Oil & Natural Gas Technology

DOE Award No.: DE-FE0024297

Quarterly Research Performance

Progress Report (Period Ending 3/31/2018)

Marcellus Shale Energy and Environment Laboratory (MSEEL)

Project Period (October 1, 2014 – September 30, 2019)

Submitted by:
Samuel Taylor

Signature

West Virginia University Research Corporation
DUN's Number: 191510239
886 Chestnut Ridge Road,
PO Box 6845, Morgantown WV, 26505
Tim.Carr@mail.wvu.edu
304-293-9660

Prepared for:
United States Department of Energy
National Energy Technology Laboratory

3/31/2018

U.S. DEPARTMENT OF ENERGY | NATIONAL ENERGY TECHNOLOGY LABORATORY

Office of Fossil Energy

U.S. DEPARTMENT OF ENERGY | NATIONAL ENERGY TECHNOLOGY LABORATORY

Executive Summary

The objective of the Marcellus Shale Energy and Environment Laboratory (MSEEL) is to provide a long-term field site to develop and validate new knowledge and technology to improve recovery efficiency and minimize environmental implications of unconventional resource development.

This quarter field work focused on moving results to publications. There were significant advances in the analysis of the large data sets generated by MSEEL using neural-network and support vector regression models to understand well behavior during and after fracture stimulation, and two publications have been submitted. Work continued and is resulting in two publications on different approaches to processing the fiber-optic distributed acoustic sensing (DAS) and distributed temperature sensing (DTS) data and for recognizing long-period long duration microseismic events with both the fiber-optic DAS data and the microseismic data. We have also been able to process the long term DTS data to better understand production changes by individual stage.

In the geochemistry area work focused primarily on determining changes in kerogen structure and bulk rock interactions and composition on interaction with fracturing fluids under simulated subsurface conditions. Kerogen was extracted and modeled, and high P-T reactors were used to determine the chemical evolution of fracturing fluids on interaction with shales of different maturity (ranging from 0.8 VRo to 2.9 VRo) at reservoir conditions. The results were surprising with a significant decrease in BTEX (benzene, toluene, xylenes) compounds and total DOC (dissolved organic carbon) with increasing thermal maturity. Metagenomic analysis has resulted recognition in improved understanding of deep biosphere microbiology in the Marcellus and even a possible new genus.

In surface impacts we have continued to monitor the flowback water and air. In terms of flowback water there are interesting trends after shut-in wells are brought back online. We do not fully understand the decrease in total dissolved solids (TDS). New work on low cost biologic methods for water treatment of flowback water show significant promise and microorganisms may be able to reduce or delay the precipitation of Ra in high sulfate produced.

Quarterly Progress Report

January 1 – March 31, 2018

Project Performance

This report summarizes the activities of Cooperative Agreement DE-FE0024297 (Marcellus Shale Energy and Environment Laboratory – MSEEL) with the West Virginia University Research Corporation (WVURC) during the first quarter of FY2018 (January 1 through March 31, 2018).

This report outlines the approach taken, including specific actions by subtopic. If there was no identified activity during the reporting period, the appropriate section is included but without additional information.

A summary of major lessons learned to this point of the project are provided as bullet points and will be added to as research is completed. New lessons are highlighted.

1) Synthetic based drilling mud is ecofriendly as well as helps with friction which resulted in faster drilling and reduced costs while leading to drilling waste from both the vertical and horizontal portions of the wells that passed all toxicity standards.
2) Microseismic monitoring does not completely define propped fractures and the extent of stimulated reservoir volume from hydraulic fracture stimulation. Requires integration of data from core, logs and slow slip seismic monitoring.
3) Production logging documents significant variations in production between completion types, stages and even clusters. Variations in production provide the necessary data for robust reservoir simulation.
4) Complex geology in laterals can lead to intercommunication between stages and reduced fracture stimulation efficiency. This can be mitigated with limited entry (engineered completions) that significantly improves fracture stimulation efficiency. NNE has continued the practice in subsequent wells. Planned production logging will help to define production efficiency.
5) The significant part of air emissions are in truck traffic, not in drilling and fracture operations on the pad. Emissions from both the pad and trucking can be reduced with operational modifications such as reducing dust and truck traffic during fracture stimulation (e.g., Sandbox) from bifuel (natural gas-diesel) engine operations.
6) Dual fuel engines demonstrated lower carbon monoxide (CO) emissions than diesel only operation. Dual fuel operations could reduce onsite diesel fuel consumption by 19 to 63% for drilling and 52% for hydraulic stimulation.
7) Biologic activity cannot be eliminated with biocides, only delayed. The biologic activity results in a unique biota that may affect operations. There may be other methods to control/influence biologic activity.
8) Water production changes rapidly after fracture stimulation in terms of volume (500 bbl/day to less than 1 bbl/day) and total dissolved solids (TDS from freshwater, 100 to 150g/L). Radioactivity is associated with produced water, not drill cuttings.
9) Drill cutting radioactivity levels were within West Virginia DEP standards of 5 pCi/g above background. This was true of both vertical and horizontal (Marcellus) sections.
10) Using the green drilling fluid Bio-Base 365, all drill cutting samples, vertical and horizontal, passed the USEPA's method 1311 (Toxicity Characteristics Leaching Procedure or TCLP) for inorganic and organic contaminants. This indicates that under Federal and West Virginia solid waste rules, these solid wastes would not be considered hazardous.

11) The absence of hazardous TCLP findings suggest that drilling fluids, not the inherent properties of the Marcellus formation, play the dominant role in determining drill cutting toxicity.
12) Concerning produced water quality, hydraulic fracturing fluid was nearly identical to makeup (Monongahela River) water. Initial produced water underwent a radical change in ionic composition and a two order of magnitude increase in total dissolved solids (TDS).
13) Produced water is highly saline and total dissolved solids (TDS) rapidly increased to a maximum between 100 and 150 g/L. There was negligible change in ionic composition between the initially produced water and that sampled five years post completion.
14) Concentrations of both 226 Ra and 228 Ra increased rapidly through the produced water cycle to combined maximum concentrations of 20,000 pCi/L in the first year post completion. These radium isotopes are critical regulatory determinants.
15) The volume of produced water decreased rapidly from nearly 500 bbl/day to less than 1 bbl/day after one year. Over this cycle produced water averaged about 6 bbl/day.
16) Developed a new frequency attribute calculated from the DAS data that reveals cross-stage fluid communication during hydraulic fracturing.
17) New microorganisms have been recognized in the deep biosphere represented by the Marcellus Shale. Understanding these organisms could reduce downhole well damage and precipitation of Ra in surface facilities.
18) Developed two different neural-network and support vector regression models to identify key parameters predicting potential screen out events and ultimate well performance
19) Developed a new process to better analysis long-term fiber-optic DTS data to better understand differences in production efficiency and relation to completion efficiency as displayed by microseismic and DAS data.

Project Management Update

Approach

The project management team will work to generate timely and accurate reporting, and to maintain project operations, including contracting, reporting, meeting organization, and general oversight.

Results and Discussion

The project team is tracking nine (9) milestones in this budget period:

3/1/2017 - Completed Production Logging (Scheduled 2/15/2017; Completed 3/15/2017)

4/30/2017 - Conduct preliminary analysis of production log data and present to DOE. (Completed and being worked into a new reservoir simulation – Review meeting held at WVU 4/11/2017)

6/30/2017 - Initial economic impact assessment completed (Scheduled 6/30/2017; Completed 6/30/2017)

8/15/2017 - Coordinate and hold MSEEL session at URTEC 2017 (Scheduled 8/30/2017; Completed 8/30/2017)

8/30/2017 - Complete rock geochemistry and geomechanical data analysis and integration with log & microseismic data to develop preliminary reservoir simulation and fracture model(s)

Simulation model is providing a good history match. (Scheduled 8/30/2017; Completed 8/30/2017)

8/30/2017 – Create a comprehensive online library of MSEEL presentations and papers that can be downloaded. Maintain with additional material through end of project. (Scheduled 8/30/2017; Completed 9/30/2017)

8/30/2017 – Reorganized MSEEL data portal and prepare to transfer to NETL for public dissemination. Data will be made public in December after the 2 year time period. (Original Schedule 8/30/2017; Completed 12/30/2017)

12/31/2017 – Completed an initial detailed reservoir simulation incorporating fracture geometry and flow simulation (Scheduled 12/30/2017) presented at review in January. Still learning through continued fiber-optic production monitoring and will revise model.

12/31/2017 - Determine changes in kerogen structure and bulk rock interactions and composition on interaction with fracturing fluids under simulated subsurface conditions. See update in this technical report. (Scheduled 12/30/2017; Revised Plan 9/30/2018)

3/30/2018 – Developed recommendations for optimal landing interval in Marcellus Shale (Scheduled: 3/30/2018). Landing zone recommendation is just below the Cherry Valley Limestone (Top of lower limestone tongue).

5/31/2018 – Decision on Phase 3 Wells

12/31/2018 – Phase 3 Drilling Initiation (if Elected)

3/31/2019 - Characterize chemical transformations during produced water storage from well 3h.

6/30/2019 – Complete Long Term Environmental Monitoring, MIP 3h, 5h

6/30/2019 – Complete Long Term Production Monitoring, MIP 3h, 5h

Topic 1 – Geologic Engineering

Approach

We presented several papers showing the importance of multidisciplinary and multi-institutional team undertaking integrated geoscience, engineering and environmental studies to develop new knowledge of subsurface geology and engineering, and surface environmental impact to identify best practices that can optimize hydraulic fracture stimulation to increase flow rates, estimated ultimate recovery to reduce the number of wells and environmental impact.

Results and Discussion

In terms of production monitoring we have developed a new method of processing distributed temperature sensing data that can be used to understand differences in production between stages. An abstract has been submitted to SPE (Tim Carr and Payam Kavousi).

Abstract: A new algorithm for processing distributed temperature sensing

Objectives/Scope: As part of the Marcellus Shale Energy and Environment Laboratory (MSEEL), a distributed temperature sensing (DTS) data covers the entire 28 stimulated stages of the Marcellus lateral MIP-3H well. MIP-3H produces mainly gas and small amount of water. We have recorded and processed daily DTS data for past 2 years, this provides the opportunity to

identify producing stages vs. ineffective stages based on the temperature variations. Raw DTS data does not reveal stage production. We propose a simple algorithm to better extract temperature patterns from the DTS data providing insight to well production.

Methods/Procedures/Process: A permanent fiber-optic cable is attached to the outside of the production casing of the MIP-3H. The fiber-optic DTS cable samples reservoir temperature along the well every 3ft (1m), several times per day. The recorded temperature depends on the daily production. To remove dependency, which is not necessarily a linear relationship, we calculate the average temperature for every DTS channel along the lateral of MIP-3H. Computed average temperatures subtracted from the recorded temperature at each DTS channel. Thus, the temperature deviation from the average daily temperature for every DTS channel is the result. This temperature difference map provides a detailed overview of daily temperature variations and can be upscaled to evaluate temperature variation for each stage and provide insight into both completion and production efficiency.

Results/Observations/Conclusions: The differential temperature map through the continued production history provides insight into daily reservoir temperature variation for every 3ft (1m) along the lateral. An upscaled map to the stage scale for the 28 stages in the MIP-3H reveals cooling close to the toe and warming close to the heel of the lateral. Variation by stage and through the production history shows a complex relationship to completion efficiency. The DTS data coupled to image and geomechanical log analysis, microseismic data, and distributed acoustic sensing (DAS) during fracture stimulation provides a link between rock properties, completion efficiency and production.

Applications/Significance/Novelty: Differential DTS has not been published by other researchers. This DTS attribute can reveal dynamic of the unconventional reservoir. We show that several stages switch from cooling to warming, suggesting decreased relative production. In contrast, several stages switch from warming to cooling, a possible sign for increased relative gas production. Overall, this novel approach provides a unique view of the dynamics of gas production from the Marcellus Shale in the subsurface which has not been previously possible.

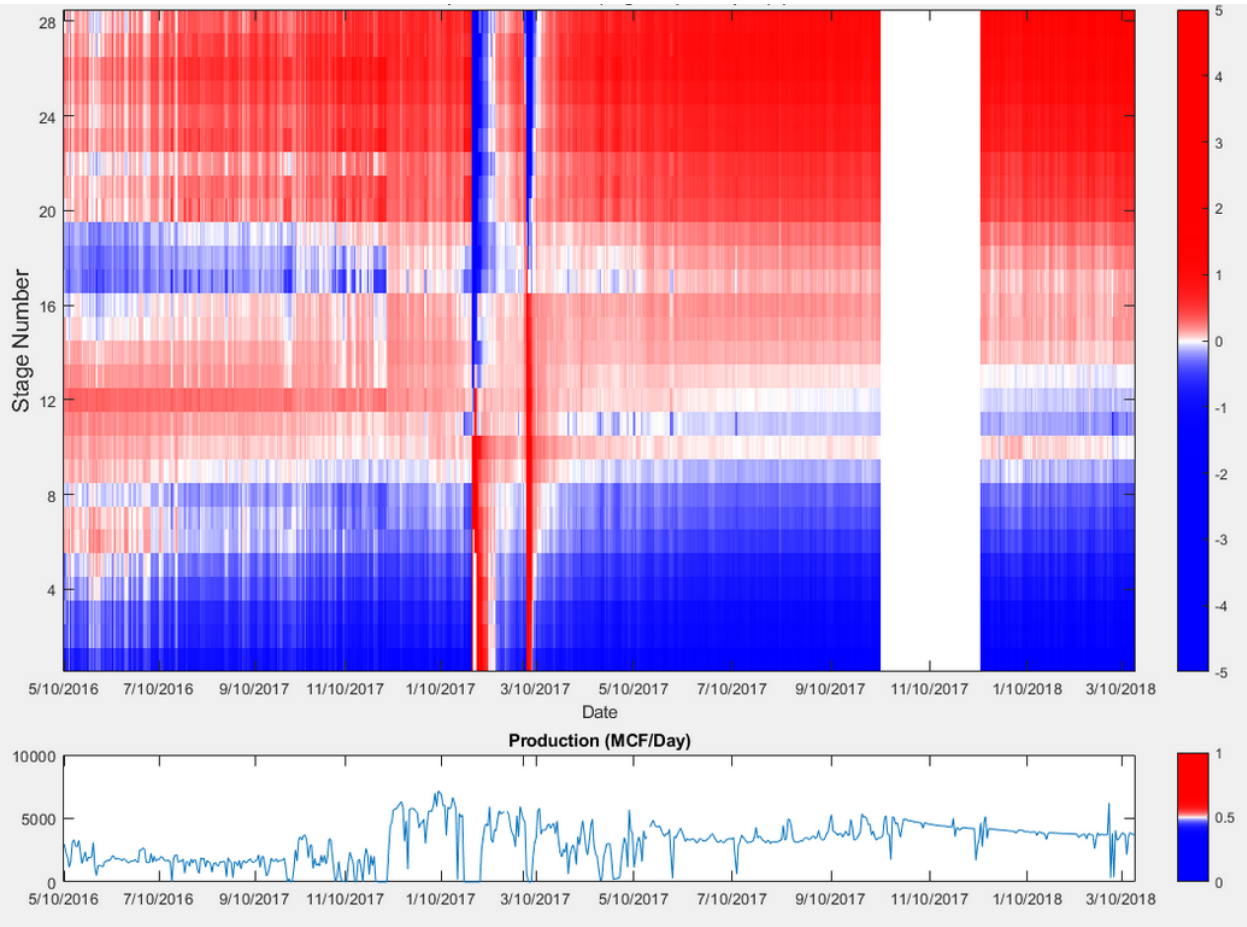

Figure 1.1: Distributed temperature sensing (DTS) map for the MIP-3h from May 2016 to March 2018 showing variations in temperature along the 28 stages in the lateral. The significant temperature perturbations in early 2017 are the result of clean-out and production logging.

We have developed two data driven machine-learning analytic techniques for advanced warning of screen out during a hydraulic fracturing treatment (Abstract for SPE - Alireza Shahkarami [St. Francis University], Payam Kavousi and Tim Carr), and prediction of gas production (Abstract for URTeC – Payam Kavousi and Tim Carr).

Technique 1. – Abstract: Application of Data Driven Analytics Techniques for Advanced Warning of Screen Out during a Hydraulic Fracturing Treatment

Objectives/Scope: Multistage hydraulic fracturing in the horizontal wells is a critical technique to improve the recovery of unconventional reservoirs such as shale and tight sand formations. Accomplishing a successful multistage hydraulic fracturing within the planned timeline is a key for an economical development of shale reservoirs. Screen out is an undesirable event that prevents an effective, safe, and economical hydraulic fracturing job. A simple and effective method of warning screen out is advantageous during a completion job.

Methods, Procedures, Process: This paper utilizes the pattern recognition capabilities of artificial intelligence and data mining techniques and the real time data during a hydraulic fracturing treatment. The field data from Marcellus Shale Energy and Environmental Laboratory (MSEEL)

project are used to develop a data driven tool that is able to predict the main characteristics of future completion jobs. The objective is to create a closed-loop system that is developed and trained during the early stages of a completion job and is able to predict the future behavior of hydraulic fracturing treatment. One application of such a tool is advanced warning of screen out.

Results, Observations, Conclusions: The data such as slurry rate, surface or bottom-hole treatment pressure, proppant concentration, etc. from the previous hydraulic fracturing treatments are used to predict the characteristics of next hydraulic fracturing job on the same well. The accurate prediction could be interpreted to warn the completion engineer of a possible screen out or used to implement of a completion schedule with a higher degree of confidence. Once a new set of data is captured it could update and train the model for the future stages.

Novel/Additive Information: Development of a tool that is able to utilize the real time, high frequency data during the completion job to predict the characteristics of operation such as treatment pressure and slurry rate ahead of time is valuable. Such a tool could be used to prevent expensive consequences of screen outs.

Technique 2. – Abstract: A fiber optic-assisted multilayer perceptron reservoir modeling: A machine learning approach in prediction of gas production from the unconventional reservoirs, a case study from the Marcellus Shale.

Objectives/Scope: This study aims to utilize the high frequency data from a fiber-optic monitoring system during multi-stage stimulation of a horizontal well drilled in the Marcellus Shale Formation in the Appalachian basin of North America. A predictive data-driven model is developed to understand the well performance and forecast the gas production using a multi-scale and multi-sensor dataset comprised of fiber optic, petrophysical, geomechanical, drilling, completion, and surface data. A spatio-temporal database is constructed and used to perform sensitivity analyses to identify the key drivers for gas production.

Methods/Procedures/Process: The 28-stage horizontal MIP-3H well, drilled in the Marcellus Shale as a part of Marcellus Shale Energy & Environment Laboratory (MSEEL) project, contains a plethora of multi-scale and multi-sensor-based spatio-temporal data, such as Distributed Acoustic Sensing, production logs, geomechanical logs, surface pressure, and surface temperature. A multi-layer perception neural network (MLPNN) was trained using eighteen input parameters to predict the daily gas production from each completed stage. The network was trained on 414 days of gas production and then tested for subsequent 102 days for validation purpose. After fine-tuning network parameters the model was iterated 500 times. Radial Basis Function-based Neural Network and Support Vector Regression were used to identify key performance indicators.

Results/Observations/Conclusions: The data-driven MLPNN model shows accuracy of ~95% in predicting daily gas production. 102 days of the test data shows that the neural network has a mean absolute error of 9.83 MCF/day for the gas production. The model can precisely predict the daily gas production using various input parameters, such as fiber-optic measurements, tubing head pressure, casing pressure, stage length, and well logs. Multiple pattern-recognition technique-based sensitivity analysis gives a robust understanding of the key drivers for hydrocarbon production. The results show that temperature, pressure, stage length, gamma, Poisson's ratio, brittleness, and minimum horizontal stress are the most important parameters influencing gas production.

Applications/Significance: This study has two main novelties. The first deals with efficient use of emerging downhole fiber-optic technology, and the second novelty concerns applying data analytics tools to predict daily gas production using multi-stage, multi-scale, and multi-sensor-based large database with high accuracy. Our work will facilitate further application of continuous stream of high-frequency fiber optic data to better understand reservoir characteristics and well performance. Incorporating fiber optic data in hydrocarbon production prediction has not been undertaken previously. Our MLPNN model integrating fiber optic, engineering, geoscientific, and surface data, can predict daily gas production with high accuracy with less computational time and cost, which can be applied to other projects worldwide.

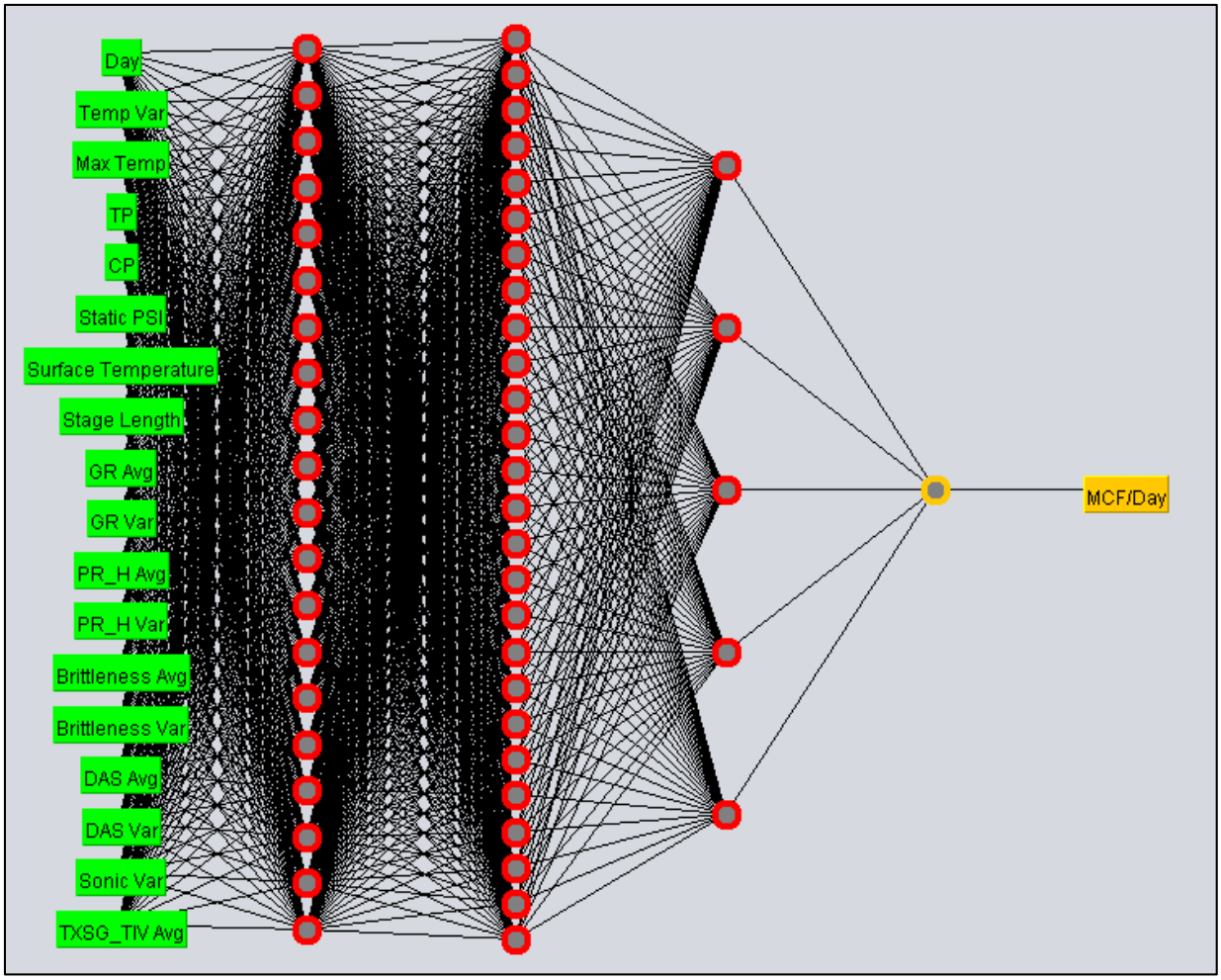

Figure 1.2: The schematic of the neural network is shown. 18 inputs are used to predict the daily gas production.

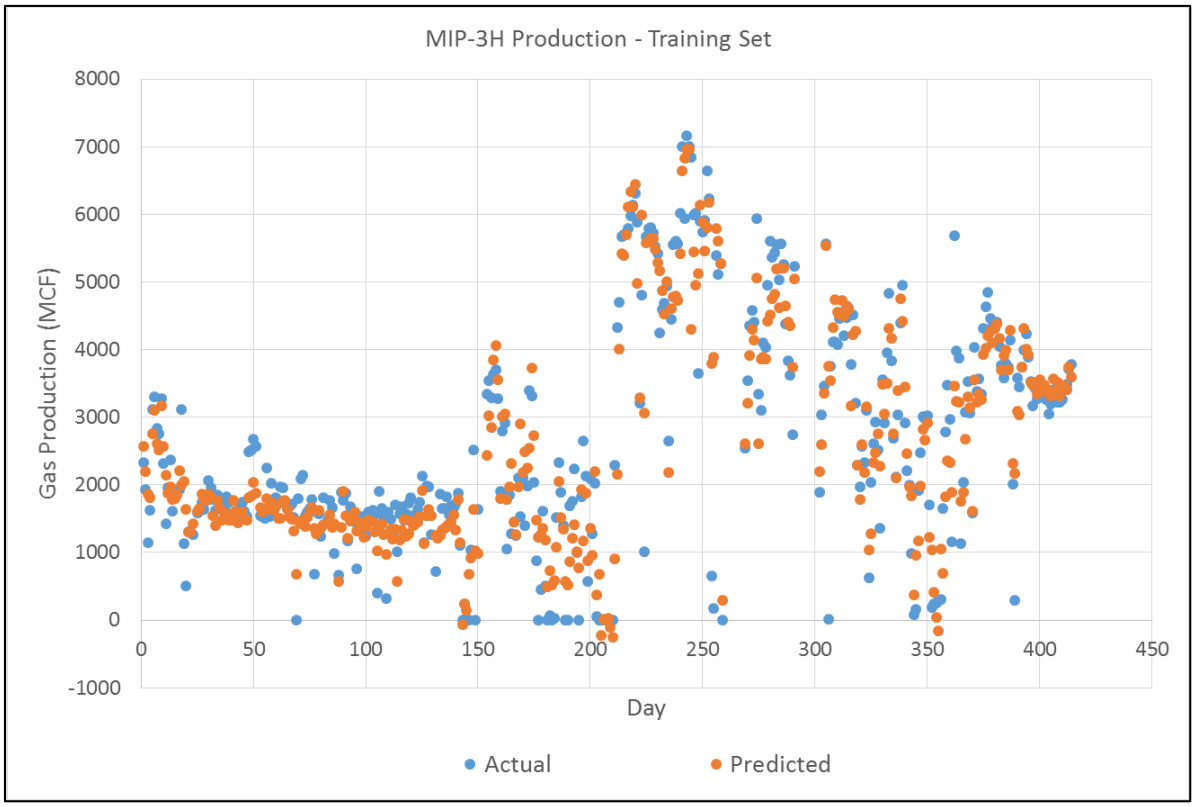

Figure 1.3: The 102 days of prediction are shown against the actual daily gas production

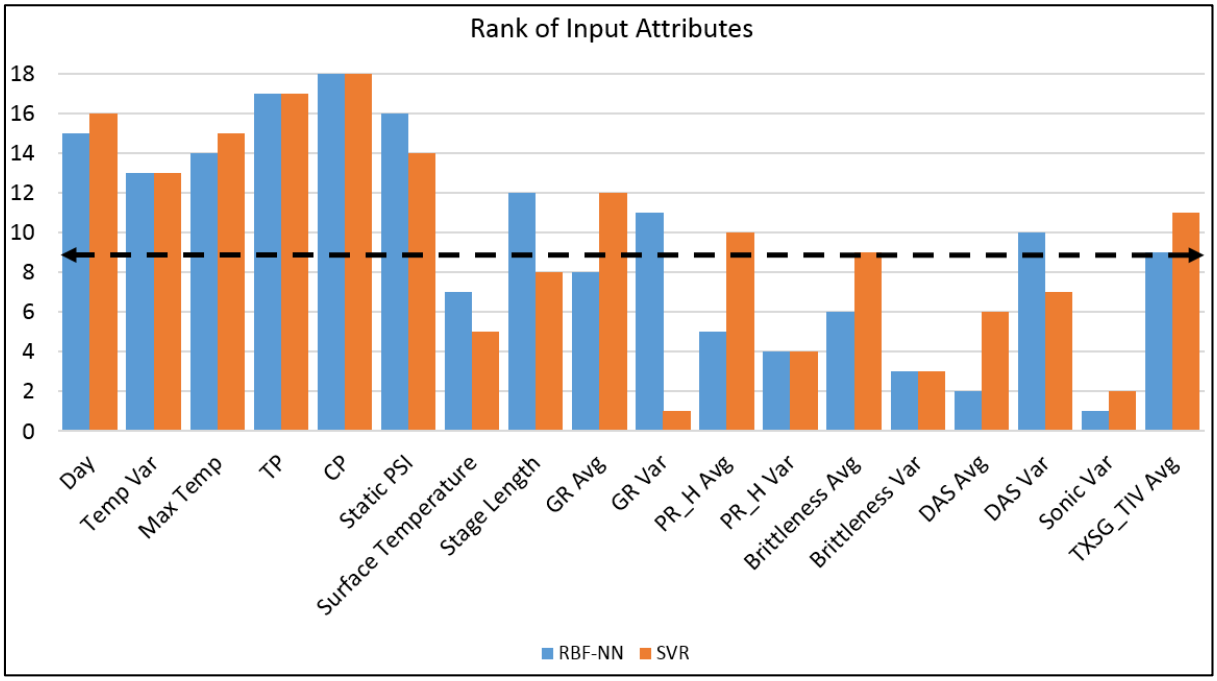

Figure 1.4: The rank of the input attributes are illustrated. RBF-NN and SVR refer to Radial Basis Function Neural Network and Support Vector Regression, respectively

Plan for Next Quarter

Continue to integrate diverse reservoir data to improve our understanding of the completion and production behavior of the Marcellus.

Topic 2 – Geophysical & Geomechanical

We have developed techniques for integrating distributed acoustic sensing (DAS) and borehole microseismic to identify long-period long-duration seismic events during stimulation (SEG Manuscript – Payam Kavousi, Thomas Wilson, Abhash Kumar and Tim Carr) and a patent application.

Approach

Geophysical:

SEG Manuscript: Integrating Distributed Acoustic Sensing (DAS) and Borehole 3C Geophone Array Data to Identify Long-Period Long-Duration Seismic Events during Stimulation of a Marcellus Shale Gas Reservoir

ABSTRACT

Microseismic monitoring, fiber-optic distributed acoustic sensing (DAS), and distributed temperature sensing (DTS) observations were made during the hydraulic fracture stimulation of the MIP-3H well in the Marcellus Shale in northern West Virginia. DAS and DTS data measure strain and temperature, respectively, along a fiber optic cable located behind the casing of the well. The presence of long-period long-duration (LPLD) events, similar in appearance to tectonic tremors, is documented in the microseismic events generated during stimulation of the MIP-3H. LPLD events are generally overlooked, but reveal the presence of significant deformation produced during hydraulic fracture stimulation. The image logs, well logs and drilling reports reveal numerous pre-existing natural fractures or faults with unfavorable orientations in the ambient stress field for tensile failures. Comparison of microseismic and DAS amplitude spectra reveal the presence of local low frequency energy events with duration of several hundred seconds. These low frequency events are interpreted as LPLD events. The spatial and temporal similarities of these events indicate that DAS data could be used to identify LPLD events during hydraulic fracture stimulation.

INTRODUCTION

Hydraulic fracturing of unconventional shale reservoirs is necessary to enhance the reservoir permeability. Hydraulic fracturing has been undertaken by various operators since 1940s (Montgomery and Smith, 2010). Companies carry out a multi-stage perforation followed by high pressure fluid/proppant slurry injection to create long hydraulic fractures within low permeability reservoirs. These hydraulic fractures combined with significant stimulation of the bounding natural fracture network increase the stimulated reservoir volume and subsequent reservoir production. The present-day stress orientation within the reservoir exerts the greatest influence on the direction of hydraulic fracture growth. However, the density, orientation, and openness of natural fractures/faults can also affect the direction and complexity of hydraulic fracture propagation.

Failure along pre-existing fractures generates low magnitude microseismic events (MSE) as high frequency seismic waveforms with clear P and S arrivals. These microseismic events are

interpreted to result from shear slip on pre-existing fractures and faults in vicinity of induced hydraulic fractures (Das and Zoback, 2013a; Rutledge and Philips, 2003; Warpinski et al., 2004). There is not always a clear correlation of microseismic cloud volume or stimulated reservoir volume (SRV) to cumulative production (Sicking et al., 2012; Wilson et al., 2016). Energy balance between microseismic events and injection energy has been compared in several researches (Kavousi et al., 2017; Kumar et al., 2017b; Warpinski et al., 2012; Boroumand and Eaton, 2012). Results show that the energy released in the form of microseismic events is only a small portion of the energy introduced into the reservoir during hydraulic fracture stimulation estimated from treatment pressure and injection volume. This energy deficit suggests that there are other mechanisms that significantly consume energy during hydraulic fracturing. Recently, LPLD events are considered to be another source for energy consumption by slow shear slip on relatively large faults (Das and Zoback, 2011, 2013a; Mitchell et al., 2013; Kweitniak, 2015). Das and Zoback, (2013a) showed that LPLD events release one to two orders of magnitude more energy than picked microseismic events and potentially affect the stimulation of the reservoirs much more than microearthquakes. Zoback et al., (2012) showed that fault orientation relative to the present-day SH_{max} could determine the slip behavior. They proposed through modeling that misaligned faults undergo slow slip while well-oriented faults immediately slip when triggered by increased fluid pressure. The reason might be that fluid pressure propagates faster along well-oriented faults than misaligned faults and triggers a rapid slip. Das and Zoback (2013a) suggested that LPLD events could happen on pre-existing faults that are unfavorably oriented in the present-day stress field or have high clay content.

Das and Zoback (2011) analyzed microseismic data from hydraulic fracturing in the Barnett Shale. They interpreted the LPLD events as low frequency energy release (between 10Hz to 80HZ) that lasts from tens of seconds to minutes. The long-period long-duration events are usually characterized by low amplitude arrivals, with highly emergent waveform characteristics, making the phase picking very difficult (Das and Zoback, 2011; Eaton et al, 2013). LPLD seismic events have similarities with observed tectonic tremors in subduction zones and transform faults (Caffagni et al., 2015). Tectonic tremors are assumed to be accompanied by slow shear slip of plates in transform or subduction zones (Obara, 2002; Shelly et al., 2006; Nadeau and Guilhem, 2009). Das and Zoback (2011) suggested that similar phenomena could happen during hydraulic fracturing when there is slow slip on pre-existing faults of sub-optimal orientation. They proposed that this non-brittle deformation process could contribute to reservoir production by significant permeability enhancement. LPLD events do not have a clear P-wave or S-wave arrival. Mitchell et al., (2013) analyzed the seismic waveform from surface and downhole geophone arrays during hydraulic fracturing of a horizontal well in the West Texas Cline Shale to detect LPLDs. The spectrogram of the stacked waveforms from the downhole array revealed the presence of several LPLDs; however, no LPLDs were detected in the surface recordings, most likely because of low signal strength. Eaton et al. (2013) studied seismic waveforms recorded during the hydraulic fracturing of a well in Montney gas reservoir in British Colombia and identified several LPLD events. They observed LPLD events in frequencies less than 10 HZ and proposed that complexity of pre-existing natural fractures could affect the spectral frequency of LPLD events. Cafagni et al. (2015) showed that downhole geophone arrays might show regional earthquakes as LPLD events because of relatively similar time duration, emergent waveform, overlapping frequency content, and apparent velocity. For regional earthquakes, P- and S-wave can be highly scattered within the crust from the source to the receiver, and hence produce a long duration signal with ambiguous arrival time (Aki, 1969; Aki and Chouet, 1975). Zecevic et al., (2016) also emphasized that regional earthquakes might show up in microseismic data with a similar signature to LPLDs. Kumar et al., (2017a) interpreted several LPLDs from the surface array microseismic data during

hydraulic fracturing of the MIP-3H well in the Marcellus Shale close to Morgantown, West Virginia in the eastern U.S. They analyzed seismic waveforms from the USArray stations and earthquakes recorded in the regional catalogs and found no temporal correlation between the detected LPLDs from surface broadband stations and known catalog events. When LPLD events are recorded in areas with high earthquake frequency, it is necessary to correct for the possibility that a potential LPLD may be the attenuated remnant waveform from a distant or unrecorded earthquake. Because a LPLD is a low amplitude event of local origin, the temporal correlation of the candidate event to a similar waveform recorded by a regional seismometer indicates that the event is most likely of earthquake origin and should not be considered a LPLD event.

Fiber-optic DAS and DTS data record strain and temperature around the wellbore, respectively. Fiber-optic sensing technology has been used by the oil and gas companies since 1990s to monitor steam injection, injection profiling, acid injection profiling, and hydraulic fracture diagnostics (Karaman et al., 1996; Rahman et al., 2011; Glasbergen et al., 2010; Sierra et al., 2008; Holly and Kalia, 2015). The DAS is sensitive to the vibrations in the local environment around the fiber and provides a measure of the relative axial strain or strain rate of the optical fiber. The technology is based on optical time domain reflectometry (OTDR). High power laser transmitter sends an accurately timed light down the sensing fiber; because of impurities inherent in the glass core, the lights are scattered back to the detector. A tiny fraction (<0.000001%) of the forward propagating light pulse backscatters toward the detector as the pulse travels through the fiber. Measuring the power and the wavelength of the backscattered light enables the detector to estimate temperature, strain, or vibro-acoustic on the fiber (Tanimola and Hill, 2009).

Ghahfarokhi et al., (2018) showed that seismic attributes such as instantaneous frequency, dominant frequency, and energy could be applied to DAS data to better monitor hydraulic fracturing. They computed the instantaneous frequency attribute of the DAS data and compared the results with the distributed temperature sensing data. They showed that low instantaneous frequency is associated with abnormal temperature rise in the Stage 9 of the stimulated Stage 10. They interpreted these abnormal findings as hydraulic connection evidence between stages during stimulation. Jin and Roy (2017) showed that low frequency (<0.05 HZ) strain rate DAS signals could reveal information about the stress shadow, fracture length, density, and width.

DAS fiber-optic data have also been used to detect microseismic events with high accuracy (Webster et al., 2016). Karrenbach et al. (2017) used DAS data to locate microseismic events and compared those locations with event locations estimated from sensors deployed in the monitoring well. Their results revealed that similar numbers of microseismic events were observed in both the DAS and monitoring well records. However, the locations of microseismic events observed by the DAS data could not be determined. The determination of location will require more than one fiber, or at least a highly deviated well.

A field trial of vertical seismic profiling (VSP) by DAS fiber-optic was conducted at Aquistore site in Saskatchewan, Canada. Oloffsson and Martinez (2017) showed that the VSPs from processed DAS fiber-optic of 3 different vendors are similar to VSP data recorded by conventional geophone arrays.

In this study, we examine the possibility that LPLD events can be detected from DAS and DTS data and compared to LPLD events from microseismic data. We use microseismic and DAS data collected during stimulation of the MIP-3H well close to Morgantown, WV (Figure 1). The DAS data were recorded in fiber deployed along the length of the MIP-3H horizontal well and the microseismic data were recorded by sensors deployed in a vertical monitoring well MIP_SW (Figure 1). The spectrogram of DAS and microseismic data are computed by using a short-time Fourier transform (STFT). In the following section analysis of the microseismic and DAS spectrogram are presented to determine if there is any correlation between them.

We propose that short-time Fourier transform of fiber-optic DAS data could show LPLD events concurrently with microseismic activity. Moreover, a temperature variation might be observed simultaneously with LPLD events on distributed temperature sensing (DTS) data because of the hydraulic connections through fractures and faults. It is very unlikely that regional earthquakes can alter the temperature around the fiber. So, the combined analysis of fiber-optic DAS and DTS can be used to differentiate LPLD events produced by stimulation and those produced by regional earthquakes.

Figure 1.1: Marcellus Shale Energy and Environment Laboratory (MSEEL) just outside Morgantown, West Virginia, USA. The MSEEL site consists of four horizontal production wells operated by Northeast Natural Energy LLC. (MIP-3H, MIP-4H, MIP-5H, MIP-6H), two pilot holes (MIP-3 and MIP-4), and a micro-seismic and sampled observation well (MIP-SW), and a grid of five surface seismometer (triangles).

In 2015 two horizontal wells, MIP-3H and MIP-5H, were hydraulically fractured in the Marcellus Shale close to Morgantown (Figure 2.1), West Virginia in the eastern United States. The fiber was deployed in the MIP-3H well. Data from stimulation of 28 stages along this well are available for analysis. The lateral of the MIP-3H is drilled just above the Cherry Valley Limestone in the Upper Marcellus Shale. The microseismic activities during hydraulic fracturing were monitored by the vertical MIP-SW well, which has twelve 3C geophones separated at 100 foot intervals (Figure 2.2). The total vertical aperture of the geophones array was 1100ft (335.28m). In addition, the permanent fiber-optic cable recorded the DAS and DTS data during hydraulic fracturing of the MIP-3H well. A total of 493 DAS channels recorded vibrations along the lateral with a spacing of ~16.74ft (5.1m). Simultaneously, the DTS data were recorded with a higher resolution of ~1ft (30.48cm) during hydraulic fracture stimulation. The focus of this study is to integrate DAS, DTS, and microseismic data of the MIP-3H well stimulation and inspect them for possible LPLD events.

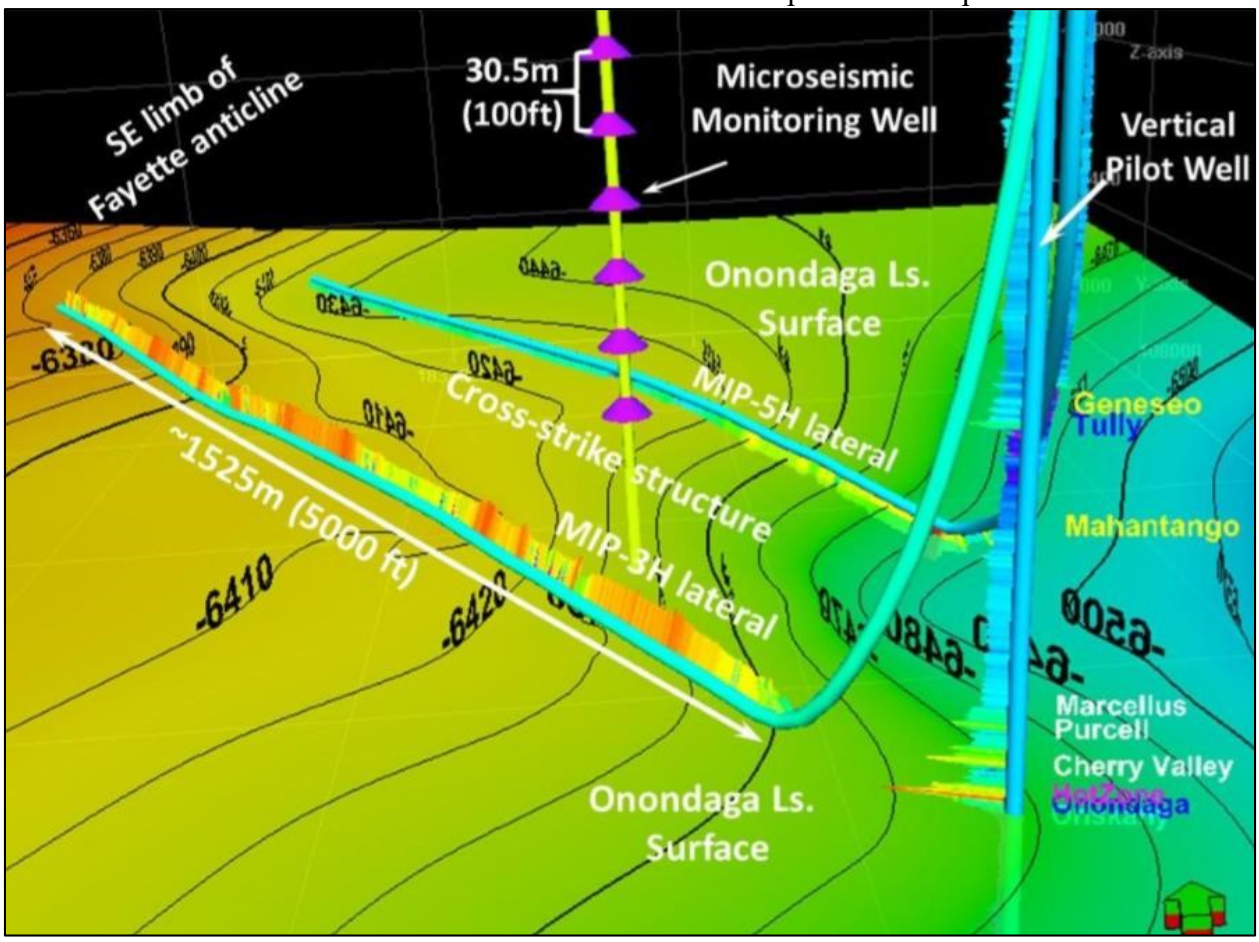

Figure 2.2: MIP-3H well is the study well with fiber-optic and microseismic are recorded in MIP-SW (after Wilson et al., 2018). Note that not all the geophones are illustrated and that the Onondaga Ls. surface is contoured by TVDSS in feet. Gamma logs are depicted along well trajectories.

From 28 stages in the MIP-3H, hydraulic fracturing of the stage 5, 10, 16, and 24 are observed to cause abnormal temperature rise in the DTS data for the stage 4, 9, 15, and 23, respectively (Amini et al., 2017). Ghahfarokhi et al., (2018) hypothesized that pre-existing faults and natural fractures act as pathways to transfer hot gassy fluids back towards the adjacent stages of the stimulated

stages. Formation image logs of the MIP-3H showed the presence of pre-existing fractures and faults in Stages 5 and 10. Several faults are also reported by the driller for base of stage 24, and 90 fractures are interpreted from the image logs for stage 16. Overall, formation image log recorded 1530 fractures along the lateral of MIP-3H well (Figure 2.3).

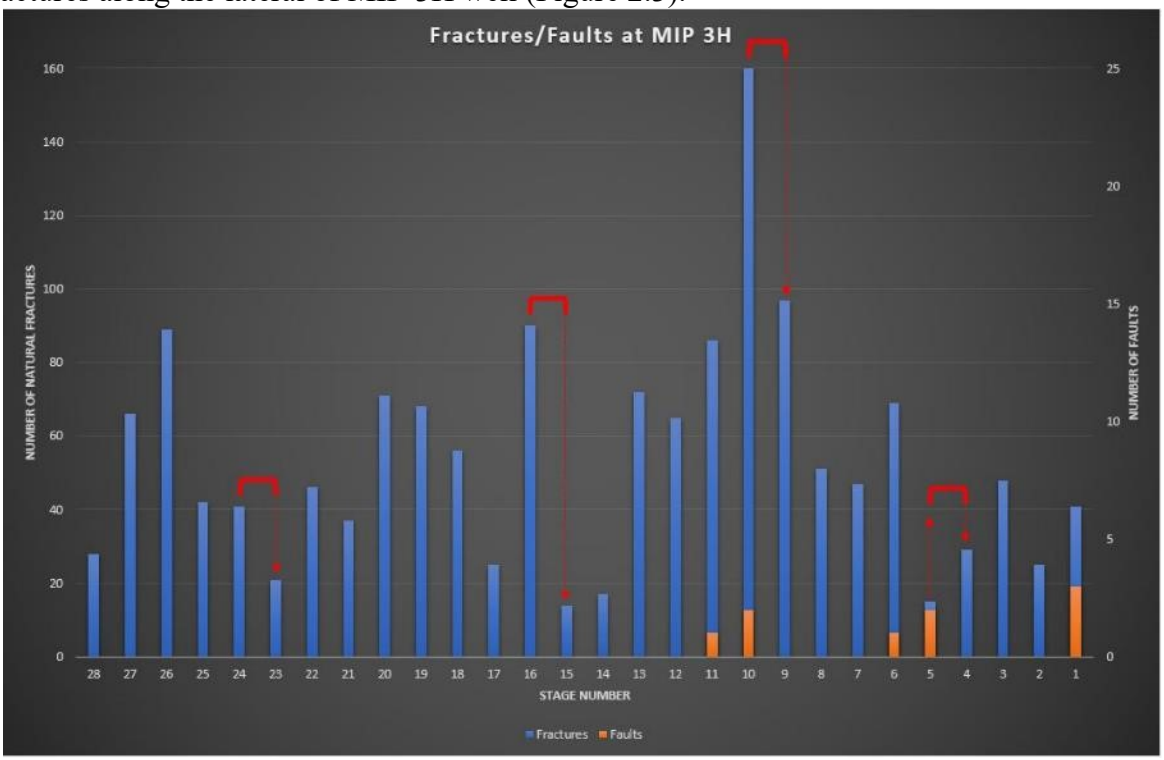

Figure 2.3: The chart that relates fracture/fault density (from fracture image log) to stages where warming was observed in DTS data during the fracture treatment of adjacent stage. Red lines connect the stage being pumped to the stage where warming was observed in DTS data (arrow points to warmed stage). Although not detected by the fracture image log, the driller reported several faults in the base of Stage 24.

Microseismic monitoring of the first 6 stages was not undertaken due to the large distance from the monitoring well. The presence of faults and fractures along the 3H lateral, along with high clay content of the Marcellus Shale facilitates the generation of LPLD events through slow-slip.

Wilson et al., (2018) analyzed the formation image logs of the MIP-3H well and reported a present-day SH_{max} orientation of N57°E based on the orientation of induced fractures observed in the vertical pilot well. As suggested by Fisher and Guest (2011) tensile failure could happen for pre-existing natural fractures with orientation of less than or equal 10° relative to the SH_{max} direction. Natural fractures and faults that are oriented at higher angels to SH_{max} most likely experience shear failure when subjected to increased pore pressure condition (Das and Zoback, 2013b).

Eaton et al., 2013 proposed that fracture network complexity could affect the dominant frequency content of LPLD events. They interpreted LPLD events from Montney Shale (British Columbia) with frequencies less than 10 Hz, while previous LPLD events reported by Das and Zoback (2013a and b) in the Barnett Shale (Texas) were found to have dominant energy in the frequency range of 10-80Hz. The lower observed frequency of LPLD events in Montney Formation, compared to the Barnett Shale, was attributed to less complex fracture network in the Montney Formation (A single fracture set). Fisher et al. (2005) categorized Barnett Shale as a formation with a very complex fracture network consists of two intersecting fracture set: a set in NE-SW and another set in NW-SE. Formation image logs of the MIP-3H vertical well reveal the

presence of two fracture sets with orientations of N87°E and N57°E while those observed in the horizontal well fell mostly in a single set with average orientation of N79°E (Wilson et al., 2018). The complex natural fracture network observed in the Marcellus Shale may facilitate higher frequency LPLD events similar to those observed by Das and Zoback 2013 study.

We assess the spectrogram of microseismic channels and compare them with the spectrogram of the DAS channels for stage 10, 16, and 24 to detect LPLD events.

DISCUSSIONS AND RESULTS

Spectral analysis of the stage 10: Ghahfarokhi et al., (2018) evaluated the DTS and DAS data of the Stage 10 stimulation to unravel low frequency zones in the DAS data (Figure 2.4). They proposed that the temperature rise in Stage 9 is because of the fluid communications through pre-existing faults and fractures that are misaligned with the present-day stress regime. This abnormal temperature rise is also corresponding to low frequency zone on instantaneous frequency attribute of the DAS data.

Two faults and 160 fractures are interpreted from the formation image log for the Stage 10. The major fractures are oriented at N80°E, almost 23° east of SH_{max} direction (N57°E). Moreover, the two faults are oriented at N30°E, 27° north of the SH_{max} direction. These faults and fractures are more prone to shear slip rather than tensile deformation during stimulation. Also, the high clay content of the Marcellus Shale would facilitate a slow shear slip on the preexisting faults and fractures during the stimulation of the associated stage. We inspect the recorded microseismic data for possible LPLD events during the hydraulic fracturing of Stage 10 and then compare them with DAS spectrogram.

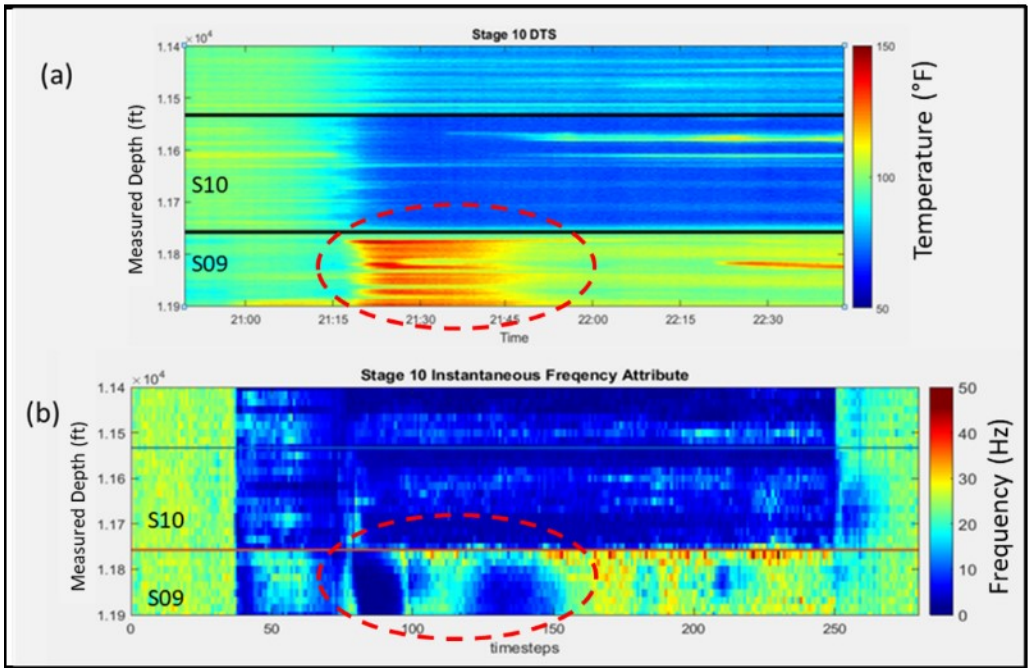

Figure 2.4: a) The DTS data for stimulation of stage 10. The warmer color shows higher temperature. The temperature is raised during Stage 10 (S10) stimulation. b) Low frequency zones are observed in stage 9 (S09) during stimulation of stage 10. Possible hydraulic connection is established between the Stage 10 and Stage 9.

The sum of the z-component response of all 12 geophones is extracted from the raw SEGY data. The raw dataset has a sampling frequency of 2004Hz, slightly higher that the DAS dataset with a 2000Hz sampling frequency. Burst of low frequency energy are observed in the microseismic spectrogram of the Stage 10 when the pumping pressure ramps up. These burst of low frequency energies are within low frequency zone (10-80HZ) and have durations of 200-300 seconds (Figure 2.5).

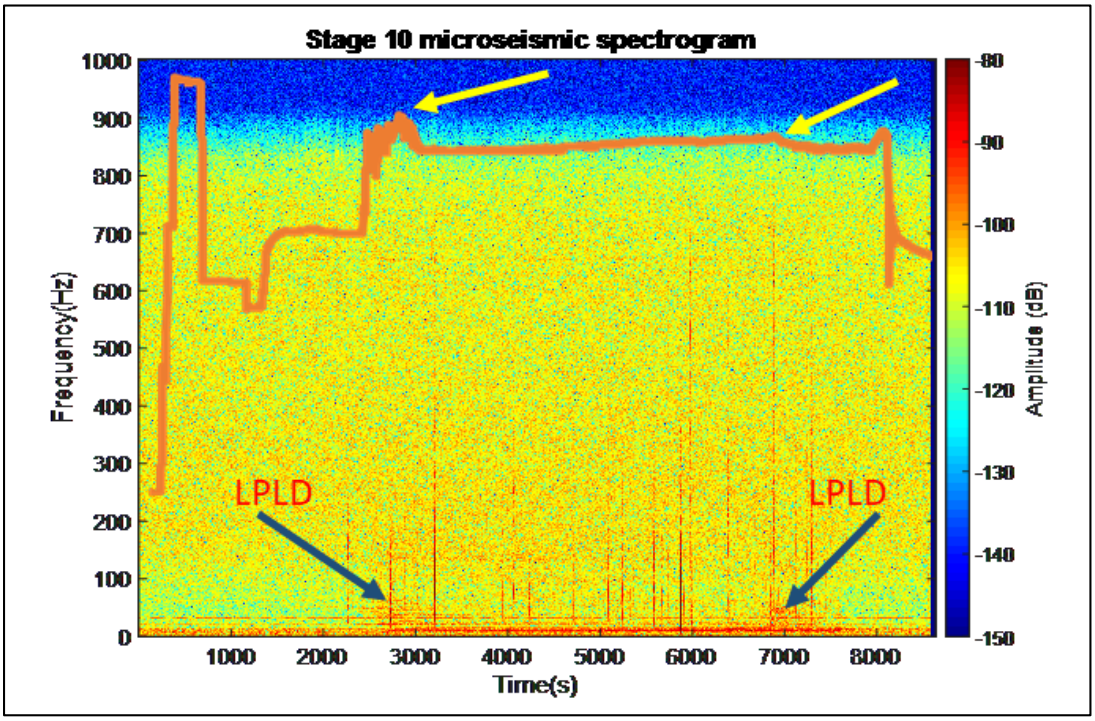

Figure 2.5: The raw unfiltered microseismic spectrogram of the Stage 10. Burst of low frequency zones are visible as the pumping pressure ramps up (yellow arrows).

In order to compare microseismic and DAS data, a bandpass filter limits the frequency content of both dataset between 10 to 80Hz. We evaluated a DAS channel at 11801.49ft, which is located in the top of the Stage 9, against the sum of the microseismic z-components recorded during the stimulation of the Stage 10 (Figure 2.6). The filtered DAS spectrogram from the Stage 9 channel reveals low frequency intervals that are interpreted to correspond to LPLDs from Stage 10 microseismic. These LPLDs are not distinguishable in the Stage 10 DAS data due to treatment noise in proximity to the injection perforations (Figure 2.7). The DAS and microseismic signals show similarities around 3000 and 7000s, which pumping pressure is ramped up (Figure 8).The slow slip shear on pre-existing faults and fractures in Stage 10 and 9 is interpreted to be the most likely cause of the interpreted LPLDs in microseismic data. The LPLD events are concurrent with the temperature rise in the Stage 9, this could suggest a flow communication through re-activated faults and fractures that undergo slow slip shear during hydraulic fracturing. The fiber-optic

proximity to the stimulated reservoir volume provides a clearer image of possible LPLDs than microseismic. There are other low frequency zones in DAS data that are not visible on microseismic spectrogram. However, the question of whether these low frequency zones are due to LPLD event remains unresolved (Figure 2.6).

The persistent very long-duration low frequency tremor between 2500 and 8000 seconds on DAS and microseismic spectrogram appears to be related to coupling of pumping induced vibrations into the subsurface (Figure 2.6). Eaton et al., (2013) noticed similar low frequency features that persist for an entire stage stimulation. DAS and Zoback (2013) also mentioned that transport of the treatment fluids inside the pipe might induce oscillations in the formation and cause LPLD like frequency zones on microseismic spectrogram. This coupling induced seismicity is clearer from the spectrogram of the trace#329 in stage 12, i.e. a trace 400ft away toward the heel from the last perforated cluster in the Stage 10 (Figure 2.9). So, the DAS response is mostly related to the vibration that is caused by passing treatment fluid through the production casing and less related to the stimulation of the Stage 10.

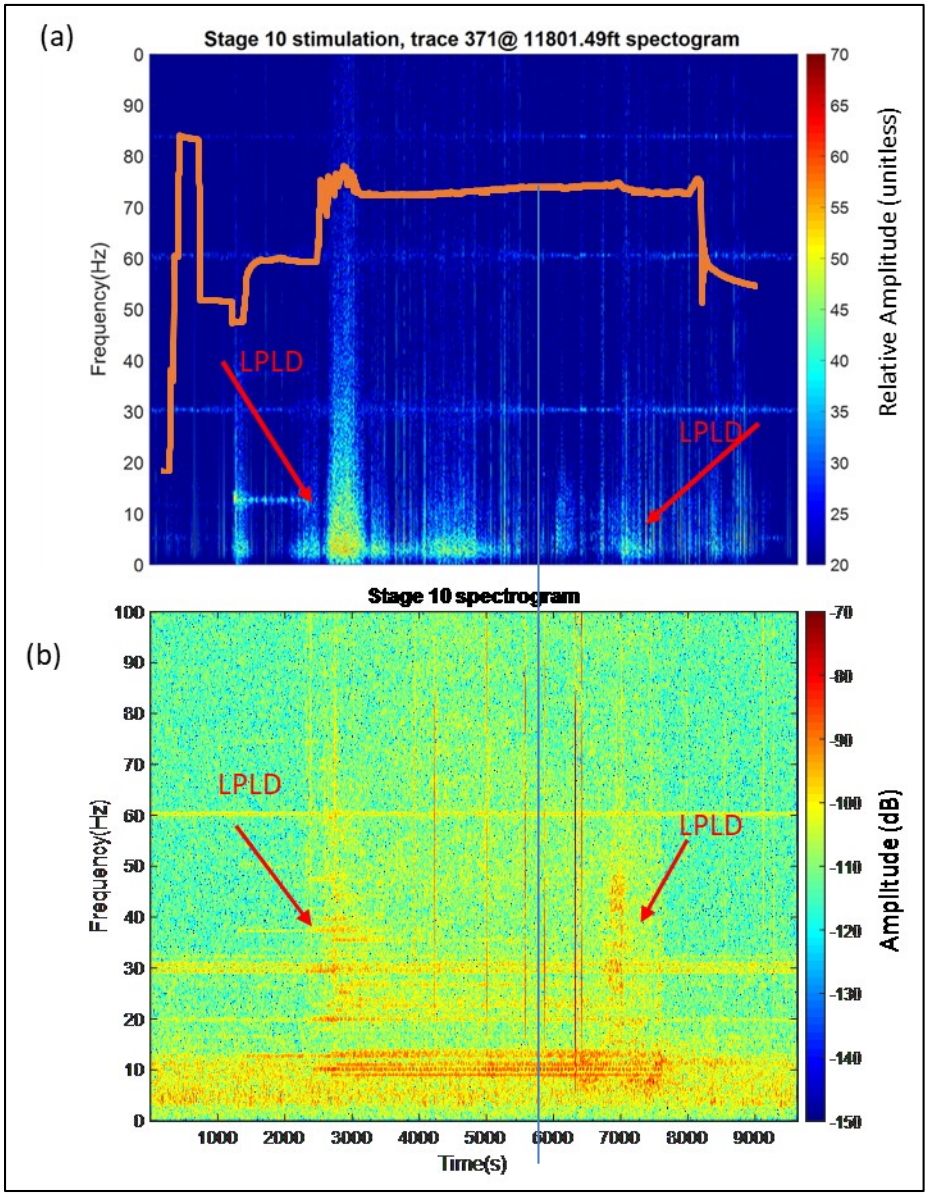

Figure 2.6: a) Stage 10 stimulation cause low frequency zones in DAS trace#371, which is in Stage 9. b) Spectrogram of sum of the z-components of Stage 10 microseismic. The low frequency strips around 10Hz, 30Hz and 60Hz appear to be pumping induced noises**.**

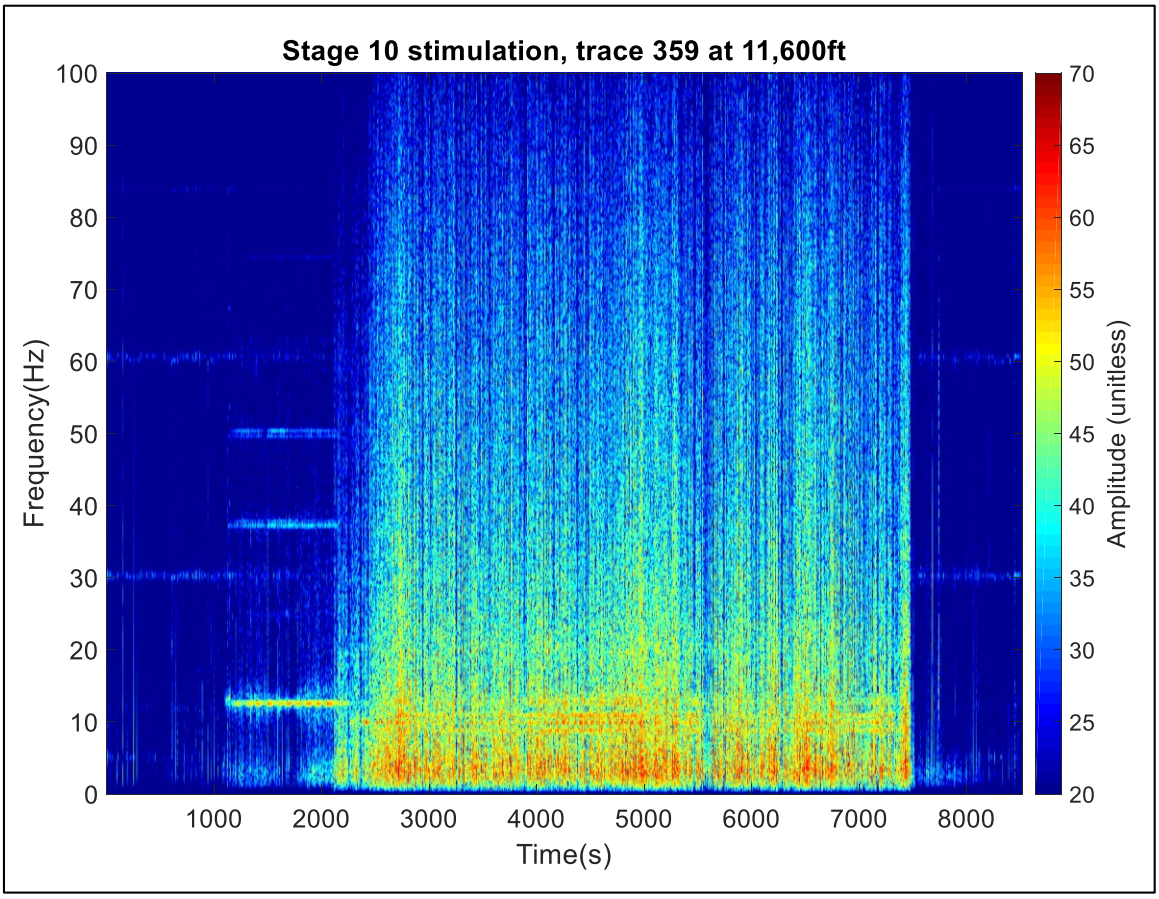

Figure 2.7: The DAS trace within the stage 10. The data is tainted by high frequency noises possibly because of proximity to the perforation clusters.

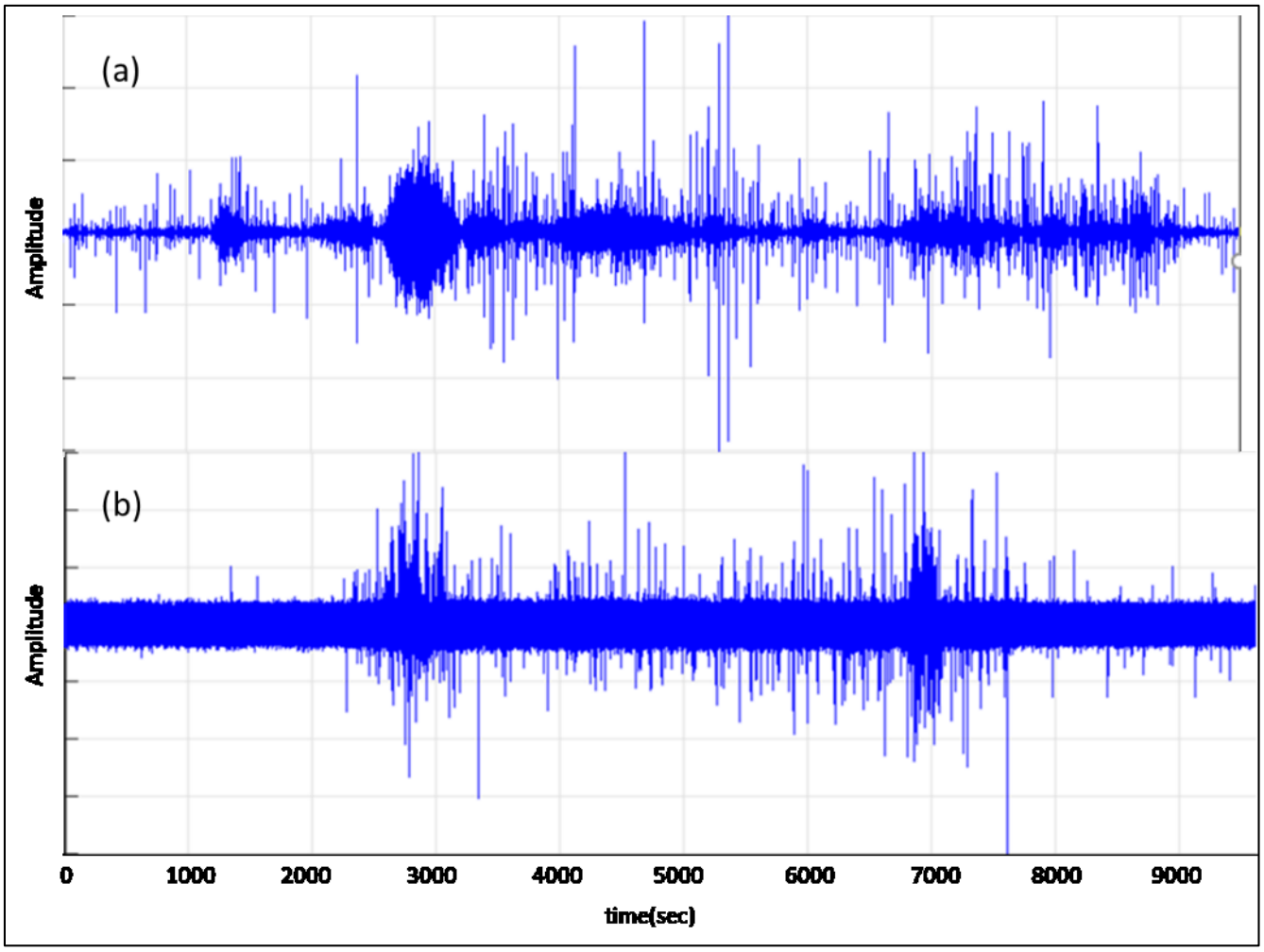

Figure 2.8: a) filtered DAS trace #371 at 11801.49ft (top of Stage 9) during stage 10 stimulation. Note that the first LPLD on the DAS trace is not visible on microseismic. b) Filtered microseismic sum of z traces during stage 10 stimulation. Compare to figure 2.3, the low frequency zones correlate in both DAS and microseismic signals. Amplitudes are not to scale.

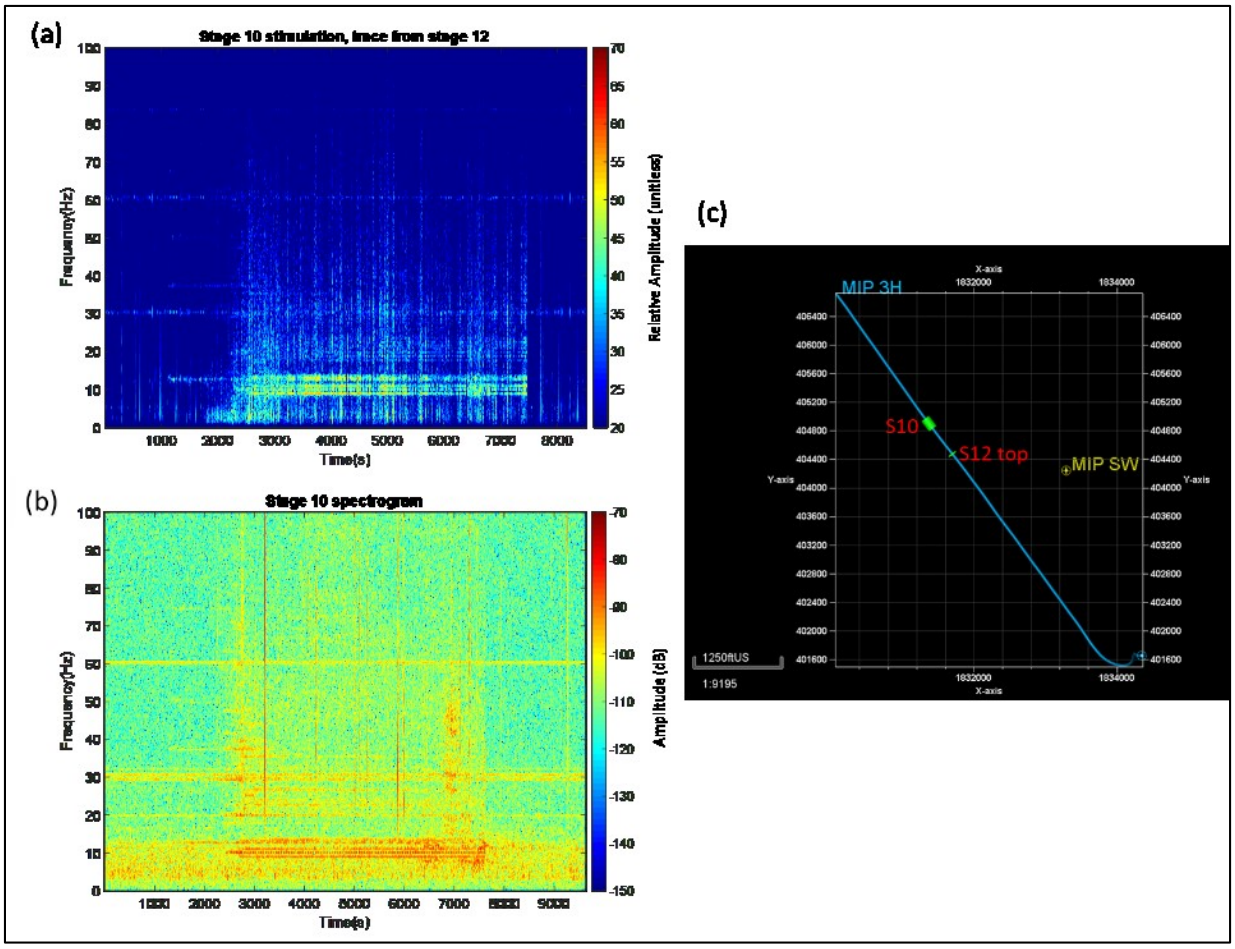

Figure 2.9: DAS and microseismic are recorded during stage 10 stimulation: a) DAS spectrogram of a trace at top of Stage 12, around 400ft away from the stimulated stage 10 b) Spectrogram of sum of the z-components of downhole geophones. Note the similarities around 10Hz, 30Hz, and 60Hz. The DAS trace is from stage 12 which had not been perforated at the time of stage 10 stimulation. c) Schematic of DAS trace 329 location relative to the stimulated stage 10.

The interpreted LPLD events in this study have similar frequency content to LPLDs from Barnet Shale interpreted by Das and Zoback (2013) in the range of 10-80 Hz. This might show that fracture networks in the Marcellus Shale in this study are similar in complexity to the Barnett Shale fracture network.

Spectral analysis of the stage 16: Similar to the Stage 10, Stage 16 stimulation caused a temperature rise in its previous stage. This temperature rise is associated with low frequency zones in the DAS data (Figure 2.10). The temperature rise is probably because of the fluid communication from stage 16 to stage 15 through pre-existing faults and fractures that were opened during the hydraulic fracturing. Ninety fractures were observed in the formation image log of the Stage 16 and majority of them are oriented N85°E. Since pre-existing fractures are not optimally oriented for a tensile failure in present-day maximum horizontal stress direction (N57°E), they can experience slow slip shear during hydraulic fracturing. We evaluate the sum of the microseismic z-components against a DAS trace at a depth of 10512.51ft, which is located in stage 15 (Figure 2.11). The spectrogram of the DAS trace from the Stage 15 during Stage 16 stimulation show several low frequency patches that could be LPLD events. However, only one of

the latter is also exist on microseismic data. The rest of the low frequency zones are probably masked by noises on microseismic data. The filtered signals are also compared to see the resemblance between LPLD events around 1000 seconds (Figure 2.12). The LPLD event at microseismic spectrum (~7200 seconds) cannot be observed from the DAS spectrum of a trace in Stage 15 (Figure 2.11). This might suggest that the second LPLD is related to faults and fractures which are not extended close to stage 15. The second LPLD might have occurred during the leak off when the pumping was stopped but pressure was still high. Instantaneous frequency attribute clearly shows the leak off period (Figure 2.10b). Similar coupling induced seismicity in Stage 10 can be observed in the Stage 16 microseismic spectrogram between 2000s and 6800s (Figure 2.11).

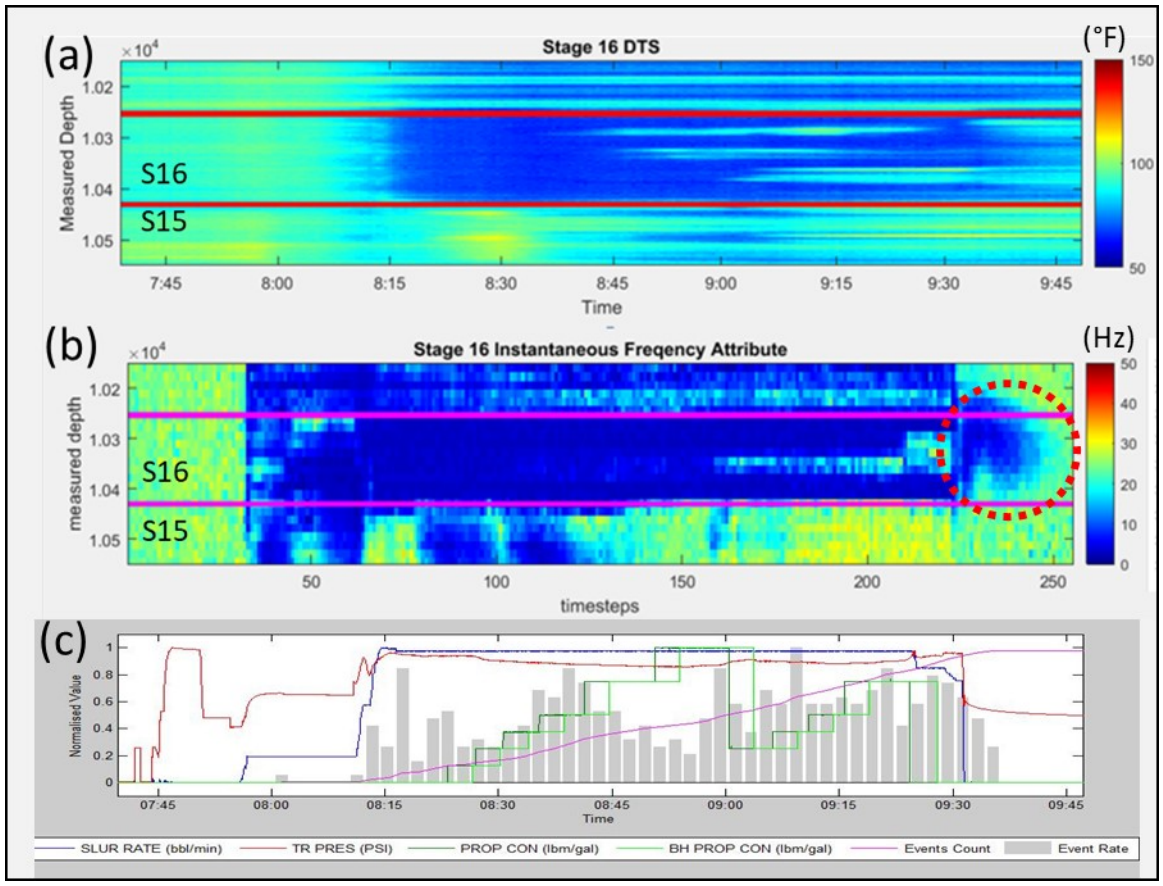

Figure 2.10: a) The stage 16 stimulation cause a temperature rise in stage 15 DTS. b) The temperature rise is associated with low frequency zones on DAS data. Note the circle around the low frequency zone after the pumping is stopped. This low frequency zone is showing the leak off time interval. c) The normalized treatment data for stage 16.

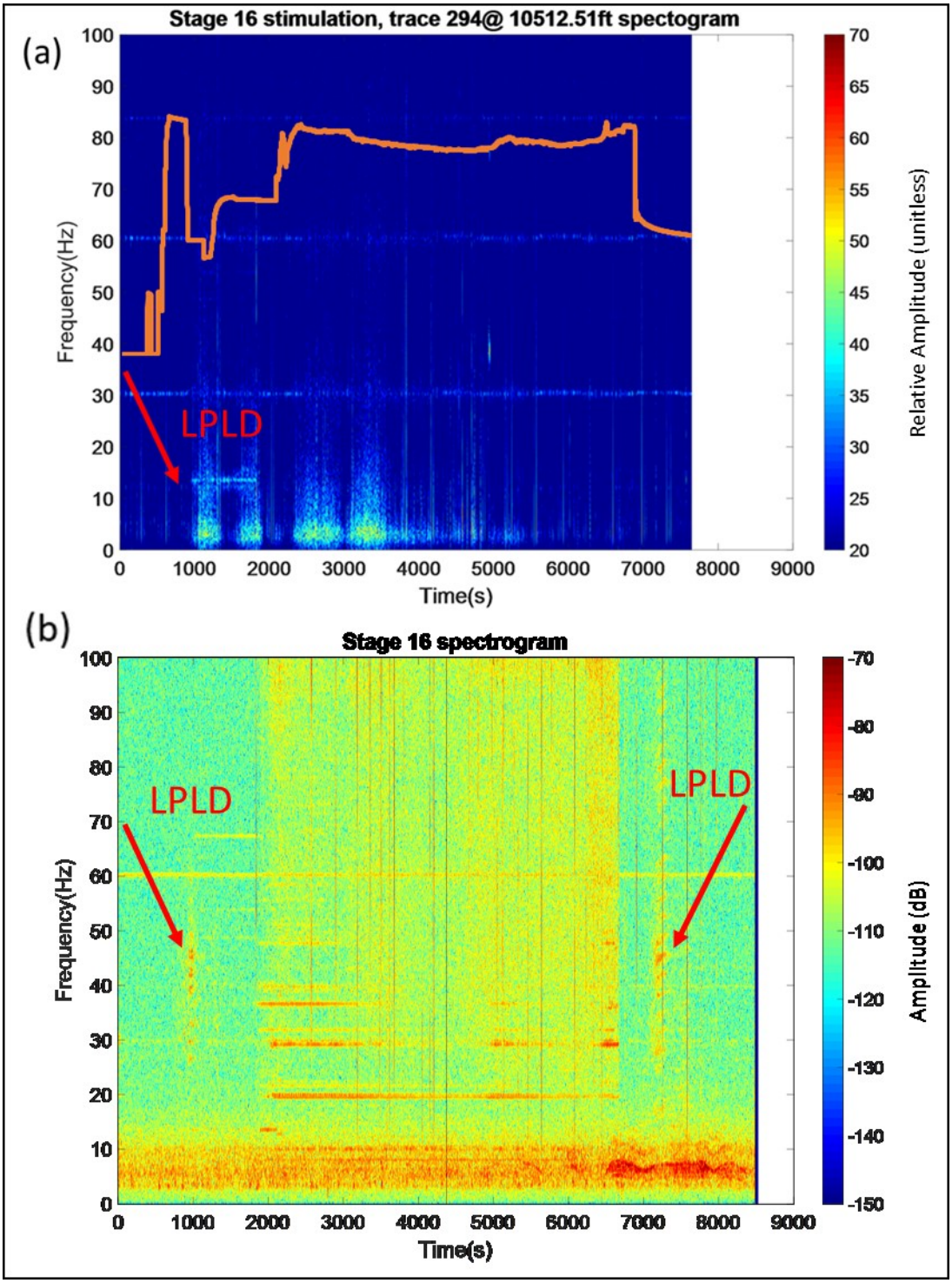

Figure 2.11: Stage 16 stimulation cause low frequency zones in DAS trace#294, which is in Stage 15. b) Spectrogram of sum of the z-components of Stage 16 microseismic. Note the common pumping noise at 30 and 60Hz.

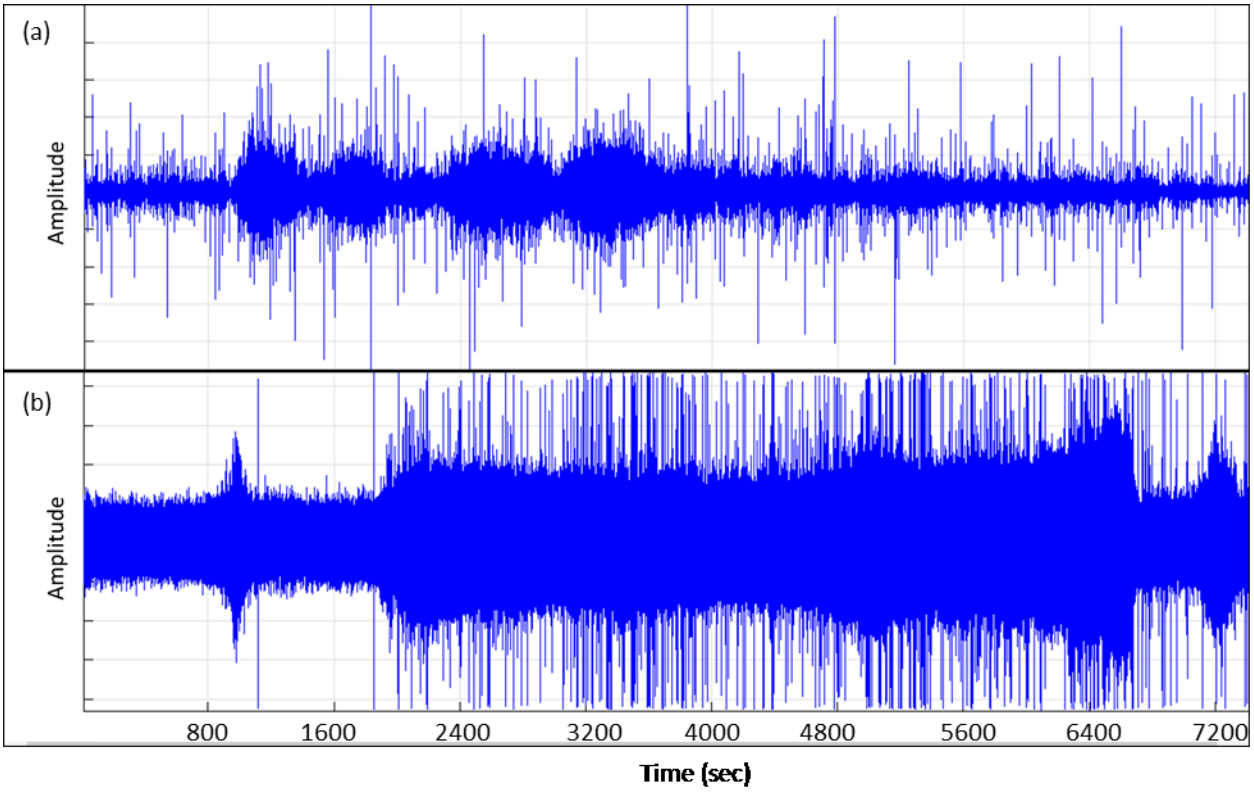

Figure 2.12: a) DAS trace number 294 from Stage 15. b) Sum of the z-components of the microseismic of Stage 16. Both DAS and microseismic traces are filtered to frequencies between 10-80HZ. Compare to Figure 9. Amplitudes are not to scale.

Spectral analysis of the stage 24: A major fault has been reported by driller at a depth between the Stage 23 and 24. The DTS and DAS of the Stage 24 stimulation show abnormal temperature and frequency variations in the Stage 23, respectively (Figure 2.13). Ghahfarokhi et al., (2018) suggested that these unusual findings are because of cross-stage flow communication that dampens the high frequencies on the DAS data. LPLD seismic events emerged in the filtered microseismics spectrogram of Stage 10 and Stage 16 where abnormal frequency and temperature present. The LPLD seismic events are assumed to be observed when there is slow shear slip on a relatively large fault. Thus, the observed fault in boundary of Stage 23 and 24 might cause the LPLD events on microseismic data. To evaluate this hypothesis, the spectrogram of Stage 24 microseismic is computed and then compared with the DAS spectrogram of a trace in Stage 23 (Figure 2.14). The filtered signals from DAS and microseismic show similarities around 2000 seconds (Figure 2.15). This similarity could suggest that LPLD events occurred as the pumping pressure ramped up and caused slow slip on relatively large faults in the stimulated stage.

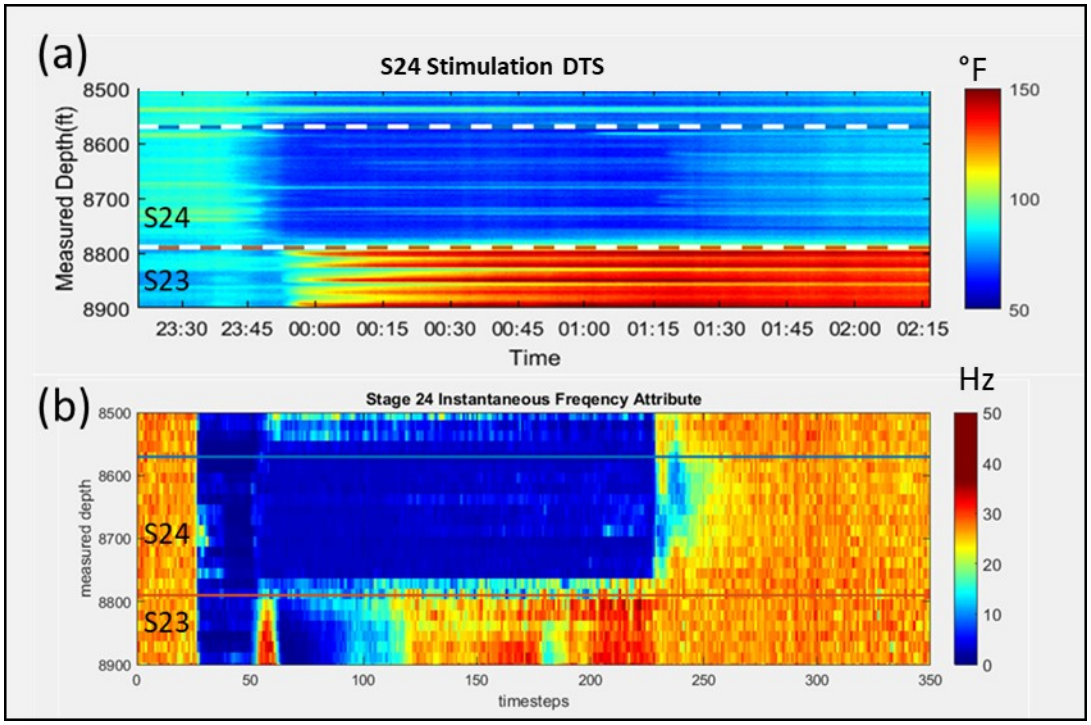

Figure 2.13: a) The recorded DTS for the Stage 24 (S24) stimulation. Low frequency zones in stage 23 (S23) is corresponding to the temperature rise in Stage 23. Each timestep is 30 seconds.

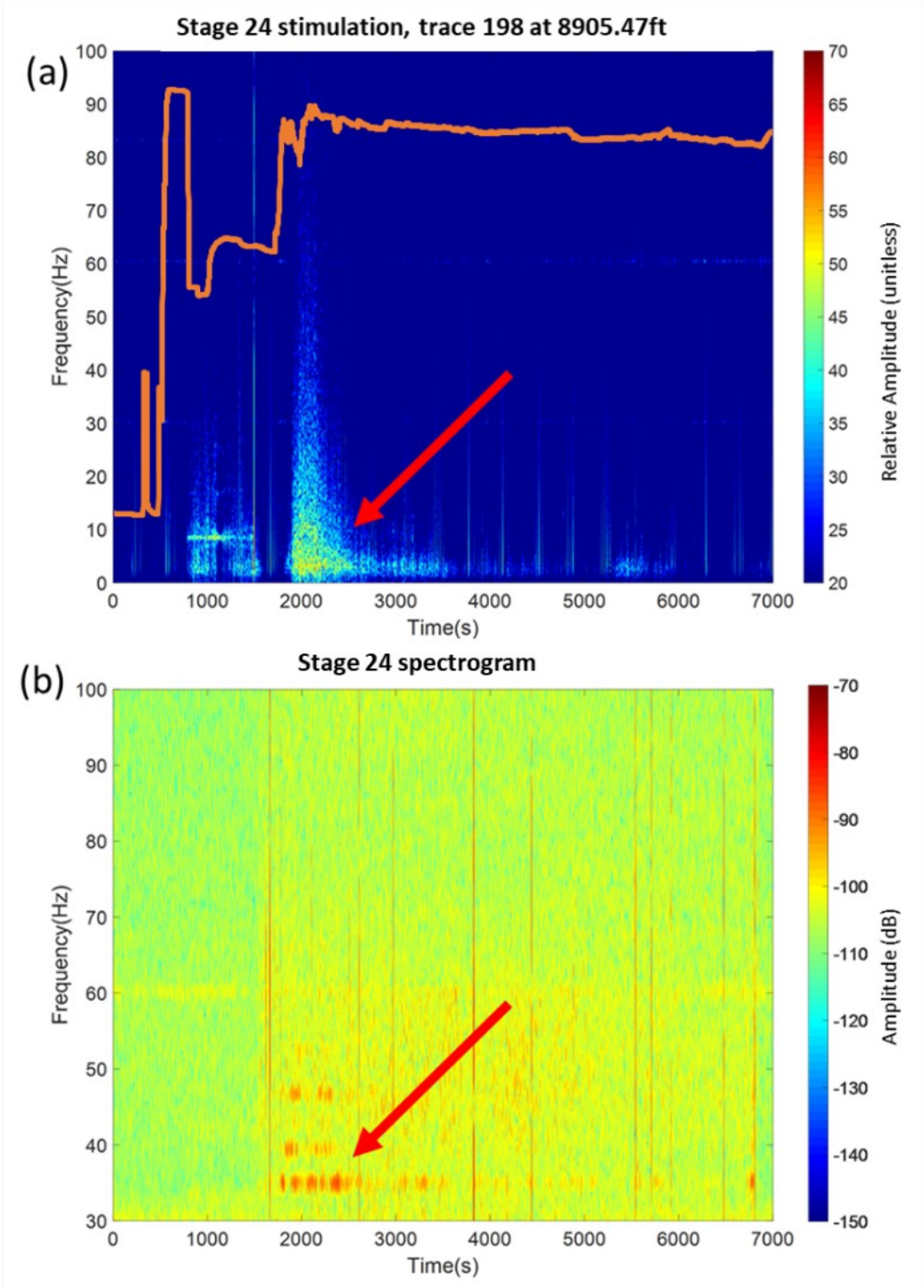

Figure 2.14: a) DAS spectrogram for trace 287 along with the treatment pressure as the solid line. b) Microseismic spectrogram of the sum of the –z component of 12 geophones in the MIP-SW.

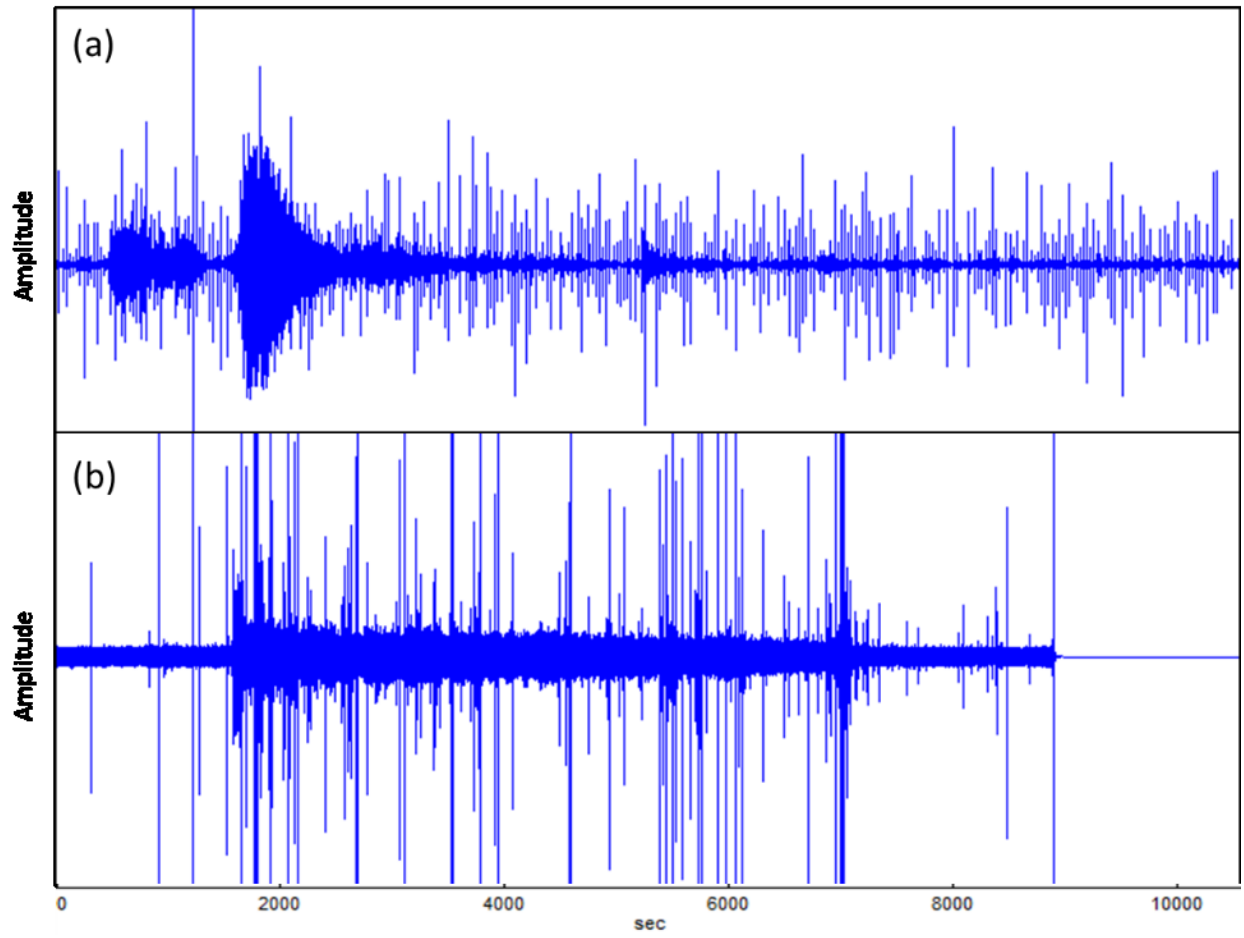

Figure 2.15: a) DAS trace 287 during Stage24 stimulation. b) Raw microseismic of Stage 24 stimulation. Both DAS and microseismic traces are filtered to frequencies between 10-80HZ. Amplitudes are not to scale**.**

CONCLUSIONS

Study of the spectrogram of the DAS and microseismic of the 3 studied stages brings the following concluding remarks:

- DAS is a valuable tool that can record possible LPLD events with better resolution than microseismic arrays. This could be due to proximity of the fiber-optic cable to the stimulated volume.
- The distributed temperature sensing data shows a warming effect in the adjacent stages of the stimulated stages when there are LPLD events in the microseismic and DAS spectrogram. It could suggest the hydraulic connections between stages which was formed as a result of LPLD events.
- Very long duration pumping induced vibrations have been reported by several researchers in microseismic data. We showed evidence of this seismicity on the DAS spectrogram where persistent constant low frequency tapes last for the entire pumping process. Care should be taken not to interpret them as LPLD events.
- Regional earthquake are very unlikely to have any effect on the DTS data. Thus, LPLD events observed in the current study in the DAS, microseismic, and DTS is most likely

related to local deformation in the reservoir during hydraulic fracturing and not an overprint of regional earthquake in the distant area.

- Studied stages have faults or pre-existing fractures which are not optimally aligned with the present-day maximum horizontal stress for tensile failure. Hence, long period slow shear slip could a major deformation mechanism for the studied stages.
- LPLD events in this study have durations of 500 seconds, this could imply slow shear slip on large faults or high clay contents in the Marcellus Shale.
-

ACKNOWLEDGMENTS

This research is funded through the U.S.DOE National Energy Technology Lab part of their Marcellus Shale Energy and Environmental Laboratory (MSEEL) (DOE Award No.: DE-FE0024297). We appreciate the Northeast Natural Energy LLC. For providing data and technical support.

REFERENCES

Aki, K. T., 1969, Analysis of the seismic coda of local earthquakes as scattered waves: Journal of Geophysical Research, **74**, 615–631.

Aki, K. T., and B. Chouet, 1975, Origin of the coda waves: Source attenuation and scattering effects: Journal of Geophysical Research, **80**, 3322– 3342.

Amini, S., Kavousi, P., and Timothy R. Carr, 2017, Application of Fiber-optic Temperature Data Analysis in Hydraulic Fracturing Evaluation--A Case Study in Marcellus Shale: Unconventional Resources Technology Conference, URTEC, Paper 2686732 .

Boroumand, N., and D. W. Eaton, 2012, Comparing energy calculations-hydraulic fracturing and microseismic monitoring: 74th Annual International Conference and Exhibition, EAGE, Extended Abstracts, EUROPEC 2012, https://doi.org/10.3997/2214-4609.20148187.

Caffagni, E., D. Eaton, M. van der Baan, and J. P. Jones, 2015, Regional seismicity: A potential pitfall for identification of long-period long-duration events: Geophysics, **80**, no. 1, A1–A5.

Das, I., and M. D. Zoback, 2011, Long-period, long-duration seismic events during hydraulic fracture stimulation of a shale gas reservoir: The Leading Edge, **30**, 778–786.

Das, I., and M. D. Zoback, 2013a, Long-period, long-duration seismic events during hydraulic stimulation of shale and tight-gas reservoirs — Part 1: Waveform characteristics: Geophysics, **78**, no. 6, KS97– KS108.

Das, I., and M. D. Zoback, 2013b, Long-period long-duration seismic events during hydraulic stimulation of shale and tight-gas reservoirs —Part 2: Location and mechanisms: Geophysics, **78**, no.6, KS109– KS117.

Eaton, D., van der Baan, M., Tary, J. B., Birkelo, B., Spriggs, N., Cutten, S., & Pike, K. , 2013, Broadband microseismic observations from a Montney hydraulic fracture treatment, northeastern BC, Canada: CSEG Recorder, **38**(3), 44-53.

Fisher, M. K., Wright, C. A., Davidson, B. M., Goodwin, A. K., Fielder, E. O., Buckler, W. S., and Steinsberger, N. P ., 2005, Integrating fracture-mapping technologies to improve stimulations in the Barnett Shale: SPE production & Facilities, **20**(2), 85-93..

Fisher, T., and Guest, A., 2011, Shear and tensile earthquakes caused by fluid injection: Geophysical Research Letters, **38**, L05307.

Ghahfarokhi, P. K., Carr, T., Song, L., Shukla, P., & Pankaj, P., 2018, Seismic Attributes Application for the Distributed Acoustic Sensing Data for the Marcellus Shale: New Insights to Cross-Stage Flow Communication. SPE Hydraulic Fracturing Technology Conference and Exhibition. Society of Petroleum Engineers, Paper 189888.

Glasbergen, G., Yeager, V.J., Reyes, R.P. and Everett, D.M., 2010, Fluid-diversion monitoring: the key to treatment optimization: SPE Production & Operations, **25**(03), 262-274.

Holley, E. and Kalia, N., 2015, Fiber-optic Monitoring: Stimulation Results from Unconventional Reservoirs: Unconventional Resources Technology Conference (URTEC), Paper 2151906.

Jin, G. and Roy, B., 2017, Hydraulic-fracture geometry characterization using low-frequency DAS signal: The Leading Edge, **36**(12), 975-980.

Karaman, O.S., Kutlik, R.L. and Kluth, E.L., 1996, A field trial to test fiber optic sensors for downhole temperature and pressure measurements, West Coalinga Field, California: SPE Western Regional Meeting, Paper 35685.

Karrenbach, M., Ridge, A., Cole, S., Boone, K., Kahn, D., Rich, J., Silver, K. and Langton, D., 2017, DAS microseismic monitoring and integration with strain measurements in hydraulic fracture profiling: Unconventional Resources Technology Conference, URTEC, Paper 2670716.

Kavousi, P., Carr, T., Wilson, T., Amini, S., Wilson, C., Thomas, M., … Hewitt, J., 2017, Correlating distributed acoustic sensing (DAS) to natural fracture intensity for the Marcellus Shale: SEG Technical Program Expanded Abstracts 2017, 5386-5390.

Kwietniak, A., 2015, Detection of the long period long duration (LPLD) events in time- and frequency-domain: Acta Geophysica, **63**, 201–213.

Kumar, A., Zorn, E.V., Hammack, R. and Harbert, W., 2017a, Seismic Monitoring of Hydraulic Fracturing Activity at the Marcellus Shale Energy and Environment Laboratory (MSEEL) Site, West Virginia: Unconventional Resources Technology Conference, URTEC, Paper 2670481.

Kumar, A., Zorn, E., Hammack, R., & Harbert, W., 2017b. Long-period, long-duration seismicity observed during hydraulic fracturing of the Marcellus Shale in Greene County, Pennsylvania: The Leading Edge, **36**(7), 580-587.

Mitchell, C., J. Kurpan, and P. Snelling, 2013, Detecting long-period long-duration microseismic events during hydraulic fracturing in the Cline Shale Formation, West Texas: A case study: 83rd Annual International Meeting, SEG, Expanded Abstracts, 2233–2237.

Montgomery, C. T., and M. B. Smith, 2010, Hydraulic fracturing: History of an enduring technology: Journal of Petroleum Technology, **62**, 26-40.

Nadeau, R.M., and A. Guilhem, 2009, Nonvolcanic tremor evolution and the San Simeon and Parkfield, California, earthquakes: Science, **325**, 5937, 191-193.

Obara, K., 2002, Nonvolcanic deep tremor associated with subduction in southwest Japan: Science, **296** (5573), 1679-1681.

Olofsson, B. and Martinez, A., 2017, Validation of DAS data integrity against standard geophones—DAS field test at Aquistore site: The Leading Edge, **36**(12), 981-986.

Rahman, M., Zannitto, P.J., Reed, D.A. and Allan, M.E., 2011, Application of fiber-optic distributed temperature sensing technology for monitoring injection profile in Belridge Field, diatomite reservoir: SPE Digital Energy Conference and Exhibition, SPE, Paper 144116.

Rutledge J. T. Phillips W. S., 2003, Hydraulic stimulation of natural fractures as revealed by induced microearthquakes, Carthage Cotton Valley gas field, East Texas: Geophysics , **68**, 441–452.

Shelly, D. R., Beroza, G. C., Ide, S., & Nakamula, S., 2006, Low-frequency earthquakes in Shikoku, Japan, and their relationship to episodic tremor and slip: Nature, **442**(7099), 188.

Sicking, C., Vermilye, J., Geiser, P., Lacazette, A., & Thompson, L., 2012, Permeability field imaging from microseismic: SEG Annual Meeting. Society of Exploration Geophysicists.

Sierra, J.R., Kaura, J.D., Gualtieri, D., Glasbergen, G., Sarker, D. and Johnson, D., 2008, DTS monitoring of hydraulic fracturing: experiences and lessons learned: SPE Annual Technical Conference and Exhibition, Society of Petroleum Engineers, Paper 116182.

Tanimola, F. and Hill, D., 2009, Distributed fibre optic sensors for pipeline protection: Journal of Natural Gas Science and Engineering, **1**(4), pp.134-143.
Warpinski N. R. Wolhart S. L. Wright C. A., 2004, Analysis and prediction of microseismicity induced by hydraulic fracturing: Society of Petroleum Engineers Journal, **9**, 24–33.
Warpinski, N.R., Du, J. and Zimmer, U., 2012, Measurements of hydraulic-fracture-induced seismicity in gas shales: SPE Production & Operations, **27**(03), 240-252.
Webster, P., M. Molenaar, and C. Perkins, 2016, DAS microseismic: CSEG Recorder **41**(6): 38-39.
Wilson, T.,H., Hart, A.,K., and Pete Sullivan, 2016 , Interrelationships of Marcellus Shale gas production to frac-induced microseismicity, interpreted minor faults and fractures zones, and stimulated reservoir volume, Greene County, Pennsylvania: Interpretation, **4**(1), T15-T30.
Wilson, T. H., Carr, T., Carney, B. J., Yates, M., MacPhail, K., Morales, A.,... & Thomas, M., 2018, Marcellus Shale model stimulation tests and microseismic response yield insights into mechanical properties and the reservoir discrete fracture network: Interpretation, **6**(2), T231-T243.
Zecevic, M., Daniel, G., & Jurick, D., 2016, On the nature of long-period long-duration seismic events detected during hydraulic fracturing on the nature of LPLD events: Geophysics, **81**(3), KS113-KS121.
Zoback, M. D., A. Kohli, I. Das, and M. McClure, 2012, The importance of slow slip on faults during hydraulic fracturing stimulation of shale gas reservoirs: Americas Unconventional Resources Conference, SPE, Paper 155476. *Geomechanical*

During this quarterly period, the influence of a discrete fracture network on the growth of hydraulic fractures was investigated through the use of numerical modeling. The numerical model updated in a previous quarter was used to compute hydraulic fracture dimensions for stage 1 through stage 10 of well MIP-5H.

Results & Discussion

Geomechanical

Table 2.16 shows the computed hydraulic fracture geometries for newly modeled MIP-5H stage 1 through stage 10. Figure 2.16 shows the hydraulic fracture geometry for one of the primary induced hydraulic fractures in stage 10 of well MIP-5H. Figure 2.17 shows the cumulative proppant mass versus time (calculated and measured), Figure 2.18 shows the slurry volume injected versus time (calculated and measured), and Figure 2.19 shows the surface pressure versus time (calculated and measured) for stage 10 of well MIP-5H.

Microseismic data was available for stage 2 and stage 4 through stage 10 of well MIP-5H. Microseismic, well, and hydraulic fracture geometry data were visualized in three dimensions. Figures 2.20 through 2.27 show side views of modeled hydraulic fracture geometries and available measured microseismic events and magnitudes for stage 2, and stages 4 through 10, respectively, for well MIP-5H. Figure 2.28 shows an overview of all 10 newly modeled hydraulic fracture geometries, available microseismic event data, and the entire MIP-5H wellbore. Figure 2.29 shows a top view of all newly modeled hydraulic fracture geometries, available microseismic event data, and the nearby section of the MIP-5H wellbore. Figure 2.30 shows an orthogonal projection of the newly modeled hydraulic fracture geometries, available microseismic event data, and the nearby section of the MIP-5H wellbore.

Table 2.1. Computed Hydraulic Fracture Geometries – Stage 1 through Stage 10 – MIP-5H

STAGE	Fracture Half-Length (ft)	Fracture Height (ft)	Average Fracture Width (in)
1	591.9	294.3	0.029143
2	547.9	295.6	0.020782
3	511.5	285.7	0.022435
4	449.7	285.2	0.016648
5	517.1	289.9	0.020991
6	574.1	310.6	0.021193
7	600.1	304	0.018286
8	564.5	309.1	0.021027
9	558	306	0.02078
10	606.6	316.7	0.027322

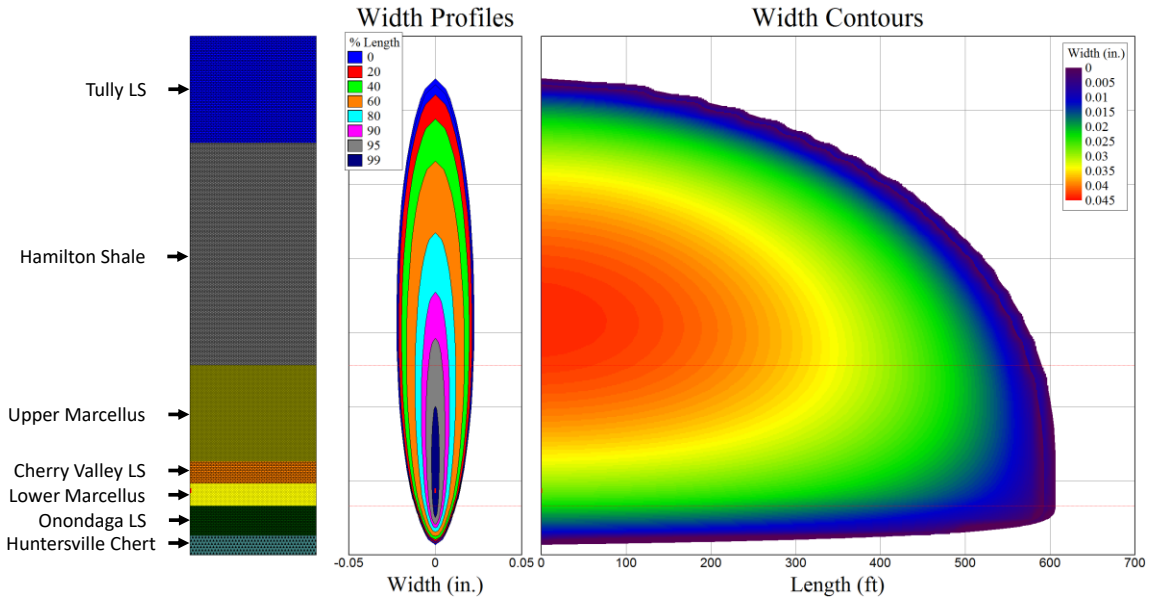

Figure 2.16. Primary Hydraulic Fracture Geometry for Stage 10 – MIP-5H

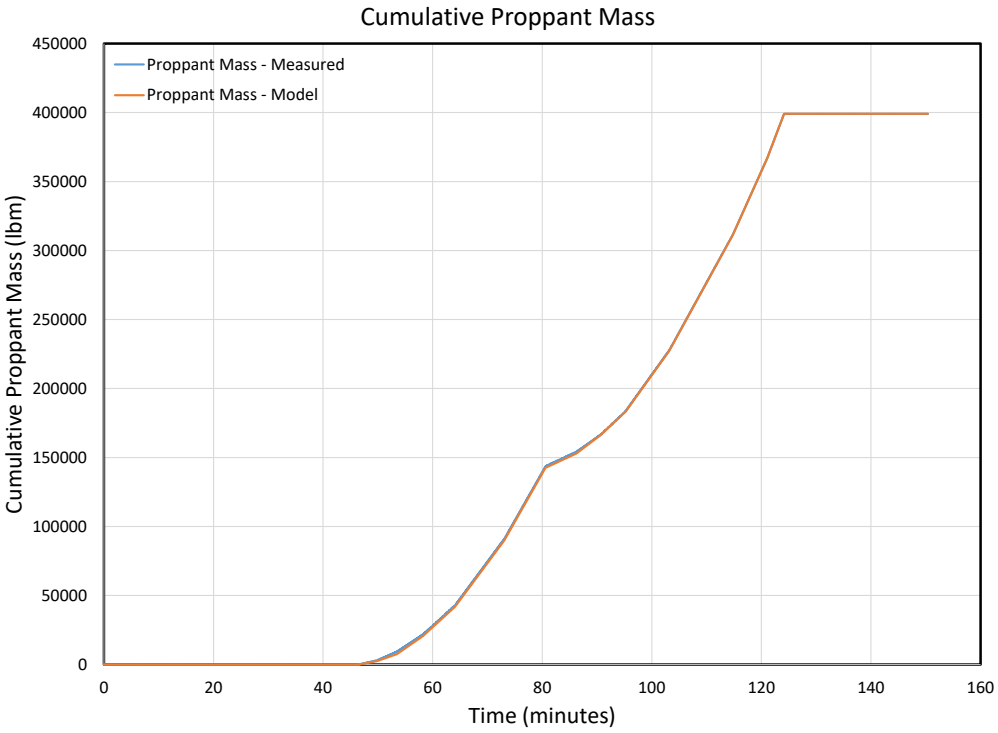

Figure 2.17. Cumulative Proppant Mass Injected for Stage 10 – MIP-5H

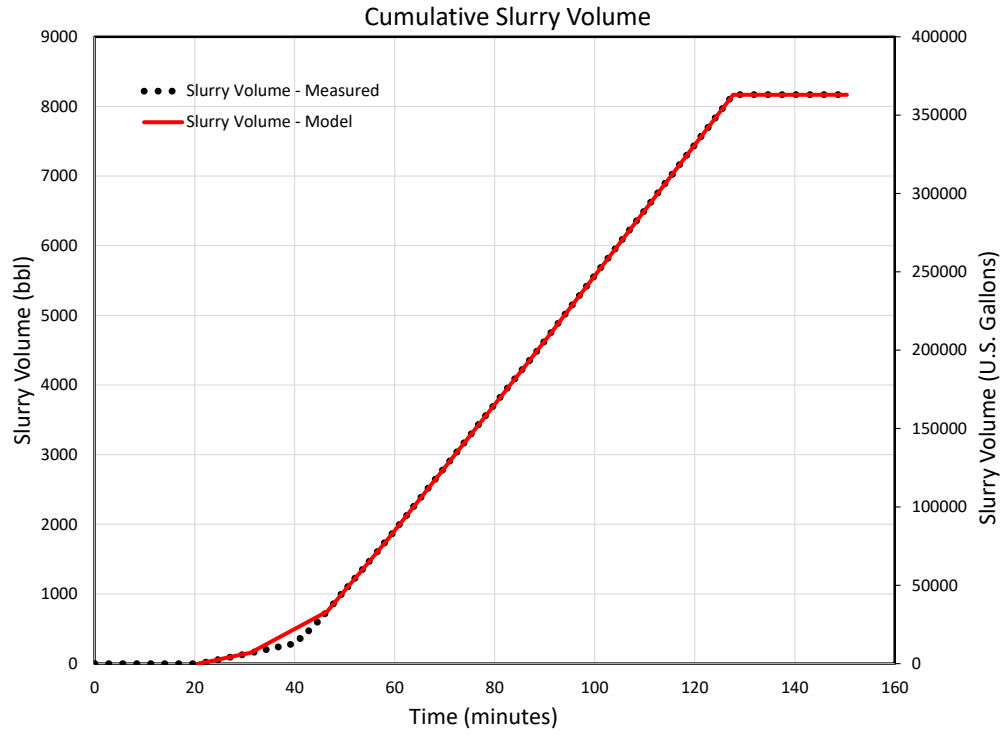

Figure 2.18. Cumulative Slurry Volume Injected for Stage 10 – MIP-5H

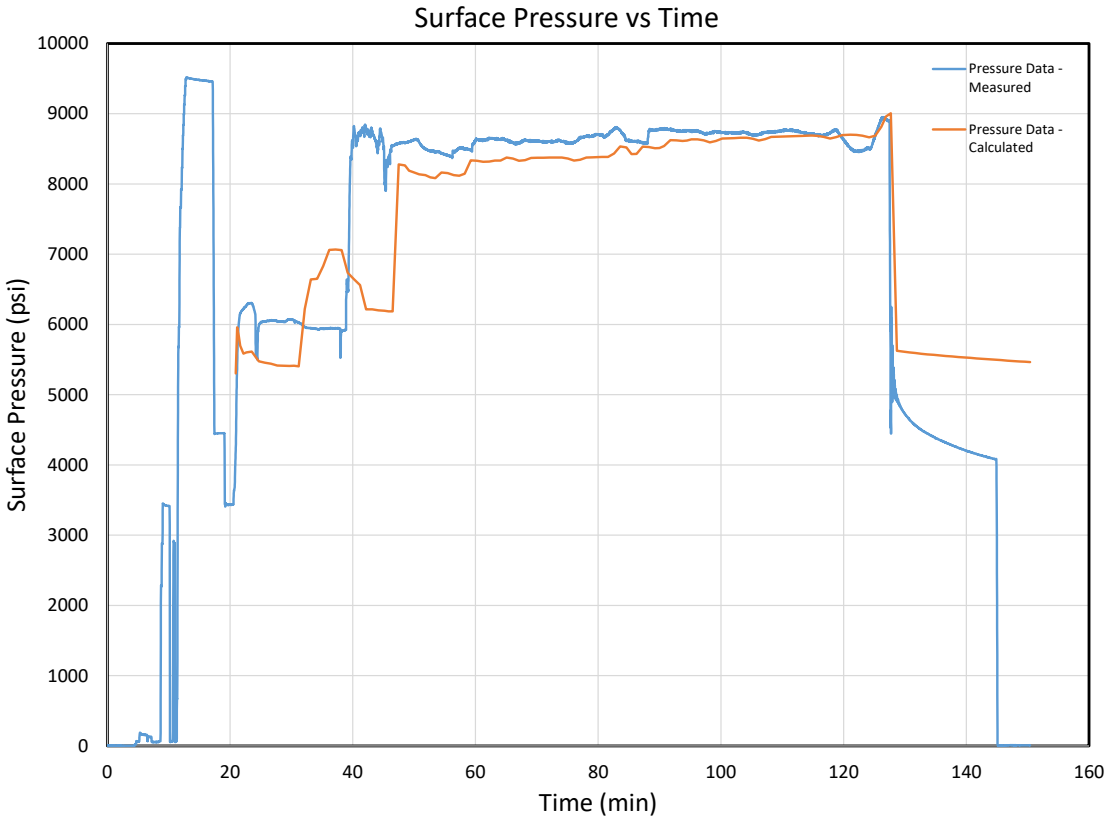

Figure 2.19. Surface Pressure versus Time for Stage 10 – MIP-5H

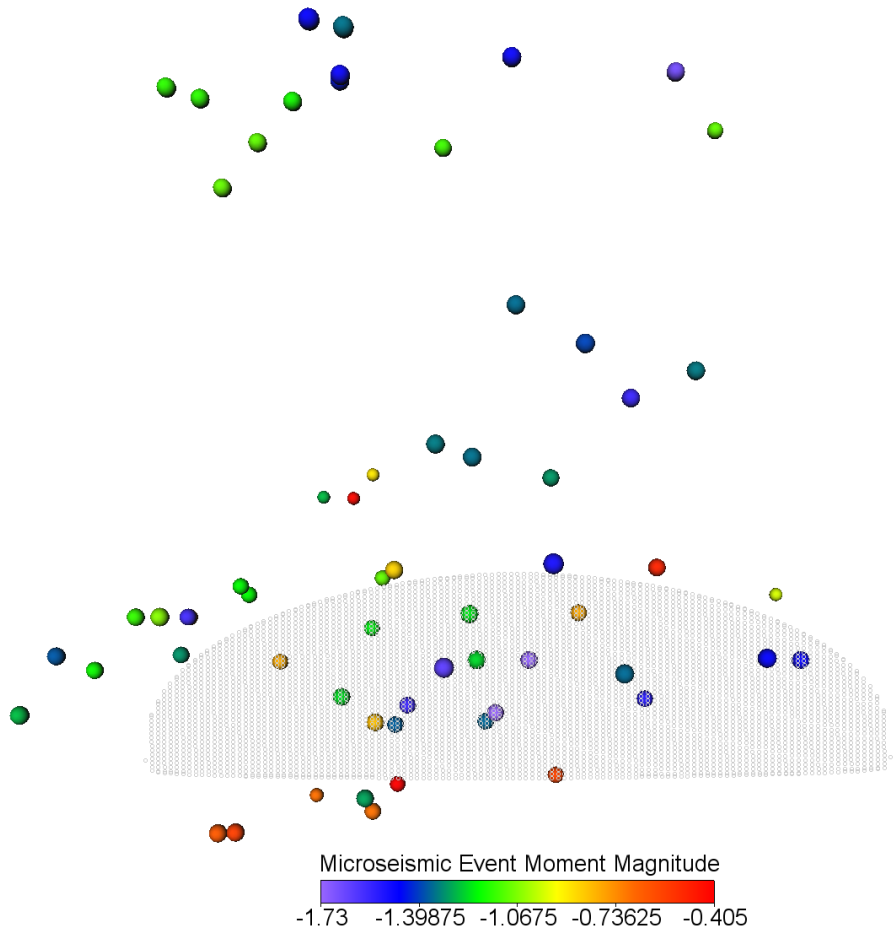

Figure 2.20. Side View of Calculated Primary Hydraulic Fracture and Measured Microseismic Events and Magnitudes for Stage 2 – MIP-5H

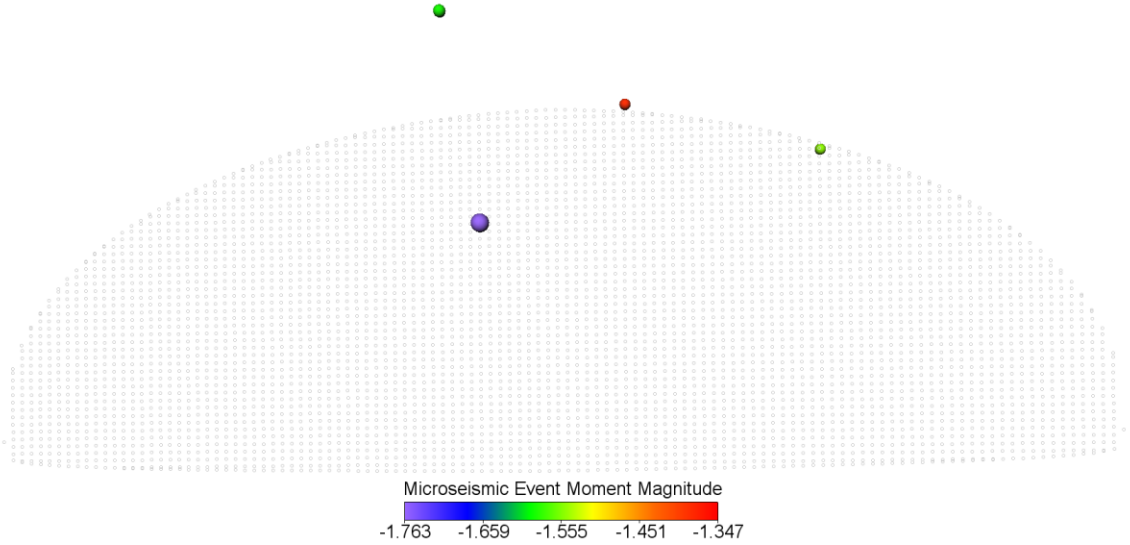

Figure 2.21. Side View of Calculated Primary Hydraulic Fracture and Measured Microseismic Events and Magnitudes for Stage 4 – MIP-5H

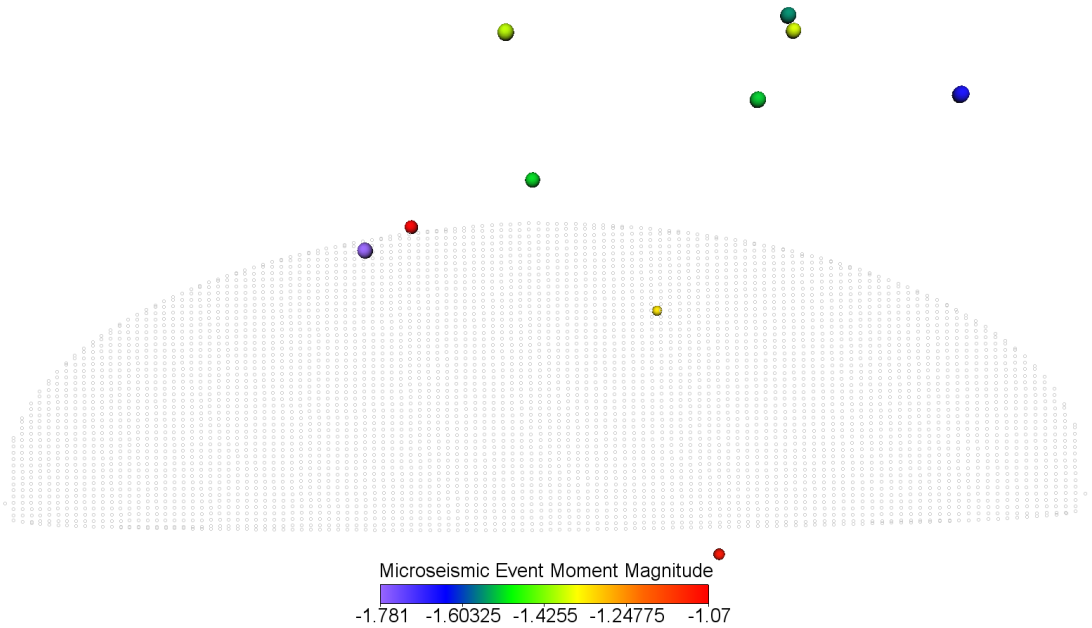

Figure 2.22. Side View of Calculated Primary Hydraulic Fracture and Measured Microseismic Events and Magnitudes for Stage 5 – MIP-5H

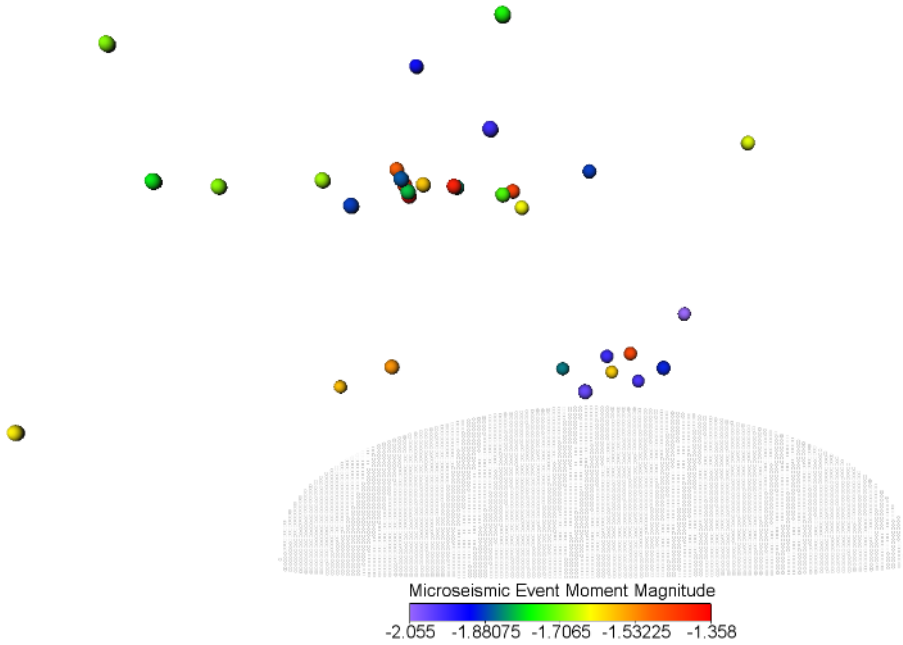

Figure 223. Side View of Calculated Primary Hydraulic Fracture and Measured Microseismic Events and Magnitudes for Stage 6 – MIP-5H

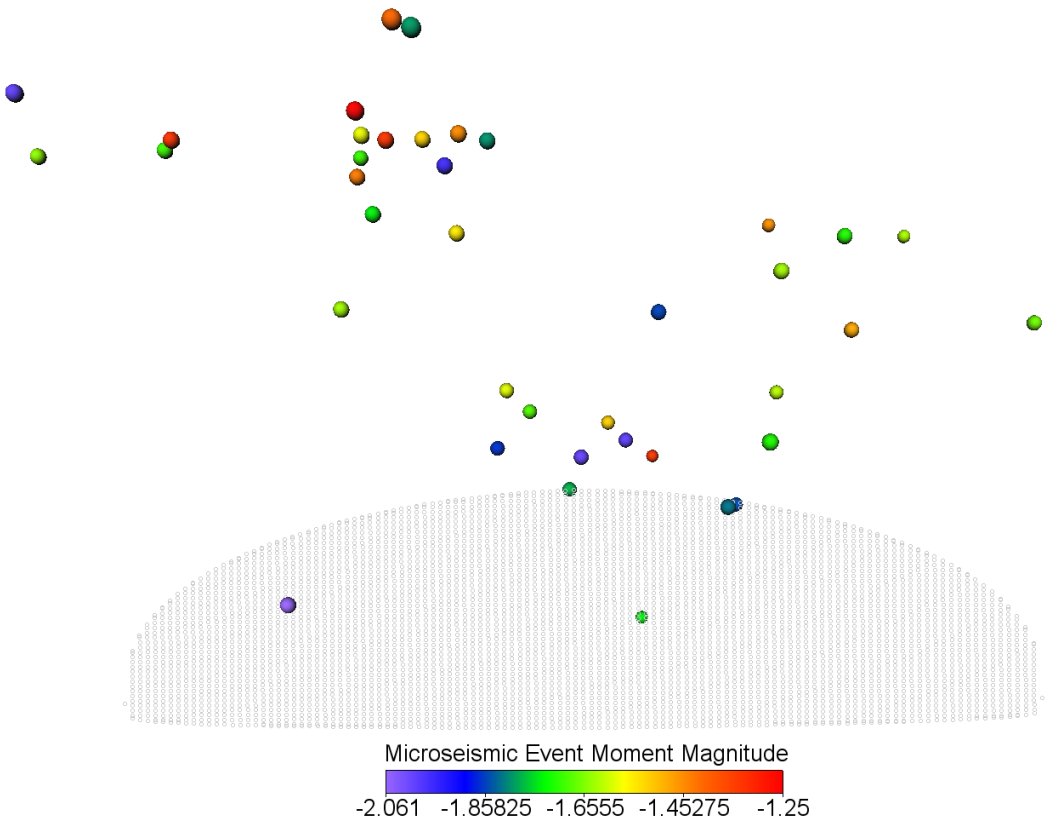

Figure 2.24. Side View of Calculated Primary Hydraulic Fracture and Measured Microseismic Events and Magnitudes for Stage 7 – MIP-5H

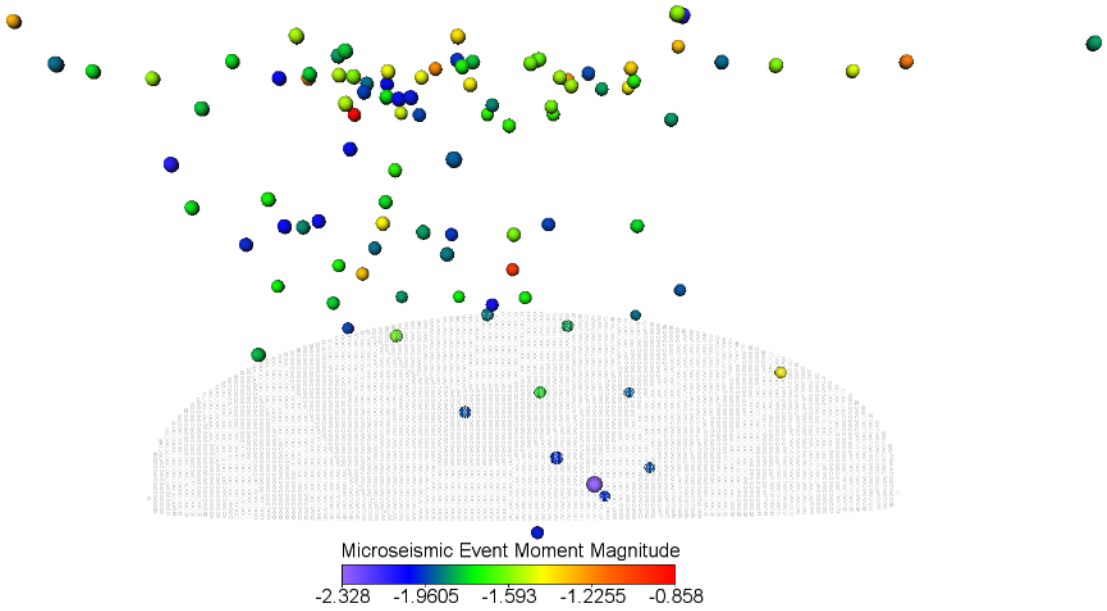

Figure 2.25. Side View of Calculated Primary Hydraulic Fracture and Measured Microseismic Events and Magnitudes for Stage 8 – MIP-5H

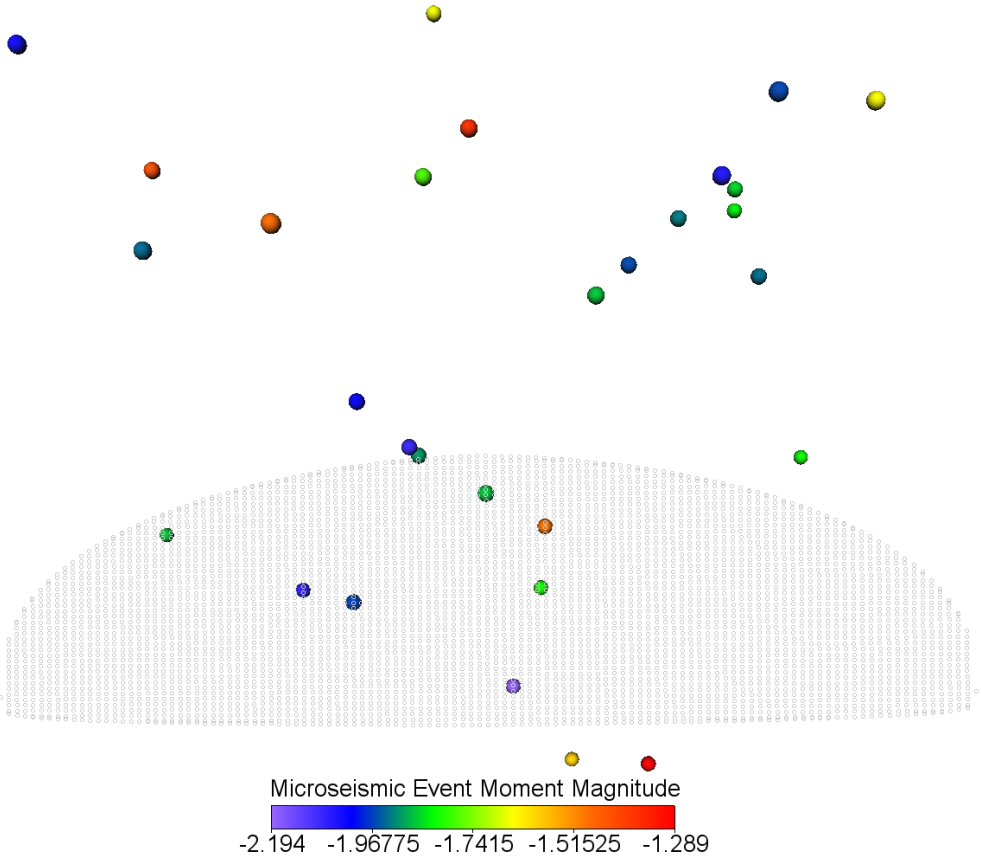

Figure 2.26. Side View of Calculated Primary Hydraulic Fracture and Measured Microseismic Events and Magnitudes for Stage 9 – MIP-5H

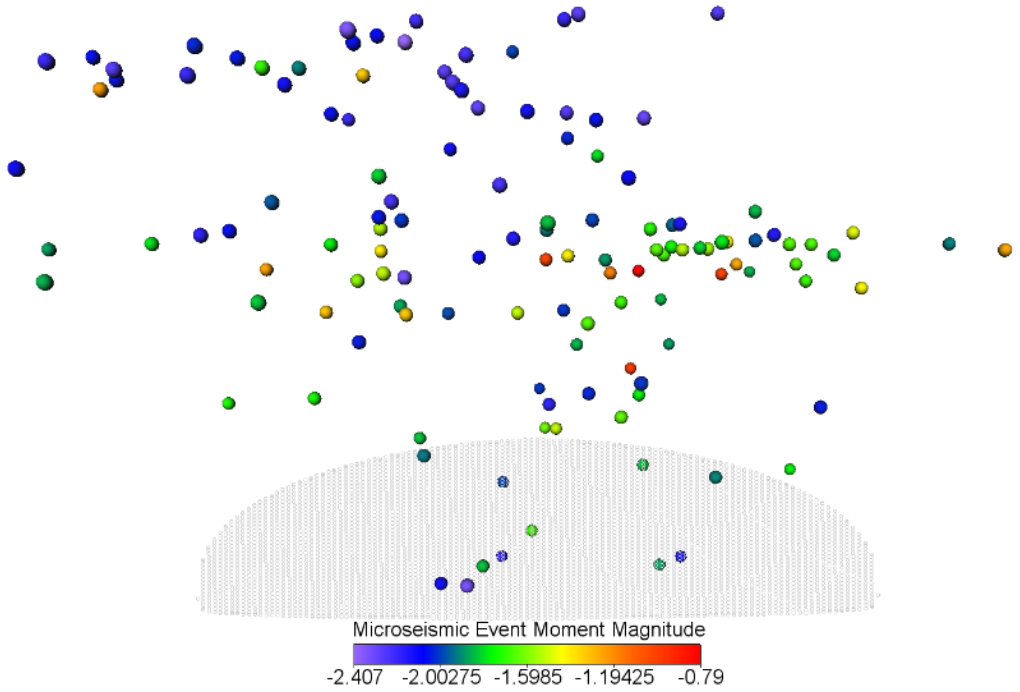

Figure 2.27. Side View of Calculated Primary Hydraulic Fracture and Measured Microseismic Events and Magnitudes for Stage 10 – MIP-5H

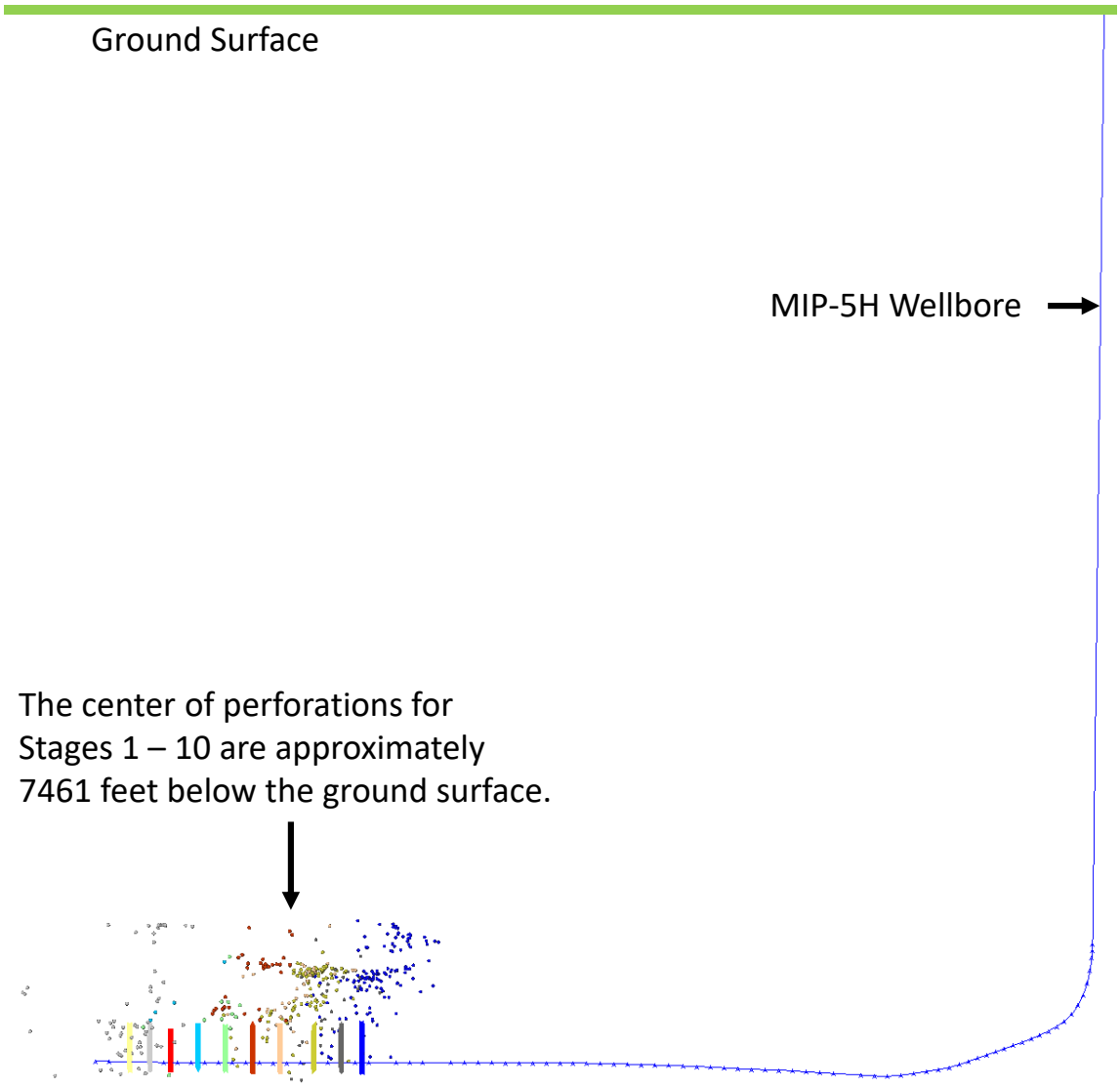

Figure 2.28. Overview of Calculated Primary Hydraulic Fracture Geometries, Available Measured Microseismic Events, and Entire Wellbore for Stage 1 through Stage 10 – MIP-5H

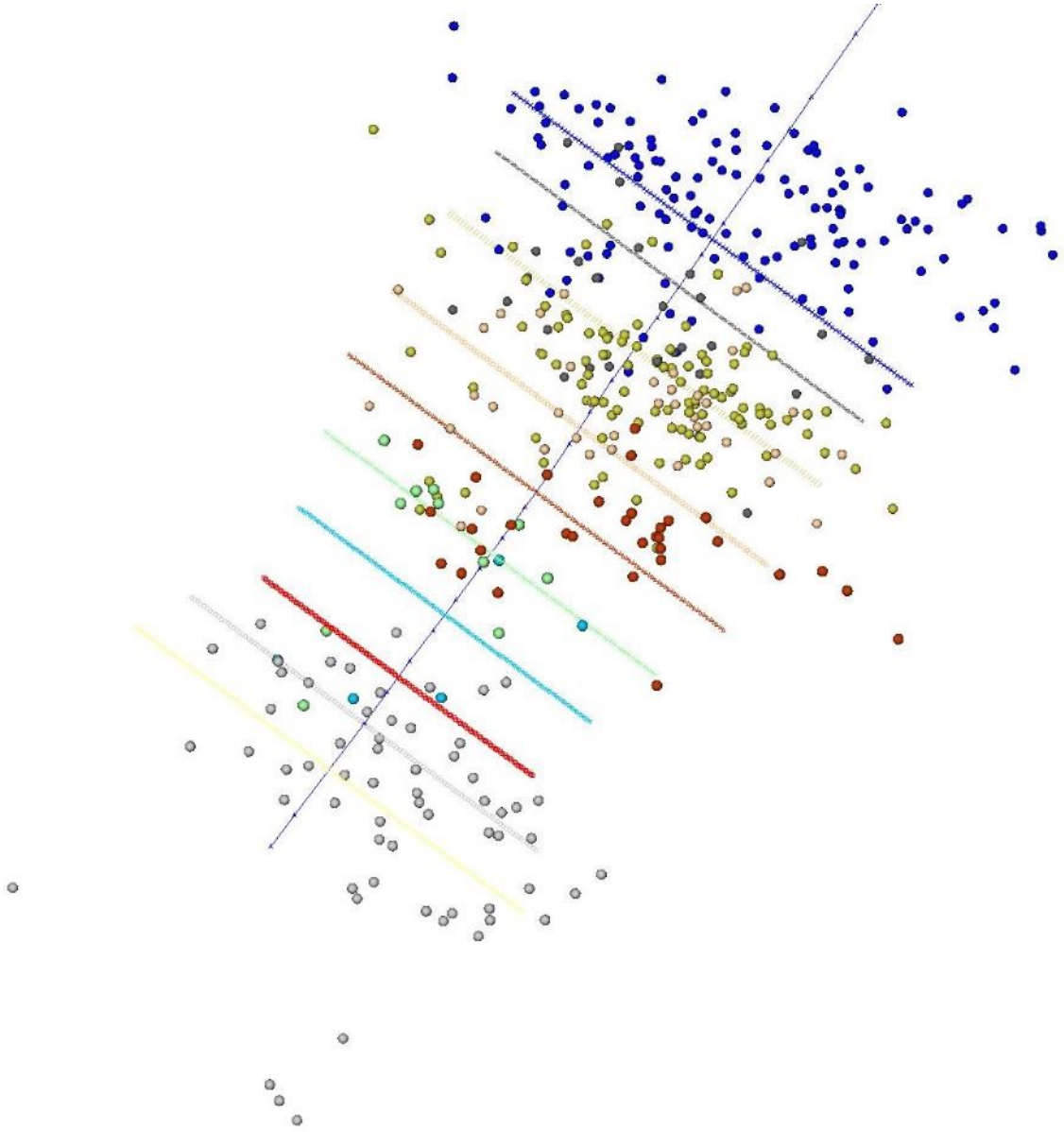

Figure 2.29 Events, and Nearby Wellbore for Stage 1 through Stage 10 – MIP-5H

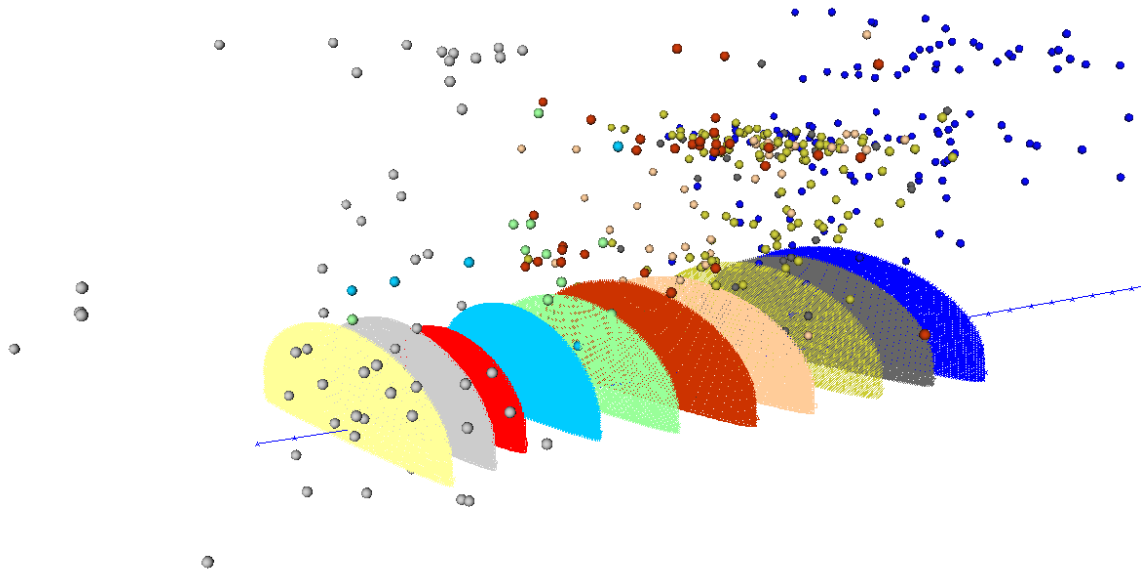

Figure 2.30. Orthogonal View of Calculated Primary Hydraulic Fracture Geometries, Available Measured Microseismic Events, and Nearby Wellbore for Stage 1 through Stage 10 – MIP-5H

Products

n/a

Plan for Next Quarter

Geomechanical

The modeling study will be continued to investigate additional stimulation stages at well MIP-5H through the use of available information on the hydraulic fracturing field parameters (fluid volumes, pumping rate, proppant schedule, and geophysical data). The analysis of microseismic data will be continued and a comparison of hydraulic fracture geometries will be made with available microseismic data.

Topic 3 – Deep Subsurface Rock, Fluids, & Gas

Approach

The main focus of the subsurface team led by Sharma this quarter was to analyze core, fluid and gas samples collected from the MSEEL site. Members of Sharma's lab group (Dr. Warrier and Mr. Wilson) and Dr. Hanson from Mouser's lab group continue to coordinate and supervise all sample collections. Samples were also distributed to the research team at OSU and NETL for analysis under different sub-tasks. Several talks and presentations were given at local and regional conferences /universities.

Results & Discussion

Sharma's Lab

This quarter's work focused primarily on determining changes in kerogen structure and bulk rock interactions and composition on interaction with fracturing fluids under simulated subsurface conditions.

To determine changes in kerogen structure on interaction with fracturing fluids, it is essential to characterize the structure of kerogen before any interaction.

Vikas Agrawal (Sharma PhD student) extracted and analyzed kerogen from upper and lower Marcellus Formation from 3 new wells (apart from MSEEL well analyzed before) namely BG-1, WV-7 and WV-6. The thermal maturity of the samples ranged from 0.8 VRo to 2.5 VRo. Using ^{13}C solid state NMR, aliphatic, aromatic and lattice structural parameters of the kerogen was determined.

The results indicate that the percentage of carbon chains such as mobile (freely rotating) and immobile alkyl without heteroatoms (with restricted rotation), and alkyl-substituted aromatic carbons decrease with increasing maturity indicating that these chains are more prone to thermal degradation. However, carbon chains such as O- substituted alkyl (ether), O_2 substituted alkyl (dioxy alkyl), amine, protonated aromatic carbons, O- substituted aromatic (phenol) and bridgehead aromatic carbons does not decrease directly with thermal maturity suggesting that these groups are either more refractory in nature. Using the stuctural parameters of kerogen, schematic models of the analyzed kerogen were also developed as shown in Figure 3.1 (Agrawal and Sharma, 2018).

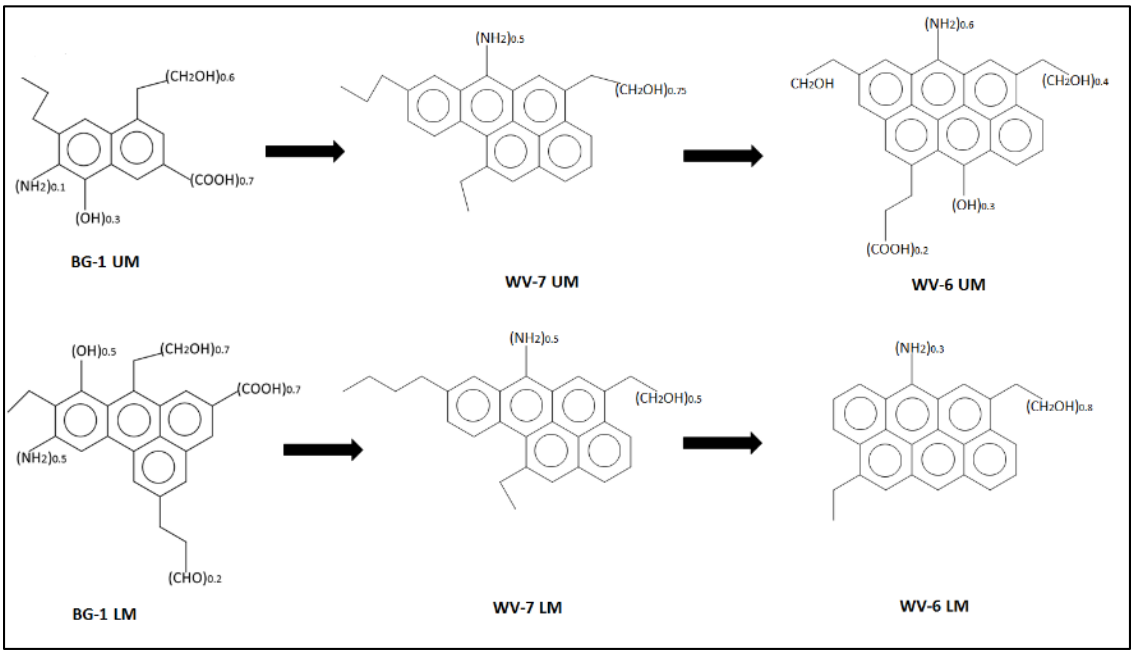

Figure 3.1. Schematic representation of transformation of a unit of kerogen cluster from low maturity BG-1 kerogen to higher maturity WV-7 kerogen to further higher maturity WV-6 kerogen. Each unit of kerogen cluster is formed using aliphatic, aromatic and lattice structural parameters a) upper Marcellus b) lower Marcellus. Values written in parentheses indicate the fraction of the particular functional group per unit of kerogen cluster. Other isomers of each kerogen unit are possible

Another MS student of Sharma, John Pilewski, carried out experiments using high P-T reactors to determine the chemical evolution of fracturing fluids on interaction with shales of different maturity (ranging from 0.8 VRo to 2.9 VRo) at reservoir conditions.

The results from the fluid analysis indicate a significant decrease in BTEX (benzene, toluene, xylenes) compounds (Figure 3.2) and total DOC (dissolved organic carbon) with increasing thermal maturity. These observations indicate adsorption of organic compounds in kerogen matrix with increasing thermal maturity. Further analysis will be conducted to determine the physical and chemical changes in kerogen structure of the shales used in this study.

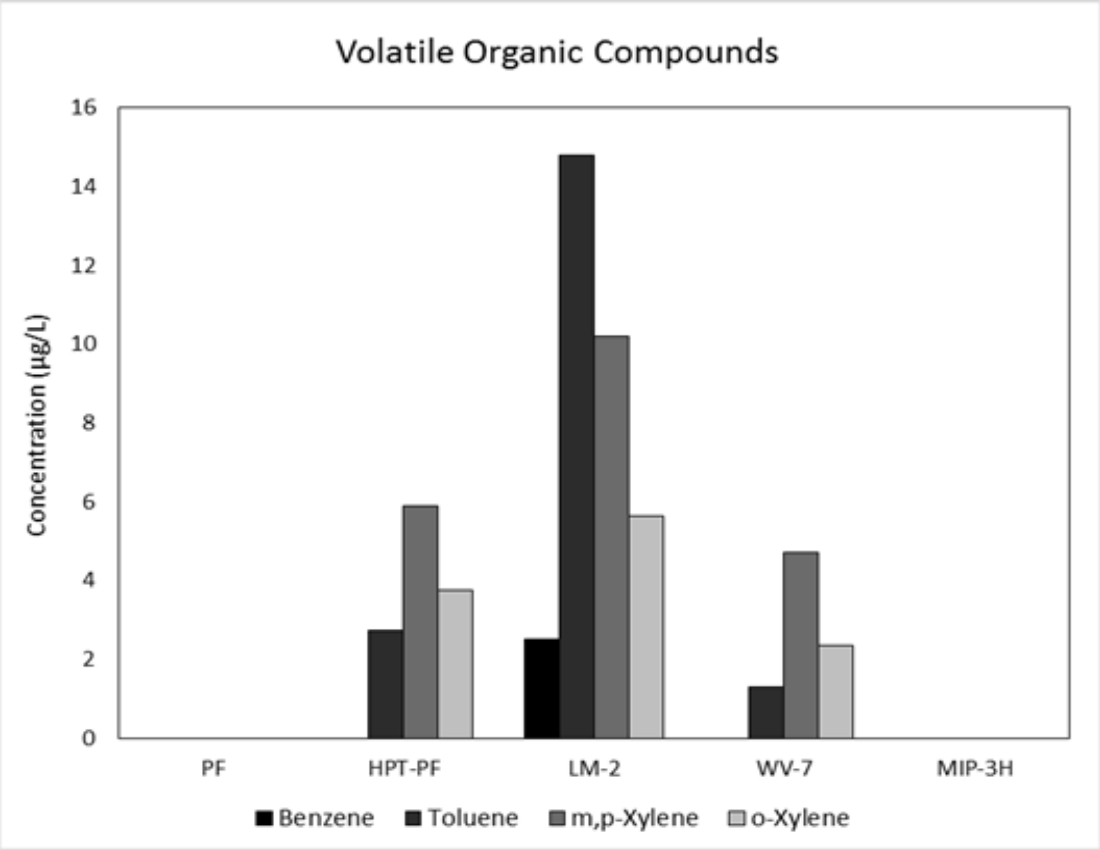

Figure 3.2. Concentration of BTEX compounds of fracturing fluid on interaction with different shale samples for 14 days. PF is fluid sample before interaction at room temperature and pressure. HPT-PF is the control fluid sample collected after it was kept for 14 days in the reactor at high P-T conditions. LM-2, WV-7 and MIP-3H are fluid collected after interaction with 3 different shales samples with thermal maturity 0.8 VRo, 1.4 VRo and 2.9 VRo respectively.

Wrighton's Lab (OSU)

All produced fluids submitted for 16S rRNA iTag sequencing have been received and analyzed. These data are being incorporated into multiple publications. Metagenomic sequencing for all produced fluids have been submitted. These data are being incorporated into multiple publications listed below.

Four manuscripts are in preparation/review from the Wrighton lab which incorporate MSEEL microbial data:

- *"*In vitro *interactions scaled to* in situ *conditions: microorganisms predict field scale biogeochemistry in hydraulically fractured shale."* Review comments have been

received from PNAS and we have been encouraged to submit a revised manuscript to PNAS. This research was led by a graduate student, Mikayla Borton, in the Wrighton lab.

- *"*Candidatus *Marcellius: a novel genus of Verrucomicrobia discovered in a fractured shale ecosystem."* To be submitted to Microbiome in May 2018. This research was led by a visiting post-doc, Sophie Nixon, in the Wrighton lab.
- *"Comparison of* Methanohalophilus *strains reveals adaptations to distinct environments."* Invited to submit to Frontiers in Microbiology special topic edition Geobiology in the Terrestrial Subsurface, to be submitted June 2018. An undergraduate researcher, Bridget O'Banion in the Wrighton lab, led this research.
- An invited review for Frontiers in Microbiology special topic edition Geobiology in the Terrestrial Subsurface, June 2018. This paper will focus on the coupling of laboratory experiments to field data analyses using shale as a model system. Kelly Wrighton is leading this work.

Wilkins Lab (OSU)

Effort in the Wilkins Group focused on preparation of two manuscripts.

1. Viruses control dominant bacteria colonizing the terrestrial deep biosphere after hydraulic fracturing. Rebecca A. Daly[1], Simon Roux[2], Mikayla A. Borton[3], David M. Morgan[4], Michael D. Johnston[4], Anne E. Booker[1], David W. Hoyt[5], Tea Meulia[6], Richard A. Wolfe[1], Andrea J. Hanson[7,8], Paula J. Mouser[7,8], Matthew B. Sullivan[1,7], Kelly C. Wrighton[1], and Michael J. Wilkins[1,4*] This is to be submitted to Nature Microbiology in the next week.

The deep terrestrial biosphere harbors a significant fraction of earth's biomass and remains understudied compared to other ecosystems. Deep biosphere life primarily consists of bacteria and archaea, yet knowledge of their co-occurring viruses is poor. Here we temporally catalogued viral diversity from five deep terrestrial subsurface locations (hydraulically fractured wells), examined virus-host interaction dynamics, and experimentally assessed metabolites from cell lysis to better understand viral roles in this ecosystem. We uncovered high viral diversity, rivaling that of peatland soil ecosystems, despite low host diversity. Many viral OTUs were predicted to infect *Halanaerobium*, the dominant microbe in these ecosystems. Examination of CRISPR-Cas spacers elucidated lineage-specific virus-host dynamics suggesting active *in situ* viral predation of *Halanaerobium*. These dynamics indicate an ongoing arms-race with repeated viral encounters and changing viral host range across temporally and geographically distinct shale formations. Laboratory experiments showed that prophage-induced *Halanaerobium* lysis releases intracellular metabolites that can sustain key fermentative metabolisms, supporting the persistence of microorganisms in this ecosystem. Together these findings suggest that diverse and active viral populations play critical roles in driving strain-level microbial community development and resource turnover within this deep terrestrial subsurface ecosystem.

2. Pressure stress drives physiological and metabolic shifts in dominant shale-colonizing *Halanaerobium*. Anne E. Booker[1], David W. Hoyt[2], Tea Meuli[3], Elizabeth Eder[2], Carrie D. Nicora[2], Mary S. Lipton[2], Michael J. Wilkins[1,4]

This manuscript is in development, and describes the observation that *Halanaerobium* (dominant microbial community member in produced fluids from MSEEL and other Appalachian Basin wells) is able to grow at pressures up to 7000 psi. Under these high-pressure conditions, the

microorganisms change their central metabolism, and generate more extracellular polymeric substances (EPS or 'slime') that causes biomass to clump together and potentially attach to surfaces. Such behavior has implications for permeability within the subsurface fracture network.

Mouser Lab (OSU)

Andrea Hanson (post-doc) finished up her position with Mouser in March 2018. Andrea has a draft of a paper summarizing lipids in rock cores and fluids that is currently being circulated with co-authors, to be submitted during the next quarter for peer review. The Cole Group was tasked to connect the rock and fluid compositions to the lipids detected. Sue's fluid chemistry for MIP 3H and the BSE and QEMSCAN imagery for Tully Limestone and Middle Marcellus are included in the paper.

The dramatic increase in energy extraction from hydrocarbon-bearing shales provides the opportunity to explore the microbiology of the deep terrestrial subsurface. Recent studies have established patterns of microbial community succession and metabolic potential in shale-derived saline produced fluids resulting from oil and gas extraction. However, the presence of indigenous microbial biomass and the physiological details of cellular-level adaptation in fractured shales are not well defined. Specifically, little is known about the intact polar lipid (IPL) composition of microbial membranes, structures that play a crucial role in osmoprotection, nutrient acquisition, and energetic balance under harsh environmental conditions.

The team characterized microbial IPLs in rock cores and produced fluids collected from a Marcellus Shale natural gas well in the Appalachian Basin using liquid chromatography coupled to tandem mass spectrometry (LC-MS/MS). Analysis detected remnant archaeal glycerol dialkyl glycerol tetraethers structures in Tully limestone (depth 7200'), and intact mono- and diglycosyl archaeol within Marcellus Shale (depth 7509'), representing pre-energy extraction chemical signs of microbial life more than 2 km below ground surface. In the highly saline produced fluids collected over 490 days, the team observed a predominance of anionic and glycosylated IPL head groups not predicted by metagenomic tools. Combined, these findings advance the understanding of microbial life in undisturbed deep shale and the dynamic physiological strategies used to survive the high salinity shale environment following energy development.

Morgan Volker completed her candidacy in December 2017 and has been wading through LC-qTOF MS data generated during a trip to Colorado State University last November. Morgan has two papers in preparation related to MSEEL; these manuscripts will be submitted for peer review in the next quarter.

Cole's Lab (OSU)

Analysis of fluid samples from the MIP 3H and 5H wells continues. The final samples from Dec 2017 were analyzed for anions by ion chromatography. All samples (including those previously analyzed) were prepared for ICP-OES and ICP-MS analysis for major and trace analysis, and analyzed on the ICP-OES for major cations and selected trace metals. There was good agreement between the charge balance for the anion and cation analysis, most within 5%, and good agreement between replicate analyses.

The total dissolved salt concentrations in the 3H brines increases from approximately 50 g/L in the early stages of flowback to approximately 150 g/L. TDS in the 5H well is more variable, reaching a high of approximately 250 g/L and then decreasing to ~ 80 g/L in the last sample collected. The brine chemistry is dominated by Na-Ca-Cl, however the brine composition changes over time, with increasing Sr/Ca and Ba/Ca ratios.

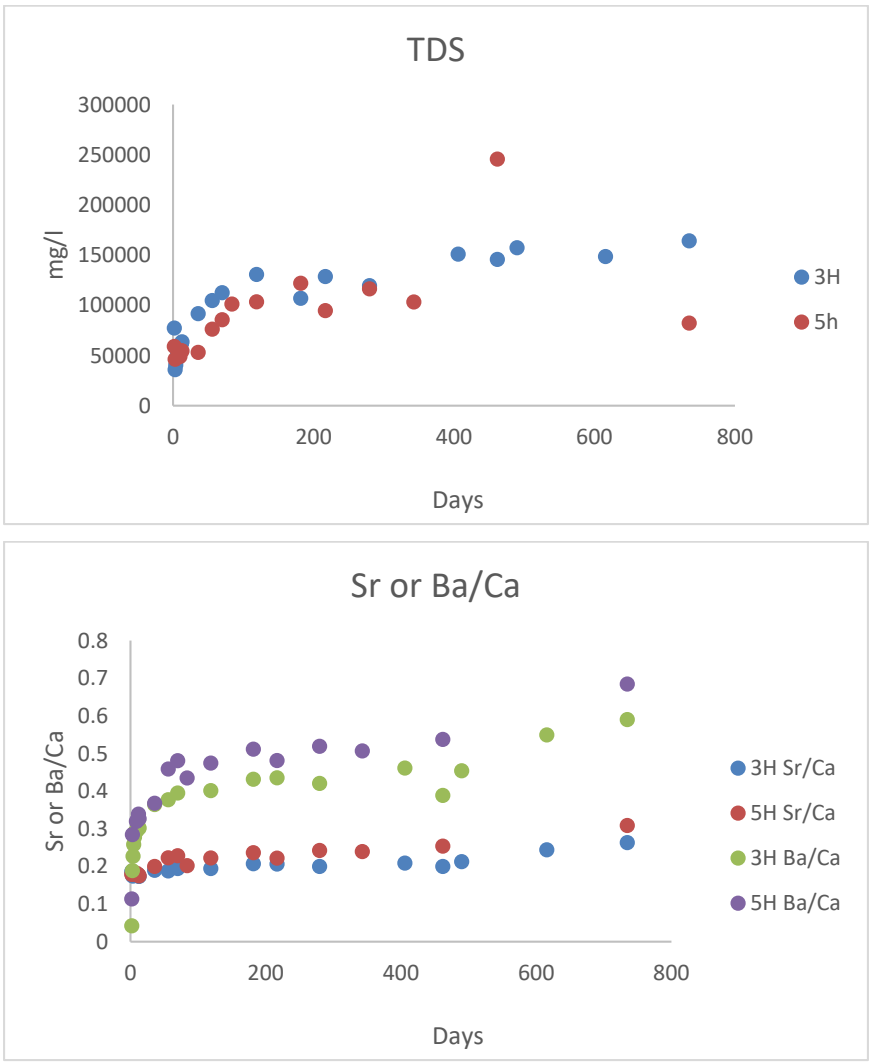

Figure 3.3. TDS Concentrations vs. Time

Products

Sharma's Lab

Agrawal ,V. and Sharma, S. 2018. Molecular Characterization of Kerogen from Marcellus Shale and its Implications for determining sources of organic matter, hydrocarbon potential and thermal maturity. Fuel (*in press*)

Agrawal, V. and Sharma, S. 2018. Testing utility of organogeochemical proxies to assess sources of organic matter, paleoredox conditions and thermal maturity in mature Marcellus Shale. Frontiers in Energy Research (*in review*)

Wrighton's Lab

"*Top-down and bottom-up controls on* Halanaerobium *populations in the deep biosphere*." Poster presentation at the Department of Energy's Joint Genome Institute 'Genomics of Energy and Environment Meeting', San Francisco, CA, March 2018. A researcher, Rebecca Daly, in the Wrighton lab, led this work.

Mouser's Lab

Luek J, Hari, M, Schmitt-Kopplin P, **Mouser PJ,** Gonsior M. (2018). Temporal Dynamics of Halogenated Organic Compounds in Marcellus Shale Flowback. *Water Research*, 136, 200-206. doi.org/10.1016/j.watres.2017.07.012.

Invited Seminars:

University of Maine, Department of Biology and Ecology. Biodegradation of Organic Compounds in the Hydraulically Fractured Shale Ecosystem, 2/2018.

Abstracts/Professional Presentations:

Mouser PJ**,** Heyob KM, Blotevogel J, Lenhart JJ, Borch T (2018). Pathways and Mechanisms for Natural Attenuation of Nonionic Surfactants in Hydraulic Fracturing Fluids if Released to Agricultural Soil and Groundwater. ACS annual conference, New Orleans, LA, Mar 19-22, 2018.

Hanson AJ, Lipp JS, Hinrich K-U, Mouser PJ (2018). Microbial lipid biomarkers in a Marcellus Shale natural gas well: From remnant molecules to adapted communities. ACS annual conference, New Orleans, LA, Mar 19-22, 2018

Plan for Next Quarter

The lab continues to work with students in Sharma's group (Akondi) to wrap up two manuscripts in review/preparation related to diglyceride fatty acid signatures in MSEEL rock cores.

Topic 4 – Environmental Monitoring – Surface Water & Sludge

Approach

The Marcellus Shale Energy and Environment Laboratory (MSEEL) is the first comprehensive field study coupling same site environmental baseline, completion and production monitoring with environmental outcomes. Almost two years into the post completion part of the program, the water and solid waste component of MSEEL has continued to systematically sample flowback and produced water volumes. During year one of the study, hydraulic fracturing fluid, flowback, produced water, drilling muds and drill cuttings were characterized by their inorganic, organic and radio chemistries. In addition, surface water in the nearby Monongahela River was monitored upstream and downstream of the MSEEL drill pad. Toxicity testing per EPA method 1311 (TCLP) was conducted on drill cuttings in both the vertical and horizontal (Marcellus) sections to evaluate their toxicity potential.

Previous findings

The MSEEL wells used green completion strategy including a synthetic based drilling fluid (Bio-Base 365). All drill cutting samples fell below TCLP thresholds for organic and inorganic components indicating that they are non-hazardous per the Resource Conservation and Recovery Act. Maximum specific isotopic activity in drill cuttings was recorded for ^{40} K which was 28.32 pCi/g. Gross alpha accounted for the highest reading at 60 pCi/g. The maximum combined radium isotope values was 10.85 pCi/g. These radioactivity levels are within the background range for the region.

The composition of the hydraulic fracturing (HF) fluids in both wells was similar to the makeup water which was drawn from the Monongahela River. Its chemistry was typical of Monongahela River water. This is true of inorganics, organics and radio chemicals. Organic surrogate recoveries were in the range of 90 to 104% indicating good quality control at the analytical laboratory. There was no evidence that Monongahela River quality was influenced by well development, completion or production at the MSEEL site.

Produced water is severely contaminated indicating care in handling. Concentrations of all parameters increased through the flowback/produced water cycle. $^{226+228}$Ra reached 20,000 pCi/L at post completion day 251 indicating an important trend that will be carefully assessed in ongoing monitoring.

Task 4a.1-Surface Environmental-Water and Waste.

Methods

Table 4.1 summarizes the produced water sampling schedule for the quarter. Produced water samples were taken at the upstream end of each well's separator.

Table 4.1. Sampling schedule for the quarter.

	Freshwater		Aqueous/Solids: drilling/completion/production								
	Mon River	Ground water	HF fluid makeup	HF fluids	flowback/ produced	drilling fluids	drilling cuttings/ muds	total aqueous	total solids	Sampling Dates	Sampling Notes
Sampling Stations											
Flowback @ 105 weeks - 3H					1			1		12/20/2017	one sample 3H
Flowback @ 105 weeks - 5H					1			1		12/20/2017	one sample 5H
Flowback @ 313 weeks - 4H					0			0		12/20/2017	4H offline
Flowback @ 313 weeks - 6H					0			0		12/20/2017	6H offline
Flowback @ 111 weeks - 3H					1			1		1/22/2018	one sample 3H
Flowback @ 111 weeks - 5H					1			1		1/22/2018	one sample 5H
Flowback @ 318 weeks - 4H					1			1		1/22/2018	one sample 4H
Flowback @ 318 weeks - 6H					0			0		1/22/2018	6H offline
Flowback @ 115 weeks - 3H					1			1		2/23/2018	one sample 3H
Flowback @ 115 weeks - 5H					1			1		2/23/2018	one sample 5H
Flowback @ 322 weeks - 4H					1			1		2/23/2018	one sample 4H
Flowback @ 322 weeks - 6H					0			0		2/23/2018	6H offline

Analytical parameters

Analytical parameters analyzed for samples flowback produced water (FPW) collected are listed in Table 4.2.

Table 4.2. Aqueous analytical parameters for FPW analyzed.

Aqueous chemistry parameters - HF fluids and FPW***						
Inorganics					Organics	Radionuclides
	Anions	Cations*				
pH	Br	~~Ag~~	Mg		Benzene	α
TDS	Cl	Al	Mn		Toluene	β
TSS	SO_4	As	Na		Ethylbenzene	^{40}K
Conductance	sulfides	Ba	Ni		Total xylene	^{226}Ra
Alkalinity	nitrate	Ca	Pb		m,p-xylene	^{228}Ra
Bicarbonate	nitrite	Cr	Se		o-xylene	
Carbonate		Fe	Sr		MBAS	
TP		K and Li	Zn		O&G	

Results & Discussion

Produced water volume trends in wells MIP 3,5H and MIP 4,6H

NNE's water production logs were used to estimate produced water volumes. While water production rates were similar in the first two months post completion, cumulative water production rates soon diverged yielding very different curves for each well (figure 4.1). It is noted that the older wells (4H, 6H) were shut in between 12 Dec 15 and 17 Oct 16, an interval of 315 days.

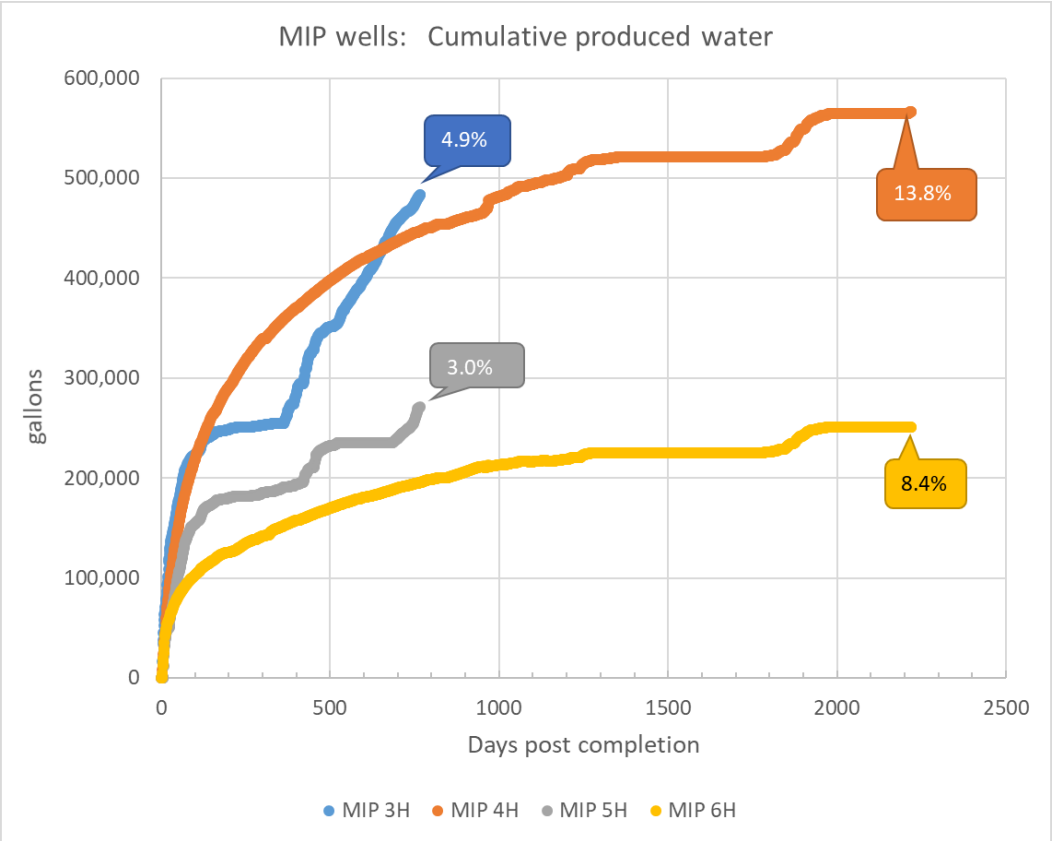

Figure 4.2. Cumulative water production at the four MSEEL wells.

The proportion of hydrofrac fluid returned as produced water, even after 2318 days (~6.5 years) was only 13.8% at MIP 4H and 8.4% at MIP 6H (table 4.3). The reason for the variation among wells both respect to cumulative and proportional produced water returns remains an unanswered question.

Table 4.3. Produced water volumes relative to injected HF fluid for each MSEEL well.

	days post	cumulative produced water		HF injected		water/gas
	completion	gal	% injected	gal	m^3	bbl/MMCF
MIP 3H	865	511,724	4.9%	10,404,198	39,380	4.18
MIP 5H	866	292,900	3.0%	9,687,888	36,669	3.75
MIP 4H	2318	576,009	13.8%	4,160,982	15,749	4.44
MIP 6H	2318	255,697	8.4%	3,042,396	11,515	4.00

Trends in produced water chemistry

Major ions

While makeup water was characterized by low TDS (total dissolved solids) and a dominance of calcium and sulfate ions, produced water from initial flowback is essentially a sodium/calcium chloride water (Figure 4.1). Other than slight increases in the proportion of barium and strontium, the ionic composition of produced changed very little through 806 days post completion.

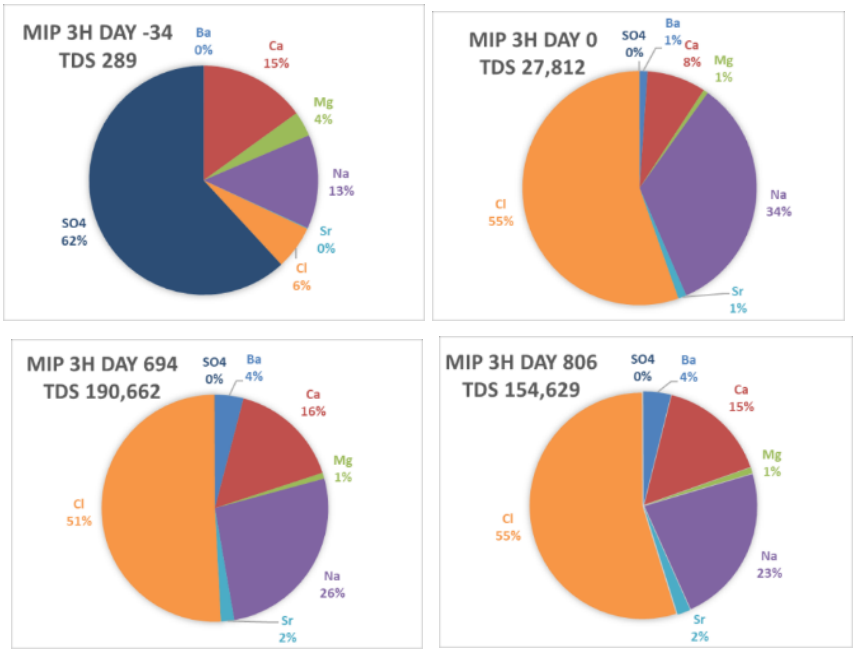

Figure 4.2. Changes in major ion concentrations in produced water from well MIP 3H. From left to right the charts represent makeup water from the Monongahela River, produced water on the first day of flowback and produced water on the 806th day post completion.

While TDS increased rapidly over the initial 90 days post completion values had been consistently between 100,000 and 150,000 mg/L through day 806 and have since continued on an upward trend, increasing to around 190,000 mg/L for 3H (figure 4.2). The older 4H and 6H

wells offer insight into the longer term TDS trend. Those wells only came back on line during this quarter after a shut in period of 315 days and those results vary but they are much lower than the current values for wells MIP 3H and 5H.

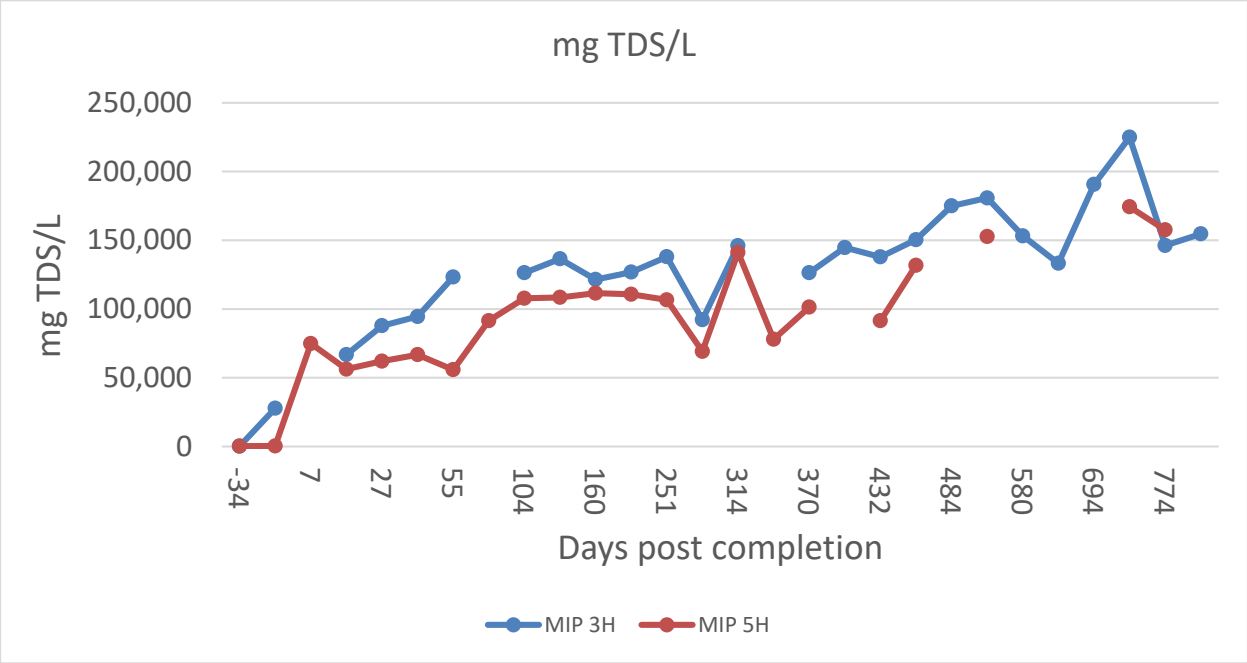

Figure 4.3. Changes in produced water TDS sdc (sum of dissolved constituents) through the first 806 days post completion (3,5H).

Water soluble organics

The water soluble aromatic compounds in produced water: benzene, toluene, ethylbenzene and xylene were never high. With two exceptions at post completion day 321 and 694, benzene has remained below 30 µg/L (figure 4.3) (the team is awaiting confirmation from the analytical lab for this reported value of 41 µg/L for day 694). Apart from the spikes, this seems to be a characteristic of dry gas geologic units. After five years, benzene has declined below the drinking water standard of 5 µg/L.

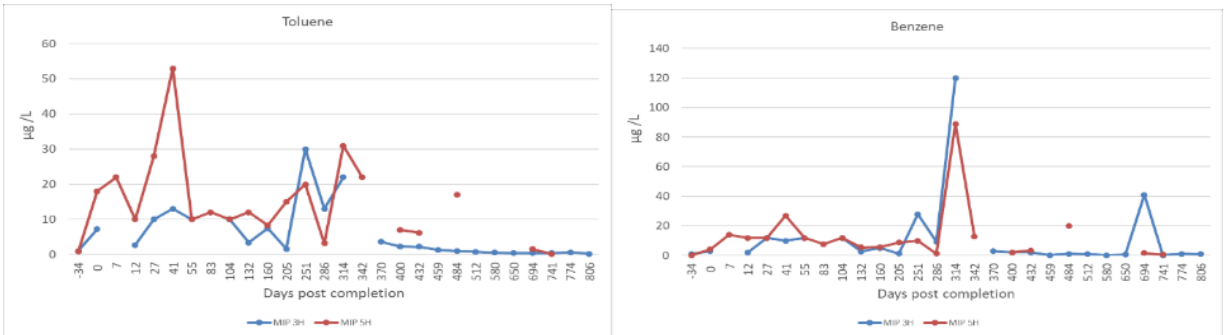

Figure 4.4. Changes in benzene and toluene concentrations. The figure shows data from well both 3H and 5H.

Radium isotopes

Radioactivity in produced water

Radium concentrations generally increased over the 806 days post completion at wells MIP 3H and 5H. Maximum levels of the radium isotopes reached about 20,000 pCi/L at the unchoked 3H well and about half that amount at 5H (figure 4.4).

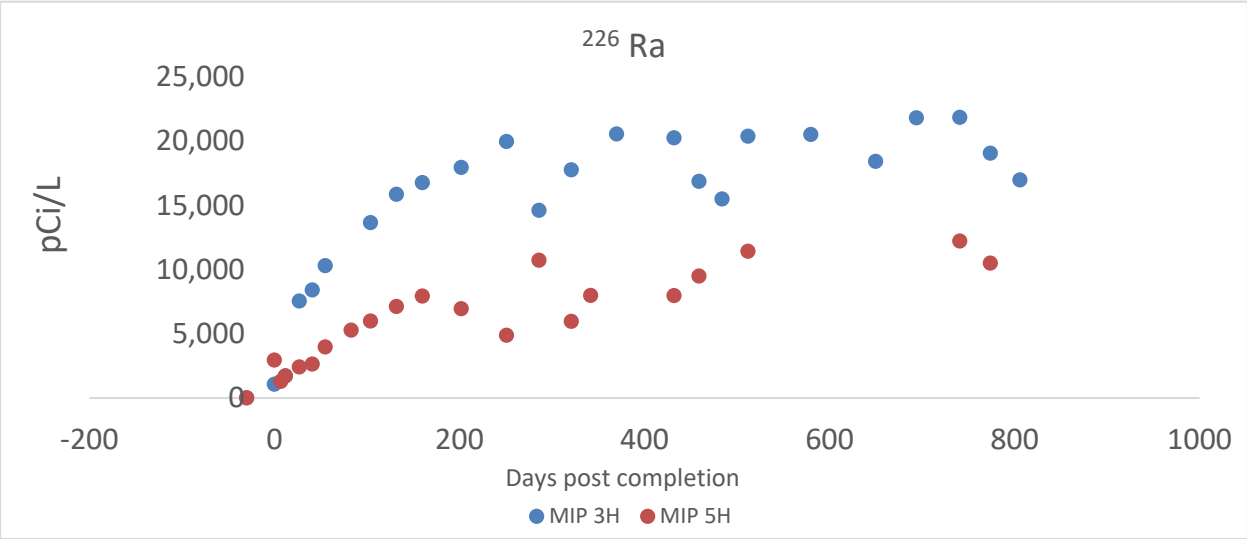

Figure 4.5. The radium isotopes are plotted against days post well completion. Well 5H was choked periodically. It produced less water and lower concentrations of radium.

Radium concentrations at wells 4H and 6H were below 9,000 pCi/L during all sampling periods. Both wells were choked at day 1963. Well 4H was reopened at day 2225, radium was 58 pCi/L on the first sampling after the reopening and 3719 pCi/L at day 2257, a month later (figure 4.5).

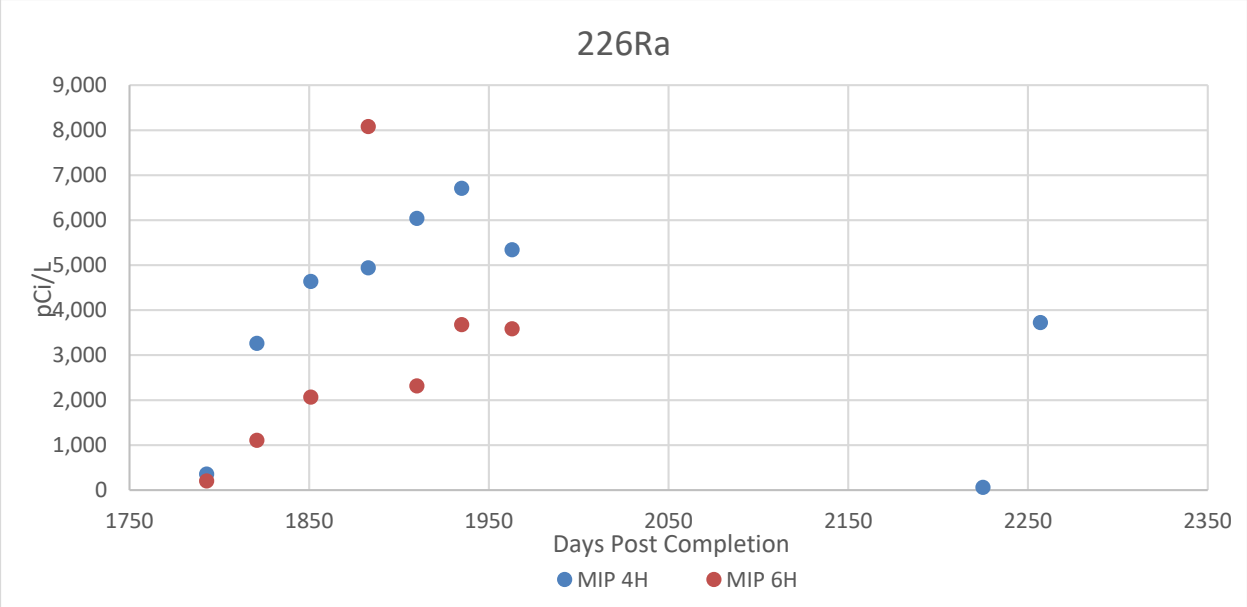

Figure 4.6. The radium isotopes are plotted against days post well completion. Well 4H and 6H were choked at day 1963. At day 2225, 4H was reopened showing a value of 58 pCi/L.

The radiochemical concentrations were determined by Pace Analytical in Greensburg PA, a state certified analytical lab. Figure 6 shows the relationship between gross alpha and ^{226}Ra. The relationship between alpha and ^{226}Ra is clear but the correlation coefficients show much more variance in the alpha readings. So, individual values can diverge to a far greater extent than the modelled values. Earlier studies e.g. Ziemkiewicz and He 2015 often relied on samples taken from several wells over short time spans so the apparent differences between alpha and, individual isotope concentrations may well be analytical artifact. The MDCs and uncertainty levels reported by the lab indicated that both the alpha and radium levels were within ranges that would be considered reliable. This may illustrate the limitations of survey level parameters such as gross alpha.

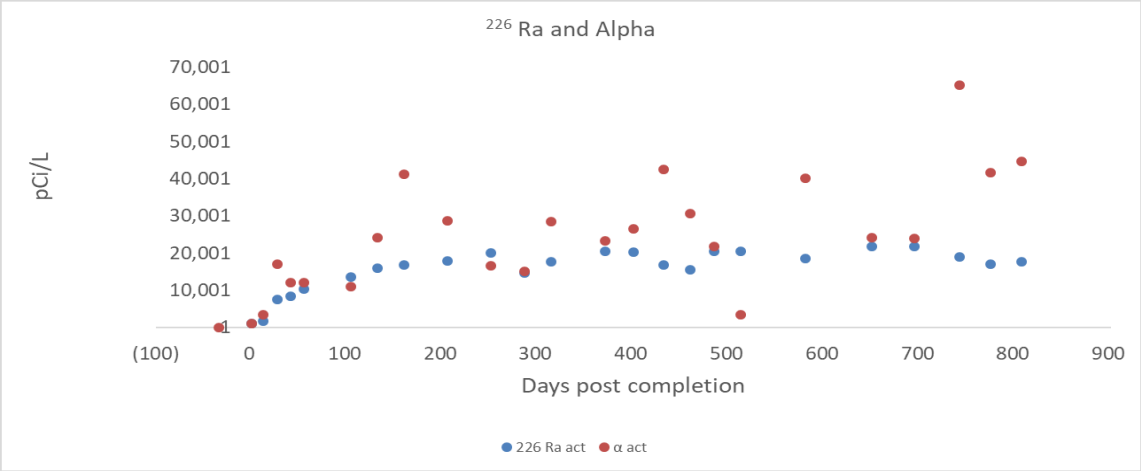

Figure 4.7. The relationship between gross alpha and ^{226}Ra as a function of time post completion.

Task 4.a.2. What is the toxicity, chemistry and radiochemistry of produced water precipitates?

Samples of tank bottom waste have not been able to be obtained through our partners at Northeast Natural Energy.

Products

Presented "Marcellus Shale Energy and Environmental Laboratory: Water and Waste" for Independent Oil and Gas Association, Charleston WV.

Plan for Next Quarter

The team will continue to sample and analyze flowback/produced water (FPW) from MIP 3H, 4H, 5H and 6H if they are online.

References

Ziemkiewicz, P.F. and He, Y.T. 2015. Evolution of water chemistry during Marcellus shale gas development: A case study in West Virginia. Chemosphere 134:224-231.

Topic 5 – Environmental Monitoring: Air & Vehicular

Approach

The research team from the Mechanical and Aerospace Engineering Department continue to focus on understanding the temporal variations in methane emissions from an actively producing shale well site. Data in the last quarterly report that was up to date regarding the quarterly audits. During this quarter, the system required systematic recalibration so that the team was unable to perform an audit in the March timeframe. The next audit is targeted for early May.

This quarter, the team focused on obtaining and implementing new equipment necessary to examine methane emissions using indirect methods or for geospatial monitoring around sites. Previously, the mobile system used the Los Gatos Research's Ultraportable Greenhouse Gas Analyzer for accurate methane concentration (the key component of our Full Flow Sampler). However, this approach limits methane measurement rates to 1 Hz. In addition, the closed path system induces sampling delay and diffusion. To overcome, the team has obtained a Li-COR LI7700 open path methane analyzer. This analyzer is capable of reporting methane concentration from 0-50 ppm at a rate of up to 40 Hz.

The next major upgrade was on the ultra-sonic anemometer. The team previously used a Gil Windsonic, which only reported data at 4 Hz. They have since obtained a Gil Windmaster Pro, which can output data up to 20Hz. In addition, the old anemometer was only a 2-axis while the new is a 3-axis, which enables vertical measurements.

Finally, the previous GPS system was only capable of 1Hz data and the team has now obtained a Reyax GPS that reports position data at up to 10Hz and includes a magnetometer-based compass. The previously used Li-COR solar sensor remains unchanged and ambient conditions will be monitored with an Omega ibthx – which provides additional slow speed averages of barometric pressure, relative humidity, and temperature. The focus is currently on implementing these new data acquisition devices within CAFEE's proprietary data logging software. The goal is for all new components to be recorded at 10Hz or 10 times faster than the old system. This should enable accurate mobile monitoring and geospatial mapping, which can later be used for quantification estimates using Gaussian Dispersion or Eddy-Covariance Flux measurements. Work is currently nearing the end of system integration. Brief details are presented below.

Results & Discussion

Figures 5.1 shows the newly purchased Li-COR LI7700 (left) and Windmaster Pro (right), respectively.

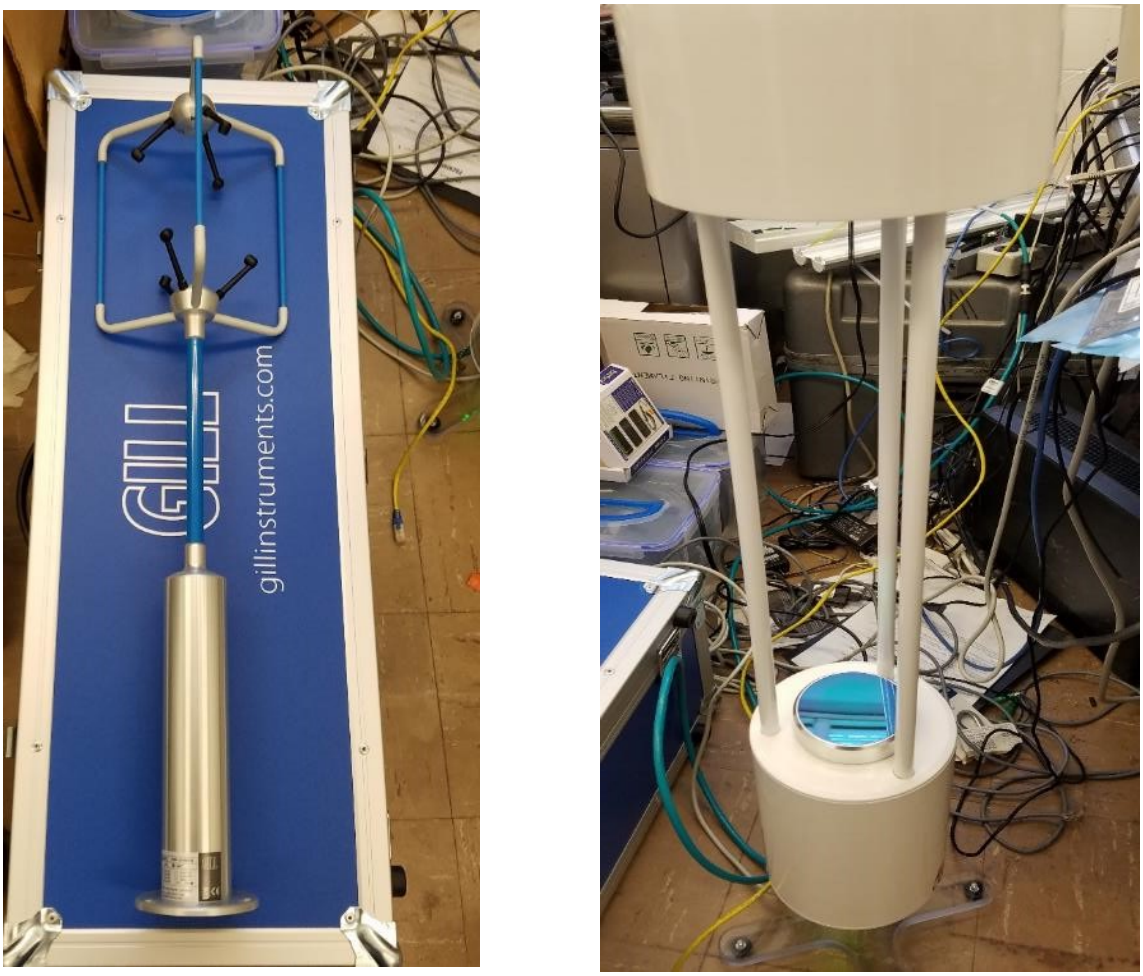

Figure 5.1. Left: new LI-7700 during DAQ interfacing and right, new Windmaster Pro.

The three key new components have been integrated into the data logging software but their electrical interface and vehicle mounting are still underway. Figure 5.2 shows an example of the LI-7700 interface in our Scimitar software including the key measurement of methane in µmol/mol (ppm). All alarm notifications and RSSI have also been integrated within the software and the system successfully collected over 21 hours of laboratory data without any faults.

Figure 5.3 shows an example of the GPS sensor on a local Morgantown route where data was collected at 10Hz. In addition, the accuracy of the GPS is increased and provides enough resolution to accurately determine the vehicle location to within a 0.5-1 meter (see lane identification).

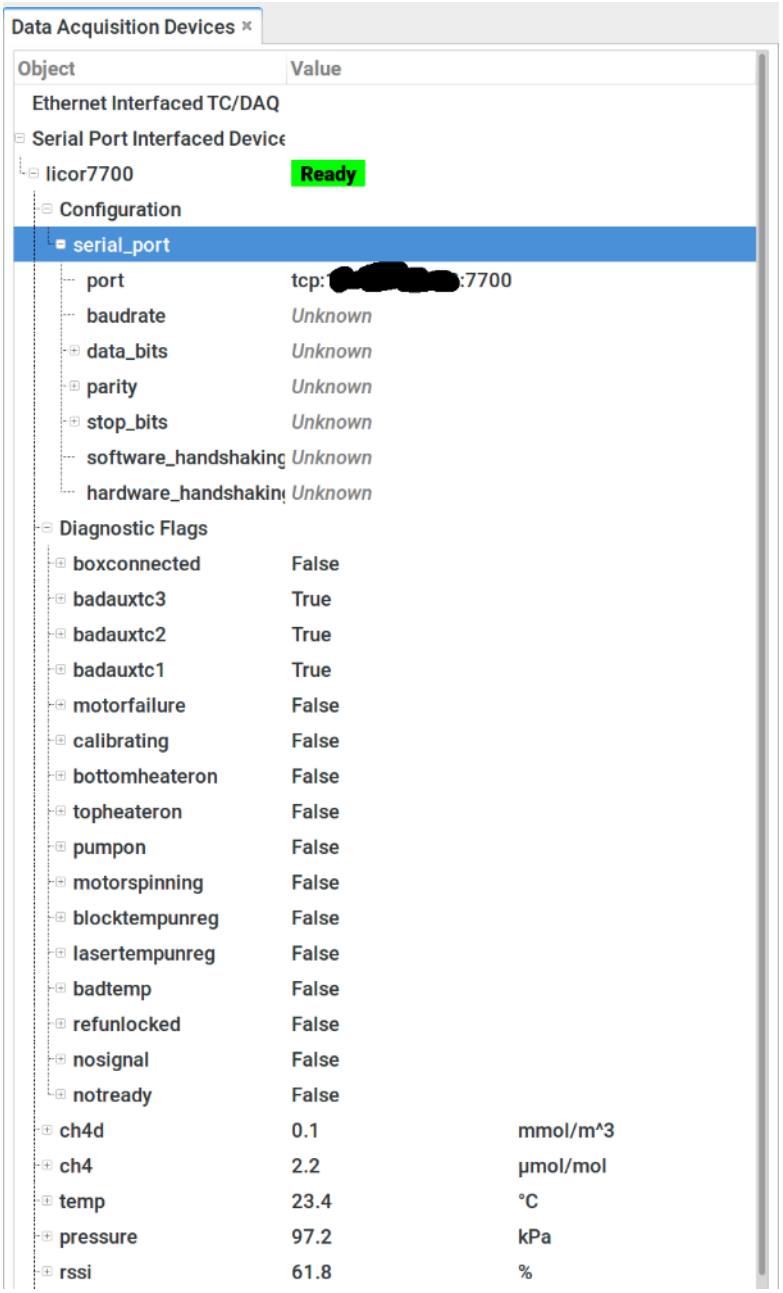

Figure 5.2. Full software integration of the Li-COR LI 7700 completed.

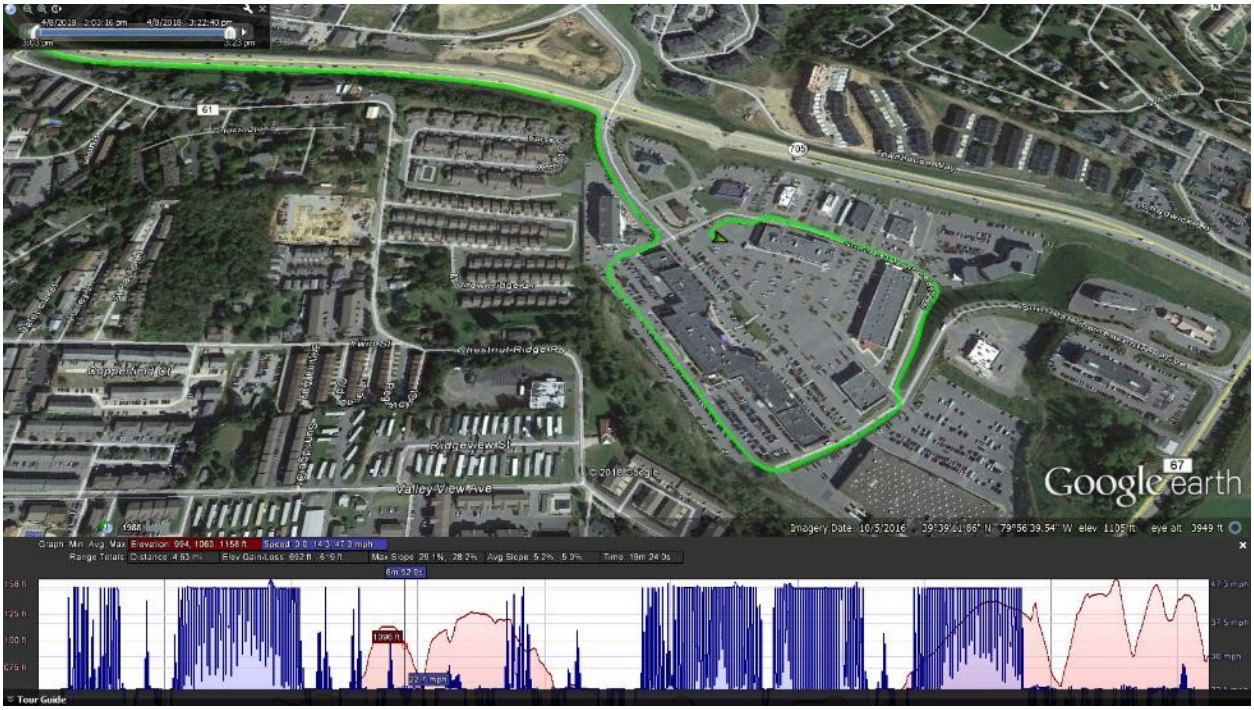

Figure 5.3. Newly integrated GPS system and data from trial run.

Products

The previous quarterly report mentioned a journal publication regarding the analysis on the temporal variability in methane emissions from the course of a year. The team has received additional reviews and will hopefully publish this quarter in the ACS open access journal – OMEGA.

Plan for Next Quarter

During the next quarter, the team will perform the next direct quantification site audit and will target the collection of ambient methane emissions and atmospheric conditions from a vehicle parked at the site during the course of the audit.

Topic 6 – Water Treatment

Approach

As part of this subtask, the Dr. Morrissey is characterizing the chemical and biological factors that influence radium accumulation in sludge from produced water. This research could lead to the development of low cost treatments for produced water that prevent the accumulation or radioactive sludge. This work is in service of Milestone 33: *Results of techniques for low cost treatment of flowback waters*. To accomplish this milestone, the team is performing a series of laboratory microcosm experiments. Produced water is incubated for 21 days in the laboratory with or without additions of sulfate (200 or 2000mg/L) and nutrients (carbon, nitrogen and phosphorus). The addition of nutrients is intended to stimulate the activity of microorganisms to immobilize sulfate and prevent it from precipitating with radium. Tests thus far have utilized produced water from the 3H.

Results & Discussion

Within the last quarter, the team completed three rounds of laboratory microcosm experiments. During these experiments, they measured microbial activity in the produced water by measuring CO_2 and CH_4 production. Although additional microcosm studies are needed for replication and statistical analysis, initial results suggest that nutrient addition stimulates microbial activity increasing the production of CO_2 but not CH_4. The high concentration sulfate treatment appears to shift microbial metabolism lowering CO_2 production but increasing CH_4 production (Figure 6.1).

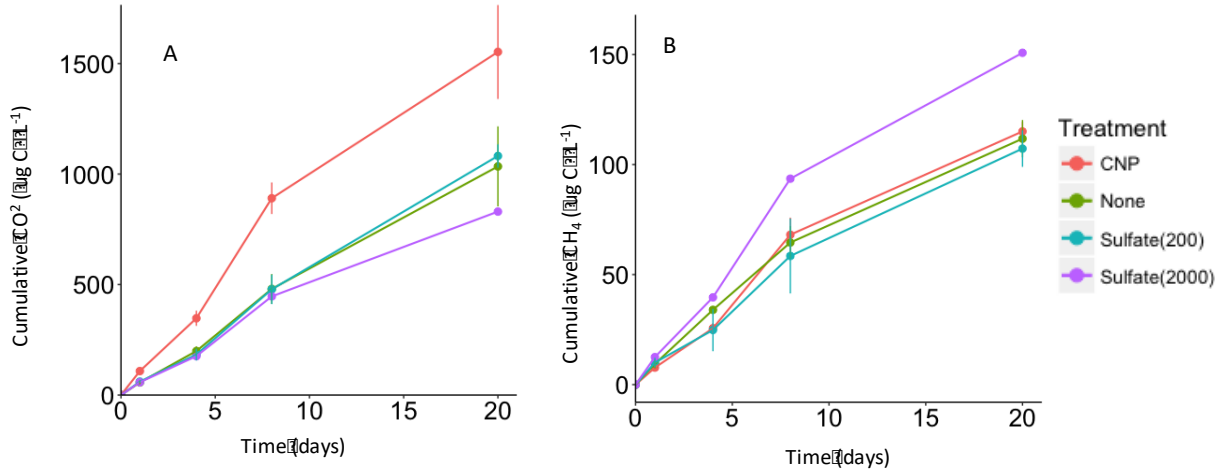

Figure 6.1. Production of CO_2 (A) and CH_4 (B) in laboratory microcosms of produced water incubated with no additions (None), with added sulfate (at 200 or 2000mg/L), and with added nutrients (CNP, carbon, nitrogen and phosphorus).

Some but not all of the chemical and radiological results and been received from the analytical laboratories. Preliminary results suggest that sulfate is below detection in the produced water from well 3H. In the absence of added sulfate, dissolved concentrations of Sr, Ba, Ra 226 and Ra 228 did not change over the incubation period (Figure 6.2) suggesting that these materials will not precipitate into solids during the holding of produced waters with chemistry similar to 3H. When high concentrations of sulfate were added (2000 mg/L) concentrations of Ba concentrations immediately dropped ~50% (Figure 6.2A) and concentrations of Ra 226 & Ra 228 declined after over time (Figures 6.2 C & D). Concentrations of Sr were unaffected by sulfate addition (Fig 2B). These results suggest that produced water with substantial sulfate and Ra concentrations could result in the rapid accumulation of Ra in to produced solids.

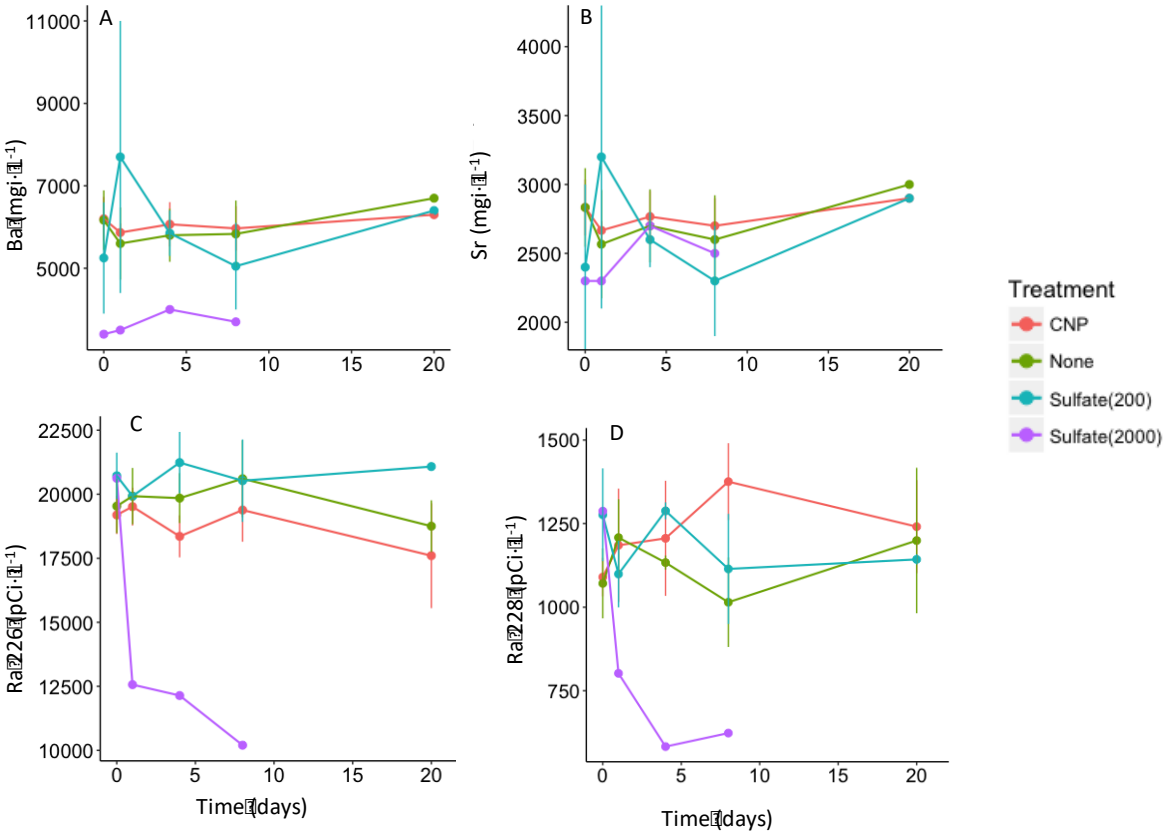

Figure 6.2. Concentrations of dissolved Ba (A), Sr (B), Ra 226 (C), and Ra 228 (D) in laboratory microcosms of produced water incubated with no additions (None), with added sulfate (at 200 or 2000mg/L), and with added nutrients (CNP, carbon, nitrogen and phosphorus).

Products

N/A

Plan for Next Quarter

In the next quarter, Dr. Morrissey will continue laboratory microcosm experiments to determine if the preliminary results reported above can be replicated and are statistically significant. As sulfate concentrations from well 3H are low, Dr. Morrissey and her team will determine if microorganisms can reduce or delay the precipitation of Ra in high sulfate produced waters by performing a microcosm study where nutrients (C,N, and P) are added in combination with sulfate.

In the next period, analysis of water chemistry in the microcosms experiments conducted this period will be completed. Solid samples of the precipitate formed during these microcosms will be analyzed for Ra 226 and Ra 228. An undergraduate research will be joining this project, this person will begin the biological analysis of samples from the laboratory microcosms. Specifically, the team will analyze the prokaryotic communities via DNA extraction, PCR and sequencing of the phylogenetic marker gene.

In the next quarter preliminary results will from this work will be presented to researchers at Kansas University who are also studying produced water.

Topic 7 – Database Development

Approach

All MSEEL data is now online and available to researchers (Figure 7.1 and 7.2). The website has been updated with the latest production beyond the end of the quarter (Figure 7.3). Work continues

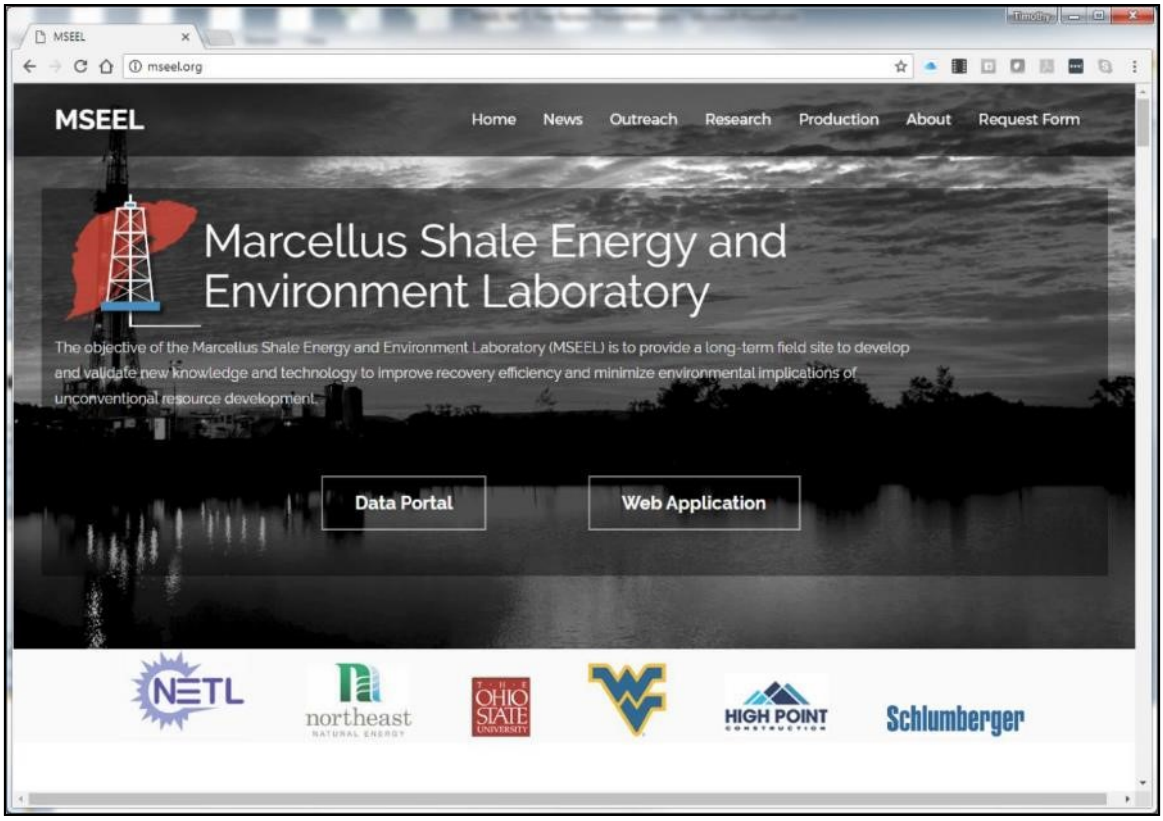

Figure 7.1: MSEEL website at http://mseel.org/.

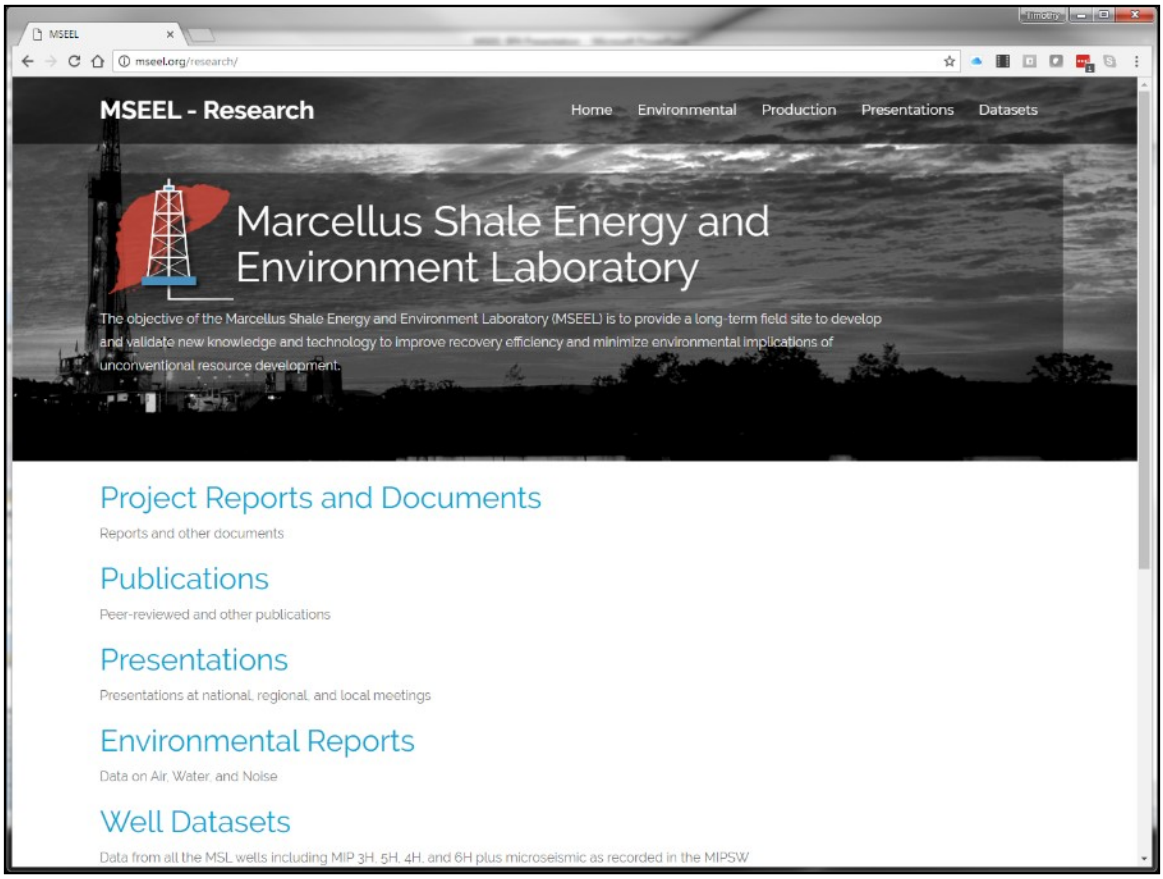

Figure 7.2: All data generated by the MSEEL project is available for download at http://mseel.org/.

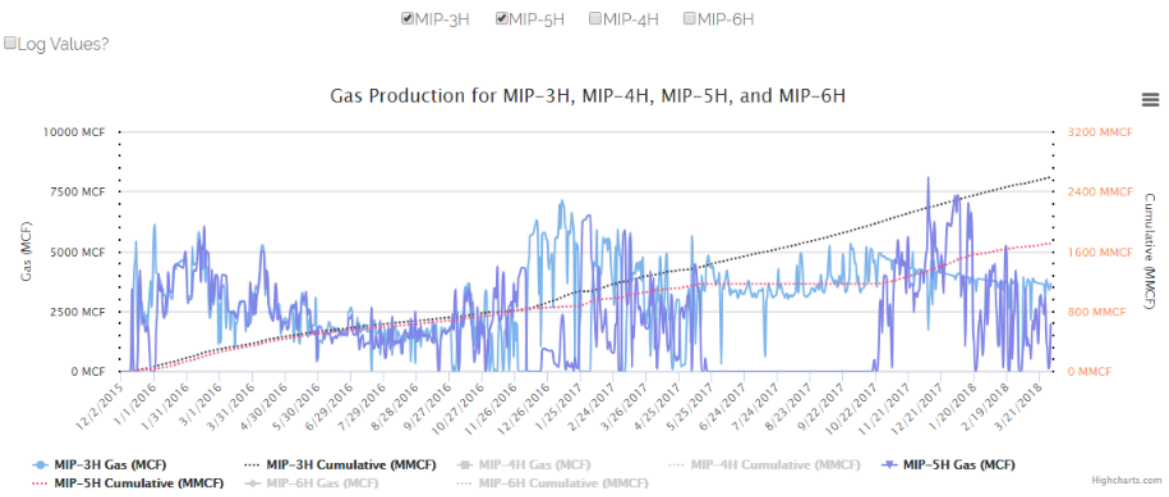

Figure 7.3: Gas and water production have been updated through the end of the quarter and are available at http://mseel.org/. Note that the MIP-3H is showing a smooth decline. This has increased our ability to understand production.

Results & Discussion

Data and publications are now available at http://mseel.org/.

Products

Web site enhanced and updated.

Plan for Next Quarter

Still working to develop interactive programs to display user selected welllogs and geochemical data. A mock-up of the type of display is shown in Figure 7.4. Should be running by 30 June.

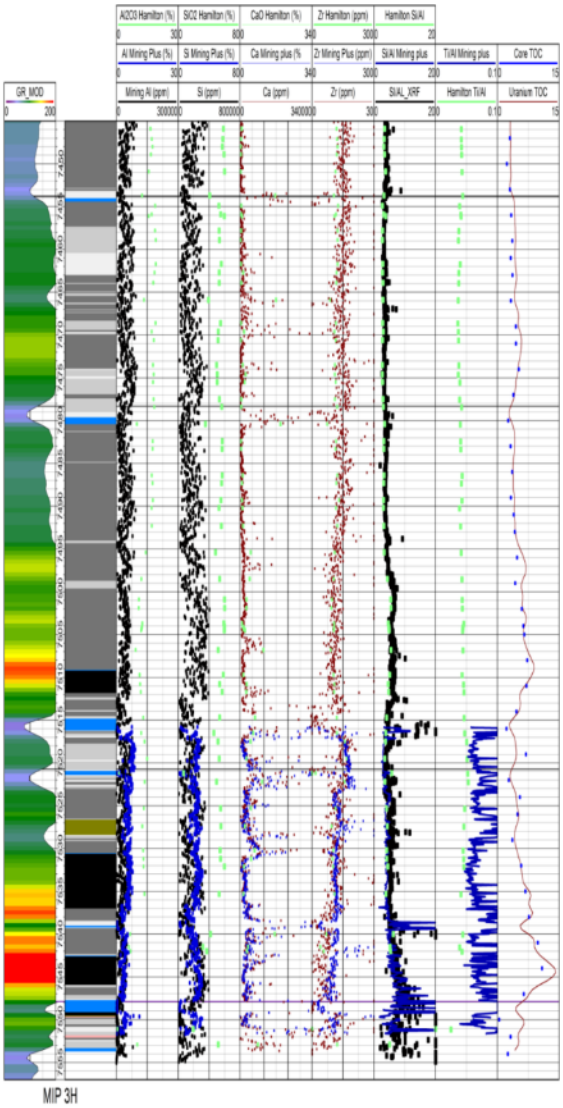

Figure 7.4: Mock up showing log and geochemical data for the MIP 3H pilot hole. The user will be able to select the type of data and scale of displays.

Topic 8 – Economic and Societal

This task is complete and will not be updated in future reports.

Cost Status

Year 1

Start: 10/01/2014 End: 09/30/2017

Baseline Reporting Quarter

	Q1 (12/31/14)	Q2 (3/30/15)	Q3 (6/30/15)	Q4 (9/30/15)
Baseline Cost Plan	(From 424A, Sec. D)			
(from SF-424A)				
Federal Share	$549,000		$3,549,000	
Non-Federal Share	$0.00		$0.00	
Total Planned (Federal and Non-Federal)	$549,000		$3,549,000	
Cumulative Baseline Costs				
Actual Incurred Costs				
Federal Share	$0.00	$14,760.39	$237,451.36	$300,925.66
Non-Federal Share	$0.00	$0.00	$0.00	$0.00
Total Incurred Costs - Quarterly (Federal and Non-Federal)	$0.00	$14,760.39	$237,451.36	$300,925.66
Cumulative Incurred Costs	$0.00	$14,760.39	$252,211.75	$553,137.41
Uncosted				
Federal Share	$549,000	$534,239.61	$3,296,788.25	$2,995,862.59
Non-Federal Share	$0.00	$0.00	$2,814,930.00	$2,814,930.00
Total Uncosted - Quarterly (Federal and Non-Federal)	$549,000	$534,239.61	$6,111,718.25	$5,810,792.59

Start: 10/01/2014 End:
09/30/2017

Baseline Reporting Quarter

	Q5 (12/31/15)	Q6 (3/30/16)	Q7 (6/30/16)	Q8 (9/30/16)
Baseline Cost Plan	(From 424A, Sec. D)			
(from SF-424A)				
Federal Share	$6,247,367		$7,297,926	
Non-Federal Share	2,814,930		$4,342,480	
Total Planned (Federal and Non-Federal)	$9,062,297	$9,062,297.00	$11,640,406	
Cumulative Baseline Costs				
Actual Incurred Costs				
Federal Share	$577,065.91	$4,480,939.42	$845,967.23	$556,511.68
Non-Federal Share	$0.00	$2,189,863.30	$2,154,120.23	$0.00
Total Incurred Costs - Quarterly (Federal and Non-Federal)	$577,065.91	$6,670,802.72	$3,000,087.46	$556,551.68
Cumulative Incurred Costs	$1,130,203.32	$7,801,006.04	$10,637,732.23	$11,194,243.91
Uncosted				
Federal Share	$5,117,163.68	$636,224.26	$1,004,177.30	$447,665.62
Non-Federal Share	$2,814,930.00	$625,066.70	($1,503.53)	($1,503.53)
Total Uncosted - Quarterly (Federal and Non-Federal)	$2,418,796.68	$1,261,290.96	$1,002,673.77	$446,162.09

Start: 10/01/2014 End: 09/30/2017

Baseline Reporting Quarter

	Q9 (12/31/16)	Q10 (3/30/17)	Q11 (6/30/17)	Q12 (9/30/17)
Baseline Cost Plan	(From 424A, Sec. D)			
(from SF-424A)				
Federal Share				$9,128,731
Non-Federal Share				$4,520,922
Total Planned (Federal and Non-Federal)				$13,649,653
Cumulative Baseline Costs				
Actual Incurred Costs				
Federal Share	$113,223.71	$196,266.36	$120,801.19	$1,147,988.73
Non-Federal Share	$0.00	$0.00	$0.00	$0.00
Total Incurred Costs - Quarterly (Federal and Non-Federal)	$113,223.71	$196,266.36	$120,801.19	$1,147,988.73
Cumulative Incurred Costs	$11,307,467.62	$11,503,733.98	$11,624535.17	$12,772,523.90
Uncosted				
Federal Share	$334,441.91	$138,175.55	$17,374.36	$700,190.63
Non-Federal Share	($1,503.53)	($1,503.53)	($1,503.53)	$176,938.47
Total Uncosted - Quarterly (Federal and Non-Federal)	$332,938.38	$136,672.02	$15,870.83	$877,129.10

Start: 10/01/2014 End: 09/30/2017

Baseline Reporting Quarter

	Q13 (12/31/17)	Q14 (3/30/18)	Q15 (6/30/18)	Q15 (9/30/18)
Baseline Cost Plan	(From 424A, Sec. D)			
(from SF-424A)				
Federal Share				
Non-Federal Share				
Total Planned (Federal and Non-Federal)				
Cumulative Baseline Costs				
Actual Incurred Costs				
Federal Share	$112,075.89	$349,908.08		
Non-Federal Share	$0.00	$31,500.23		
Total Incurred Costs - Quarterly (Federal and Non-Federal)	$112,075.89	$381,408.31		
Cumulative Incurred Costs	$12,884,599.79	$13,266,008.10		
Uncosted				
Federal Share	$588,114.74	$238,206.66		
Non-Federal Share	$176,938.47	$145,438.24		
Total Uncosted - Quarterly (Federal and Non-Federal)	$765,053.21	$383,644.90		

National Energy Technology Laboratory

626 Cochrans Mill Road
P.O. Box 10940
Pittsburgh, PA 15236-0940

3610 Collins Ferry Road
P.O. Box 880
Morgantown, WV 26507-0880

13131 Dairy Ashford Road, Suite 225
Sugar Land, TX 77478

1450 Queen Avenue SW
Albany, OR 97321-2198

Arctic Energy Office
420 L Street, Suite 305
Anchorage, AK 99501

Visit the NETL website at:
www.netl.doe.gov

Customer Service Line:
1-800-553-7681